The Compounding Effects of Obesity on the Development of Intimal Hyperplasia Following Vascular Intervention:

A Histopathological Analysis

by

Melanie Kim Black, Dip. Med. Tech.

BLCMEL 002

SUBMITTED TO THE UNIVERSITY OF CAPE TOWN

Dissertation in fulfillment of the requirements for the degree of

M.Sc. (Med) Cardiothoracic Surgery

Faculty of Health Sciences

UNIVERSITY OF CAPE TOWN

2009

Supervisor: Dr Paul Human

HOD: Professor Peter Zilla

Declaration

I, Melanie Kim Black hereby declare that the work on which this dissertation is based is my original work (except where acknowledgements indicate otherwise) and that neither the whole work nor any part of it has been, is being, or is to be submitted for another degree in this or any other university.

I empower the University to reproduce for the purpose of research either the whole or any portion of the contents in any manner whatsoever.

Signature:

Date: 1 September 2009

Acknowledgements

I would like to extend my sincere appreciation to the following individuals, without whom this thesis would not have been possible.

Professor Peter Zilla for his visionary attitude towards research and his perseverance in a challenging economic climate. I thank him for giving me the opportunity to complete a Masters degree in his department. It is both an honor and a privilege to be employed in his Cardiovascular Research Unit.

Dr Paul Human for his steadfast guidance and encouragement throughout this project, and for being a dedicated and enthusiastic supervisor. Thank you also for your patience as a teacher and for giving up many precious hours in the task of combing through the details.

To the members of the Cardiovascular Research Unit who were involved in this project, in particular Mrs Subash Govender for her excellent histological support, Mrs Helen Ilsley for her assistance with TEM, to Mr Noel Maakgraaf for the anesthesiology, Dr Siyamak Saleh for the surgical procedures and to Mr Raymond Michaels for his assistance during surgery.

Lastly I would like to thank my family for supporting me through a demanding but rewarding journey.

Publications:

The techniques involved in resin embedding were a prequel to the analytical methods required for this study, therefore the following two publications, of which I was a co-author are included for reference as Appendix B.

Comparison of Processing and Sectioning Methodologies for Arteries Containing Metallic Stents

Peter Rippstein, Melanie Black, Marie Boivin, John P Veinot, Xiaoli Ma, Yong-Xiang Chen, Paul Human, Peter Zilla, Edward R O'Brien.

Journal of Histochemistry & Cytochemistry (2006) 54: 673-681

Utilization of shape memory in external vein-graft meshes allows extreme diameter constriction for suppressing intimal hyperplasia: A non-human primate study

Peter Zilla, Michael Wolf, Nasser Rafiee, Lovendran Moodley, Deon Bezuidenhout, Melanie Black, Paul Human, Thomas Franz.

Journal of Vascular Surgery (2009)

Contents

Abbreviations

AA – Aortic Artery

ARTISTIC – Angiorad Radiation Technology for In Stent Restenosis Trial in Native Coronaries

atm – atmospheres

BMA – Butyl Methacrylate

BMI – Body Mass Index

BMS – Bare Metal Stent

CA – Coronary Artery

CABG – Coronary Artery Bypass Graft

CAD – Coronary Artery Disease

CCA – Common Carotid Artery

CIA – Iliac Artery

Col – Collagen

CRP – C-Reactive Protein

CS – Chondroitin Sulfate

CSPG – Chondroitin Sulfate Proteoglycan

CVD – Cardiovascular Disease

DAB – Diaminobenzidine

DDP – Dipeptydal Pepsidase

DES – Drug Eluting Stent

DM 2 – Diabetes Mellitus Type II

DSPG – Dermatan Sulfate Proteoglycan

EC – Endothelial Cell

ECA – External Carotid Artery

ECM – Extra Cellular Matrix

EG – Endothelial glycocalyx

EGL – Endthelial Glycocalyx Layer

ePTFE – Expanded polytetrafluoroethylene

FDA – Federal Drug Association

FFA – Free Fatty Acids

FGF – Fibroblast Stimulating Growth Factor

FIELD – Fenofibrate Intervention & event lowering in Diabetes

FSS – Flow Shear Stress

GAG – Glycosaminoglycan

GLP – Glucagon Like Peptide

HA – Hyaluronic Acid

HDL – High Density Lipoprotein

HEPES – 4-(2-hydroxyethyl)-1-piperazineethanesulfonic acid

HRP – Horse Radish Peroxidase

HS – Heparan Sulfate

Hs-CRP – High Sensitivity C-Reactive Protein

HSPG – Heparan Sulfate Proteoglycan

IA – Image Analysis

ICA – Internal Carotid Artery

IDF – International Diabetics Federation

IDL – Intermediate Density Lipoprotein

IEL – Internal Elastic Lamina

IgA – Immunoglobulin A

IgG – Immunoglobulin G

IH – Intimal Hyperpplasia

IL – Inter Leukin

I:M – Intima-media

IR – Insulin Resistance

ISR – In Stent Restenosis

ITA – Internal Thoracic Artery

IVUS – Intravascular Ultrasonography

JUPITER – Justification for use of statins in primary prevention: an intervention trial evaluating Rosuvustatin.

Jv/A – filtration rate /unit area of capillary wall;

KS – Keratan Sulfate

LCC – Left Common Carotid

LDL – Low Density Lipoprotein

MACE – Major Cardiac Event

MCP-1 – Macrophage Chemotactic Protein

MI – Myocardial Infarction

MMA – Methyl Methacrylate

MMP – Matrix Metalloproteinase

MS – Metabolic Syndrome

NAC – N-Acytylcysteine

NI – Neointimal

NIDDM – Non-Insulin- Dependant Diabetes Mellitus

NIH – Neo-intimal Hyperplasia

NK – Nuclear Kappa

NO – Nitric Oxide

Pa – Pascal

PBS – Phosphate Buffered Saline

Pc – Pressure in capillary lumen

PCI – Percutaneous Coronary Intervention

PCL - Polycaprolacton

PDGF – Platelet Derived Growth Factor

PFA – Para fomaldehyde

PG – Proteoglycan

PPAR – Peroxisome Proliferator Activated Receptor

PSI – Pounds per square inch

Pt – Pressure in the tissue

PTCI – Percutaneous Transluminal Coronary Intervention

PU – Poly Urethane

RA – Radial Artery

RANTES – Regulated upon Activation, Normal T-cell Expressed and Secreted

RCC – Right Common Carotid

ROS – Reactive Oxygen Species

SA – South Africa

SCRIPPS – Schripps Coronary Radiation to Inhibit Proliferation Post

SMA – Smooth Muscle Actin

SMC – Smooth Muscle Cell

SNS – Sympathetic Nervous System

SOD – Super Dioxide

SV – Saphenous Vein

TBS – Tris Buffered Saline

TEM – Transmission Electron Microscopy

TGF – Transforming Grpwth Factor

TIMP-1 – Tissue Inhibitor Metalloproteinase

TNF – Tumour Necrosis Factor

TG – Triglycerides

TVR – Target Lesion Revascularization

VEGF – Vascular Endothelial Growth Factor

VLDL – Very Low Density Lipoprotein

VSMC – Vascular Smooth Muscle Cell

VWF – Von Willebrand Factor

WBC – White Blood Cell

WHO – World Health Organization

WRIST – Washington Radiation for IN Stent Restenosis Trial

WSS – Wall Shear Stress

ZD – Zucker Diabetic

ZDF – Zucker Diabetic Rat

ZFR – Zucker Fatty Rat

ZL – Zucker Lean

ZO – Zucker Obese

α - alpha

β - beta

δ - delta

γ - gamma

Abstract

Introduction:

Intimal hyperplasias is the most significant factor limiting vascular intervention therapy, with an incidence of between 30-50% following coronary or femoral angioplasty, and between 10 and 30% of coronary artery saphenous vein bypass grafts (CABG). Extensive research over the past decade into the pathology and pharmacological treatment of this condition has not yet provided a reasonable solution to the multifactorial etiology of restenosis. Patients with metabolic syndrome have a higher risk for cardiovascular disease and mortality, and those with Diabetes mellitus Type II are at an even greater risk post intervention. It is our hypothesis that obesity has a significant impact on the pathology in the neointima, specifically with respect to the development of intimal hyperplasia (IH). In addition, the pro-inflammatory nature of obesity is known to elicit an increased inflammatory response that may contribute to the increase in stenosis.

Methods:

This study examines the histopathological response to injury following both balloon angioplasty and endovascular stenting in the Zucker rat, a model that allows interpretation of the role of obesity as well as progressive glucose intolerance and hyperinsulimaemia. Lean and obese Zucker fatty rats and Zucker diabetic fatty rat (ZDF) were subjected to balloon injury with or without stenting. The development of IH, along with the histological response to injury was analyzed.

Results: Following balloon angioplasty alone, the obese group displayed a greater degree of IH than the lean group, whereas the ZDF group unexpectedly was largely devoid of a hyperplastic response. There were very few inflammatory cells at the 21 day time point defined in this study. There was a high level of C-reactive protein staining in the obese group. In the stented groups, there was very little variation in the degree of IH between the three genotypes, with only a slight increase observed in the obese group. Inflammatory cells were more evident on the stented groups. Evidence of increased endothelial glycocalyx following balloon injury was also demonstrated.

Conclusion:

Our results confirmed the role of obesity in the development of IH. In the stented groups, the degree of IH was controlled by the presence of the endovascular stent. The mean intimal thickness between the wires (that is from the lumen to the IEL) was (129.8 ± 60.0μm, 120.3 ± 33.2μm and 141.4 ±100.8μm for the ZFR-F, ZFR-L and ZDF rats respectively; p=N.S). The intimal thickness after 21 days following stent deployment over the three groups was non-significant. The mean intimal thickness between the wires (that is from the lumen to the IEL)

was (129.8 ± 60.0µm, 120.3 ± 33.2µm and 141.4 ±100.8µm for the ZFR-F, ZFR-L and ZDF rats respectively; p=N.S). The intimal thickness over the wires (that is from the lumen to the stent wire, but excluding the stent area) was non-significant (79.5 ± 66.3µm, 96.4 ±58.3µm and 95.6 ± 97.6µm). The twenty-one day time point proved to be optimal for the analysis of IH, but was not ideal with regard to inflammation. The prominent endothelial glycocalyx observed post angioplasty proved to be an interesting and novel finding, which may help to further elucidate mechanisms behind the pathology of IH.

Chapter I

Introduction and Background

1.1 Introduction

Cardiovascular disease (CVD) remains the leading cause of death in the world today *(Table-1)*. Histological studies have shown that the precursors of heart disease begin in adolescence and evolve over decades (4). The arteries most commonly affected are the coronary arteries that emanate from the aorta and supply the heart muscle with oxygenated blood. Focal thickening of the intima layer by proliferating smooth muscle cells (SMC) and the accumulation of lipids or fatty streaks form the basis of an atherosclerotic lesion. These lesions may develop into fibrous plaque capsules, which typically rupture exposing the blood to a thrombogenic surface resulting in thrombus formation (5). These lesions cause vascular occlusion restricting the blood flow through the coronary arteries supplying the heart muscle, and eventually resulting in myocardial infarction (MI) *(Fig-1)*.

According to the Australian Institute of Health, Russia has the highest death rate from CVD, and Japan has the lowest incidence, most likely due to their low fat, high fish diet (6). In America, CVD has remained the leading cause of death since 1990, with 40% of deaths resulting from heart disease and with more than 1 million percutaneous coronary interventions (PCI) being performed annually. According to the World Health Organization (WHO) 11,8 million people died of CVD in 2005 and this is estimated to rise to 20 million in 2015.

Table 1 Top ten causes of death in high & low income countries (7).

High-Income Countries	**Deaths in Millions**	**% of deaths**
Coronary heart disease	1.33	16.3
Stroke & other cerebrovascular diseases	.076	9.3
Trachea, bronchus, Lung cancers	0.48	5.9
Lower respiratory infections	.031	3.8
Chronic obstructive pulmonary disease	0.29	3.5
Alzheimer and other dementias	0.28	3.4
Colon & rectum cancers	0.27	3.3
Diabetes mellitus	0.22	2.8
Breast cancer	0.16	2.0
Stomach cancer	0.14	1.8
Low-Income Countries	**Deaths in Millions**	**% of deaths**
Lower respiratory infections	2.94	11.2
Coronary heart disease	2.47	9.4
Diarrhoeal diseases	1.81	6.9
HIV/AIDS	1.51	5.7
Stroke & other cerebrovascular diseases	1.48	5.6
Chronic obstructive pulmonary disease	0.94	3.6
Tuberculosis	0.91	3.5
Neonatal infections	0.90	3.4
Malaria	0.86	3.3
Prematurity & low birth weight	0.84	3.2

The pathophysiological and molecular mechanisms driving these diseases are a focus of this thesis in an attempt to gain a better understanding of the inter-relationship between CVD and metabolic syndrome (MS). MS refers to a cluster of risk factors with a high correlation to the prevalence of obesity, diabetes and a raised low-density lipoprotein (LDL) (8).

CVD places a major health and economic burden on the world, especially in developing countries. In low to middle income countries, health care budgets are sub-optimal, making it imperative to use the limited resources effectively, to make primary health care available to the whole population. According to the American Heart Institute, health care costs are estimated at around $475.3 billion in the USA for 2008. This figure includes both the cost of health care as well as the loss of productivity burden. In the UK this figure was £30.7 billion in the same year (9).

The death rate from CVD is escalating in developing nations. The incidence of diabetes mellitus (DM) is expected to double between 2005-2050, and is one of the major risk factors for CVD. The reduction of this epidemic is largely dependent on prevention of such risk factors (9) *(Table 2)*.

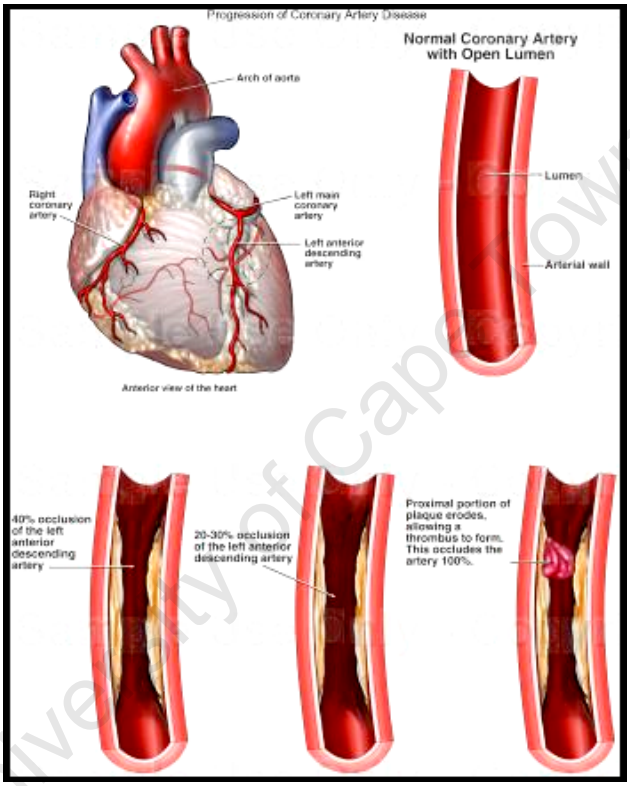

Figure 1 Coronary arteries, providing blood supply to the heart together with vascular sections showing the development of disease to the point of occlusion (10).

1.1.1 Metabolic Syndrome

MS or syndrome X, as it was previously known constitutes a set of metabolic changes that increase the risk of CVD and diabetes mellitus type II (DM2). One out of every five people are affected by MS (11). The main features of MS include obesity, DM2, hypertension and elevated LDL levels (12). MS is diagnosed when there is central obesity plus any two of the factors mentioned *(Table 2)*.

The incidence of DM and MS has risen to alarming rates worldwide. A quarter of the world's population presents with MS and this state is therefore driving CVD. In the USA alone, 20-25% of adults and 90% of DM2 patients present with MS (12).

The two most significant factors of MS are obesity and insulin resistance (IR). Hereditary factors, physical inactivity, ageing and a pro-inflammatory state contribute to the etiology of this disorder. Early diagnosis and treatment is therefore an essential component of heart disease prevention (13).

The International Diabetics Federation (IDF) has drawn up a universally accepted diagnostic tool that is simple to use in clinical practice *(Table 3).* In addition to these criteria, they have described additional parameters for research purposes, which are also implicated in MS *(Table 4).*

Table 2 Criteria for the Diagnosis of MS. (14)

Criteria For Metabolic Syndrome		
Criteria		Measurement
Waist Circumference	Men	>102cm
	Women	>88cm
Blood Pressure	Systolic	>130mm Hh
	Diastolic	>85mm Hg
Serum HDL-C	Men	<1.03mmol/L (<40mg/dL)
	Women	<1.3mmol/L (<50mg/dL)
Serum Triglycerides		>1.7mmol/L (>150mg/dL)
Serum Fasting Glucose		>5.6mmol/L (>100mg/dL)

Table 3 The new IDF definition of MS

The New International Diabetes Federation (IDF) Definition	
According to the IDF definition, for a person to be defined as having metabolic syndrome they must have: Central obesity (defined as waist circumference with ethnicity specific values) Plus any two of the following four factors:	
Raised Triglycerides	>150mg/dL
Elavated HDL Cholesterol	Males <40mg/dL (1.03mmol/L) Females <50mg/dL (1.29mmol/L)
Hypertension	Systolic BP >130 or diastolic BP >85mm Hg
Raised Fasting Plasma Glucose	>100mg/dL (5.6mmol/L) or previously diagnosed DM2

The above parameters can all be measured during the diagnosis of MS and the related disorders. One explanation for IR is that, due to the increase in free fatty acids (FFA) in the blood of obese individuals, they are utilized as an energy source instead of the glucose present in the muscle tissue, leading to a build up of excess glucose in the blood. This leads to increased insulin output from the Beta cells of the pancreas as the body tries to compensate in order to cope with the excess glucose. Eventually the pancreas stops producing insulin leading to glucose intolerance and severe and life threatening hyperglycemia.

Table 4 Metabolic Measurements For Research (13).

Additional Parametres for Research	
Abnormal body fat distribution	General body fat deposition Central fat distribution Adipose tissue biomarkers leptin, adiponectin Liver fat content
Atherogenic dyslipidaemia	ApoB Small LDL particles
Dysglycaemia	OGTT
Insulin resistance	Fasting insulin/proinsulin levels Elevated free fatty acids Insulin resistance by Bergman minimal model
Vascular dysregulation	Measurement of endothelial dysfunction Microalbuminuria
Proinflammatory state	Elevated high sensitivity C-reactive protein Elevated inflammatory cytokines (TNF alpha, IL-6) Decreased adiponectin levels
Prothrombotic state	Fibrinolytic factors Clotting factors
Hormonal factors	Pituitary-adrenal axis

The excess accumulation of adipose tissue in the abdominal region in obese individuals also results in a pro-inflammatory state, impacting on vascular pathology (15). Elevated body mass index (BMI), which compares body weight to height, has an abrogating effect on CVD. It is measured by dividing body weight by the square of the patient's height. BMI is frequently used to identify weight problems such as obesity (14). However, it is the measurement of waist circumference or waist to hip ratio, which is a more accurate indicator of a metabolic syndrome profile than BMI. A waist measurement >102cm in males and >88cm in females indicates the presence of MS (14).

Statins have been successfully administered as treatment for the symptoms of MS. They have anti-inflammatory effects and lipid lowering properties, as well as protective effects on the vascular wall by lowering oxidative stress. They are reported to increase availability of nitric oxide (NO) by this mechanism and thereby improve endothelial function. Endothelial cell (EC) dysfunction involves an impaired vasodilatory response and changes in the cell to matrix or cell-to-cell interactions (5, 16). The reduction of plasma cholesterol is also known to decreases the risk of plaque formation (16).

As a combined therapy, rosuvistatin and fenofibrate, a drug known to reduce low-density lipoprotein (LDL) and triglycerides (TG), have been used to treat more than one factor of MS, and have shown improvements in lipid & metabolic values (12, 17).

The normal artery wall consists of three cell layers, the tunica intima, tunica media and the tunica adventitia *(Fig-2).* The lumen of the vessel layer is lined with a single layer of endothelial cells resting on a basement membrane made up of extracellular matrix (ECM) components, namely collagen, laminin and proteoglycans (PG). The media consists of concentric layers of SMC with alternating bundles of elastic fibres, forming distinct bands or lamellae. The SMC respond to stimuli from the endothelium in response to contraction and dilation. The adventitia is composed of a collagen matrix, vasa vasorum (a network of blood vessels), lymphatic system, elastin and nerve fibres. The internal elastic lamina (IEL) separates the tunica intima from the tunica media and the external elastic lamina (EEL) separates the tunica media from the tunica adventitia.

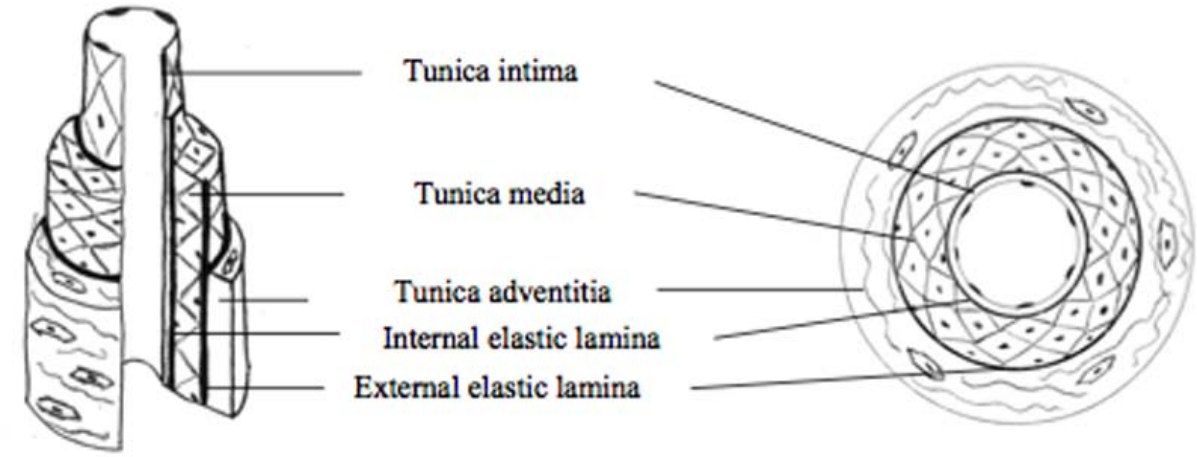

Figure 2 Histological structure of the normal artery wall (19)

The proliferation of SMC and their secretion of ECM components in the inner lining of the vasculature is referred to as intimal thickening, and is known to pre-dispose arteries to the development of atherosclerotic lesions. This occurs in arteries from birth and progresses throughout life, particularly in the coronary and carotid arteries (18).

The early histopathological changes are less easily monitored but due to excess FFA in the blood of obese individuals, fatty streaks or lipid droplets accumulate beneath the endothelium. These vascular lesions may consist of macrophages, foam cells, T lymphocytes, connective tissue elements and debris and place the patient at significantly increased risk of cardiovascular complications (19) *(Fig 3)*.

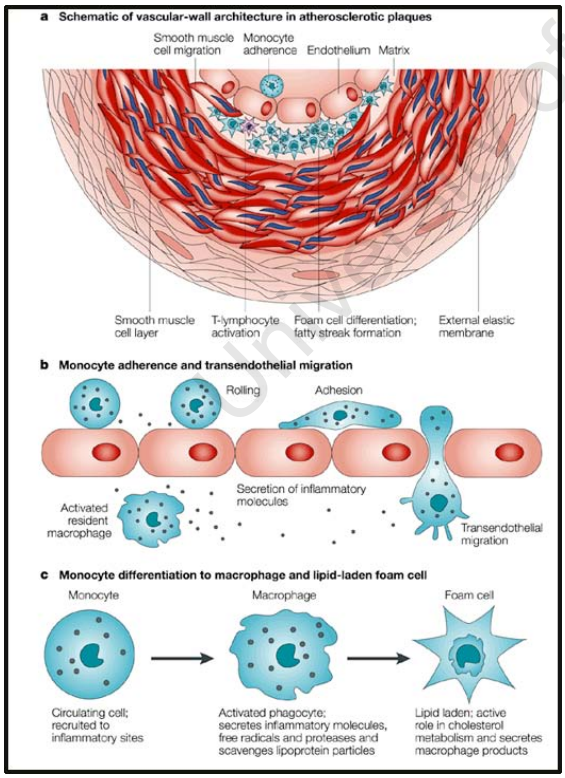

Figure 3 A Schematic representation of the development of atherosclerosis (20)

1.1.2 Obesity

Obesity is fast becoming a global health concern as the number of obese individuals is rising steadily, with estimated costs to the health care system in the USA of $92 billion in 2002 (14). The lack of physical activity combined with high fat and high sugar diets is the primary cause of this disorder. Abdominal obesity can be used to define obesity. The degree of obesity correlates to the degree of IR, which in turn correlates to the extent of intracellular stores of triglycerides (TG). A BMI > 30kg/m^2 meets the criterion for obesity in adults, but this problem is not confined to adults only. There has been a threefold increase in obesity in children under 20 years of age from 1980-2007. Obesity is associated with several health complications including DM, IR, MS and CVD. A large proportion of the increased risk, due to obesity can be attributed to an

inflammatory process. Fat mass behaves much like an endocrine organ, secreting adipokines and FFA, which influence lipid metabolism and insulin sensitivity. The metabolic and immune pathways are inter-connected, as the prevalence of obesity over-activates the immune system, creating a chronic low-grade inflammation or a pro-inflammatory state (14).

1.1.3 Hyperglycemia, Insulin Resistance and glucose Intolerance

The term, hyperglycemia refers to an elevated blood sugar. High blood glucose levels have been implicated in tissue and organ damage as well as degradation of the endothelial glycacalyx layer (EGL), lining the vasculature (21). The EGL is a network of membrane-bound PG and glycoproteins covering the endothelium on their luminal surface (22). The disruption of this glycocalyx layer results in increased reactive oxygen species (ROS) and raised levels of hyaluronic acid (HA) in the blood circulation, which leads to dysfunction of the EC (21) *(Fig-4)*.

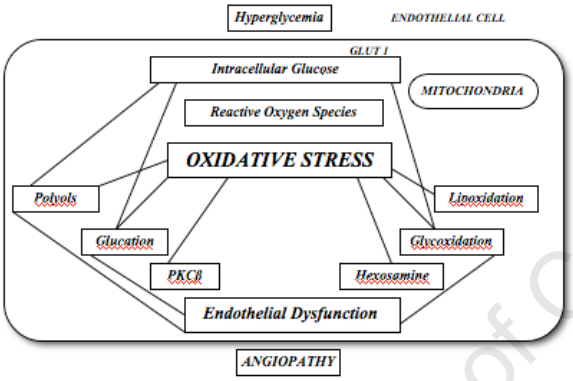

Figure 4 The effect of hyperglycemia on ROS and Endothelial dysfunction (16)

Impaired glucose tolerance refers to the association with a pre-diabetic state of dysglycemia. It is associated with insulin resistance and an increased risk of CVD, and it occurs some time before DM2 manifests itself (23).

The inability of the body to adequately respond to insulin in the liver, muscles or adipose tissue, is referred to as IR. IR in fat cells results in a decrease in the effect of insulin and therefore increased hydrolysis of stored TG. Increased mobilization of stored lipids elevates FFA in blood plasma. IR in the muscles causes reduced glucose uptake with excess glucose being stored as glycogen. IR in liver cells results in impaired glycogen synthesis and failure to deal with elevated levels of glucose. These three forms of insulin resistance all contribute to increased blood glucose levels (23).

The production of insulin by the beta cells of the pancreas regulates glucose levels in the blood stream. IR, however, results in excess accumulation of glucose in the blood, triggering the need for more insulin production. The result is both hyperinsulinemia and hyperglycemia. This can lead to destruction of the beta cells (24). Insulin resistance is believed to be the origin of MS and type II DM and is present long before the onset of DM. At diagnosis, approximately 50% of beta cell function has already been lost (13).

There have been more than 15,000 publications in recent years regarding insulin resistance and CVD. Research on Pima Indians from SW Arizona, revealed that they appear to have a protective mechanism against heart disease in spite of being overtly obese. In humans the association between obesity and the sympathetic nervous system (SNS) has been reported, and confirmed by studies on animal models (25). In the Pima Indians there is no correlation between SNS activity and insulinemia. This could explain how the inability of insulin to activate the SNS in response to obesity may contribute to the low incidence of hypertension. Pima Indians have a greater percentage of obesity but a lower percentage of hypertension and CVD. Their SNS activity level is 20-30% lower than the white population. Thus a low SNS activity level would be desirable, as it appears to be protective against the development of hypertension (25).

1.1.4 Diabetes Mellitus-Type II

Type II diabetes, previously referred to as non-insulin-dependent diabetes mellitus (NIDDM), resulting from impaired glucose tolerance, has become a worldwide epidemic. The health care costs for individuals suffering from diabetes, is escalating not only in the Western world, but globally. Research in this field is ongoing to gain a better understanding of the pathogenesis of this disease and to formulate more effective drugs or combinations of drugs. Type II diabetes is the most common form of diabetes, accounting for 90-95% of the disease in Western societies. There is a relative insulin deficiency combined with defects in insulin action, with 80% of patients being obese or with a history of obesity. The complications of this disease include micro vascular and macro vascular chronic disorders (26).

The excess glucose concentration in the blood, or hyperglycemia, in DM2 is associated with oxidative stress and causes early functional changes to the endothelium. This endothelial dysfunction may be detected by measuring change in microcirculation using flow mediated vaso-dilation and could be useful in diagnosis and treatment prior to the development of angiopathy in DM. In a review by Skhra et al. it was concluded that the use of antioxidants reduced formation of ROS, confirming that oxidative stress plays a role in endothelial dysfunction before the development of angiopathy in DM (16).

There is an increased susceptibility to atherosclerosis in the presence of hyperglycemia, and an increase in the generation of ROS. Known histological changes are an increase in wall thickness, impaired architecture and increased permeability of basement membrane in DM (16).

The coagulation cascade and fibrinolysis is activated in the presence of excess glucose, which is confirmed by thrombin generation (21). These factors all contribute to the escalation of vascular disease that is associated with DM.

Atherosclerosis and CVD occur at an earlier age in diabetic patients. Management of all the metabolic risk factors, cholesterol & TG levels, blood pressure and obesity as well as a low fat controlled diet would do much to delay the complications of DM.

1.1.5 Lipidology

Lipid profiles together with clinical assessment are needed to diagnose MS. Lipoprotein macromolecular micelles transport fats around the body. They are classified into five groups according to size. From the largest to smallest they are: i) Chylomicrons ii) Very low-density lipoproteins (VLDL) iii) Intermediate density lipoproteins (IDL) iv) LDL and v) High density lipoproteins (HDL). Lipoproteins are made up of a water-soluble outer layer of phospholipids, cholesterol and apolipoproteins, with TG and cholesterol esters in the centre *(Fig-5)* (27).

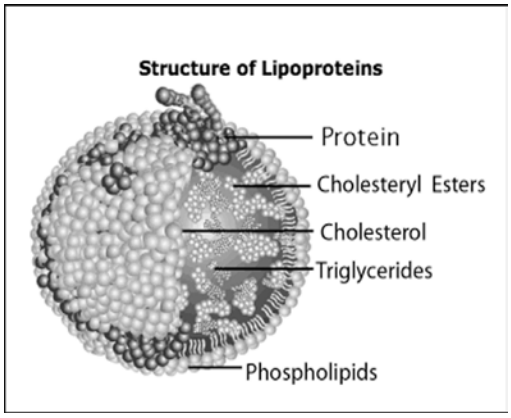

Figure 5 Lipid structure (29)

Hypercholesterolemia and increased LDL levels are associated with an increased risk of CVD. Monitoring of these parameters is a general guideline for evaluating the risk of heart disease. TG are components of VLDL, which play an important role in metabolism and supply of energy but do not dissolve in the blood. An increase in TG is an indicator for higher risk of atherosclerosis, and is often accompanied by low HDL, high LDL levels and IR. Excess calorie intake is stored in fat cells as TG and released by hormones as required. High LDL and TG together with a low HDL is a typical profile of an individual presenting with MS and is a predictor for the development of atherosclerosis (28).

1.1.6 Hypertension

Hypertension or raised blood pressure, is one of the important criteria in the diagnosis of MS and commonly found together with DM. In the presence of IR, the pancreas is stimulated to produce more insulin. An increase in insulin, is in turn, associated with an increase in blood pressure (12).

1.1.7 Atherosclerosis

The intimal layer of arteries is defined as the endothelial cell surface to the medial region and is composed of two sub-layers. The inner layer contains an abundance of PG and SMC, both synthetic and contractile, occurring as single cells rather than layers. The second layer is termed the muscoelastic layer due to the presence of elastin fibres and collagen with SMCs in closely associated layers (29). Intimal thickening is understood to be areas of healthy intima, into which SMC migrate and proliferate resulting from mechanical stress due to variations in blood flow, or flow shear stress (FSS). These areas may develop into atherosclerotic lesions and can be referred to as “atherosclerotic-prone” areas. They are also referred to as intimal cushions, focal intimal hyperplasia, muscoelastic plaque or diffuse intimal fibrosis. Atherosclerotic lesions as they are now commonly known, were previously referred to as “fatty streaks” or “fibrous plaque” (30) and are described by the WHO as “atheroma”.

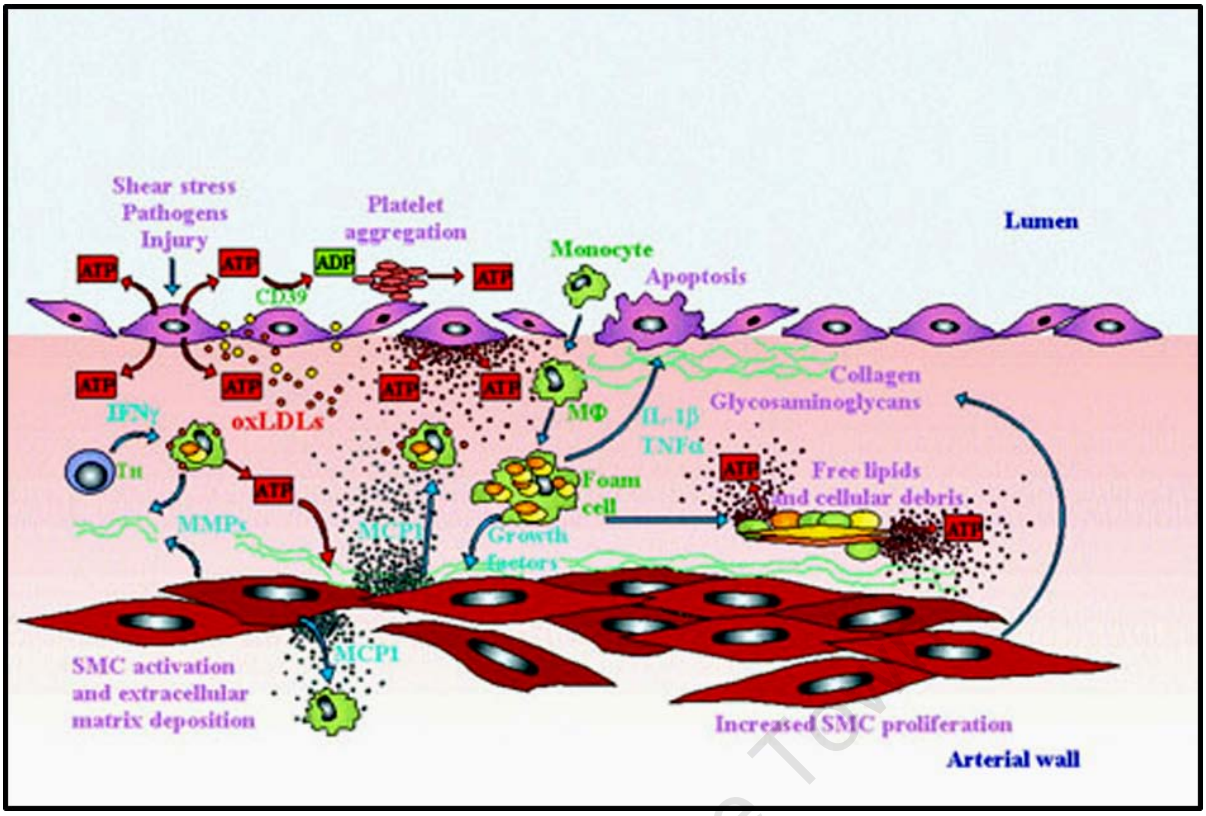

Figure 6 The key players in the early development of Atherosclerosis. EC injury allows LDL to penetrate the sub-intimal space. This is phagocytosed by macrophages, differentiated monocytes from the blood stream, which ultimately become foam cells and die, releasing their contents into the necrotic core. Increased SMC proliferation and EC apoptosis follows. (33)

The centre of an atheroma is made up of foam cells and lipid droplets surrounded by a cap of SMC and a collagen-rich matrix. These lesions can result in thrombus formation and acute vascular occlusion, thereby restricting the blood flow through the coronary arteries resulting in a MI. This may be caused by two factors, endothelial erosion or rupture of the plaque, resulting in the exposure of thrombotic material from the core of the plaque to the blood surface (5). The progression of the vascular disease to the point of atherosclerosis can be seen in *(Fig-7)*.

The EC layer is vital as a non-permeable barrier and plays a role in protecting SMC against proliferation and migration. These cells modulate homeostasis and thrombolysis and synthesize growth factors such as fibroblast growth factor (FGF), platelet derived growth factor (PDGF) and transforming growth factor (TGF). EC damage results in secretion of ECM proteins and the formation of neointimal hyperplasia (NIH). The greater the degree of endothelial damage, the greater the intimal thickening (31). The EC plays a pivotal role in the formation of atherosclerosis as retention of LDL in the intima initiates inflammation (29).

Subsequent oxidation of LDL results in activation of EC. Their functions include mediation of vascular tone, control of inflammation and immune response, thrombo-resistance and membrane barrier permeability (29). Plaque rupture is thought to involve inflammatory cytokines, coagulation factors and matrix metalloproteinases (MMP) as key players (5). EC injury or disruption of the

glycocalyx layer found on the surface of vascular EC, is suggested to be the primary event in the formation of atherosclerosis. In 2008, Noble et al. proposed that the glycocalyx lining the endothelium is the first line of defense against atherosclerosis in DM and MS and suggested that sites of low shear stress resulted in decreased NO, an anti-atherogenic factor release, due to glycocalyx disruption (32). The glycocalyx will be discussed in detail later in this section.

Atherosclerosis is an inflammatory disease, associated with raised levels of inflammatory cytokines. Plasma markers such as C-reactive protein (CRP) and macrophage chemotactic protein (MCP-1) are considered predictors for atherosclerotic risk and restenosis following PCI (33). Inflammatory cytokines, tumor necrosis factor alpha (TNF-alpha) and Interleukin (IL) 6 are up regulated following injury (5). TNF alpha levels were increased 100,000-fold for at least 6 days following injury and inhibition of TNF alpha has been shown to improve vascular recovery (34). The results from the JUPITER 'Justification for the Use of Statins in Primary Prevention: an Intervention Trial Evaluating Rosuvastatin' trials in 2008 confirmed that high sensitivity-C-reactive protein (Hs-CRP) levels, were indeed strong predictors of atherosclerosis and cardiovascular disease (35). Inflammation is associated with atherosclerosis, restenosis, IR and MS.

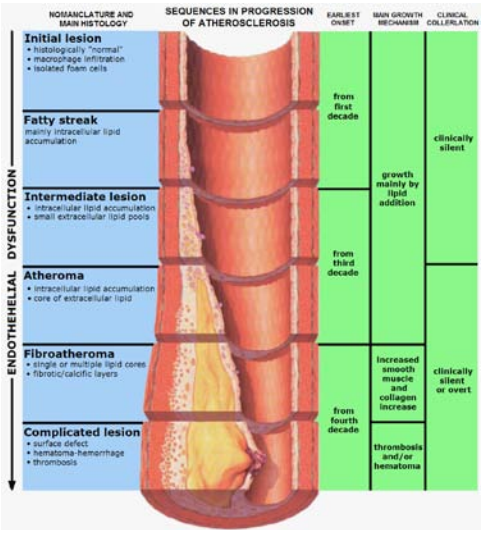

Figure 7 Chronology of the Atherosclerotic Disease Process (2)

Local and systemic inflammatory mediators are critical during the development of atherosclerotic plaque. The inflammatory cells found within the plaque, are activated by cytokines, chemokines, hormones and growth factors, inducing a pro-inflammatory state involving adipose tissue and the liver (36). Adiponectin is a cytokine-like hormone secreted by adipose tissue, which has been found to be protective in obesity related MS and CVD. Okamoto et al suggest that adiponectin has anti-inflammatory effects on macrophages, whereby T cell recruitment is suppressed. The low levels of adiponectin present in patients with MS, DM and obesity, result in the recruitment of T lymphocytes that are key contributors to an immune response in atherosclerosis (37). The mechanism of this can be attributed to a mutation in the adiponectin gene (I164T), which is associated with hypo-adiponectinemia resulting in disturbed secretion into the circulation. This may contribute significantly to MS (38).

Immunosuppressant or anti-inflammatory agents can be employed to treat atherosclerotic lesions. Immunosuppressant agents block activation of T-cells and SMC proliferation as well as prevent intimal lesions and restenosis following angioplasty (5). Anti-inflammatory agents enhance NO production and fibrinolysis (5). (See therapy section below)

1.2 The formation of Intimal Hyperplasia (IH) Following Coronary Intervention

1.2.1 Background

Injury to the vascular wall by balloon angioplasty, results in cellular proliferation, migration and inflammation. Release of inflammatory cytokines and growth factors follows. A critical phenotype change occurs in vascular SMC, changing from a contractile to a synthetic phenotype. This enables them to proliferate and migrate from the media to the intima and to produce PG and collagen in this layer. One of the signal transduction mechanisms, which control the formation of IH in diabetic states, is protein kinase C and mitogen activated protein kinase. Endothelial dysfunction also plays an important role with decreased NO production. The degree of hyperplasia is proportional to the extent of the injury induced by the balloon inflation and the transmural pressure applied (39)

The formation of IH is primarily then a combination of two factors, SMC proliferation and ECM formation. Nikkari et al. described the ECM gene being a "late event" following balloon injury to the rat carotid, with some genes expressed in the intima, while others were expressed in both intima and the media (40). In the process of arterial wall repair after endothelial denudation, there is an increase in elastin and tropoelastin, in a controlled manner in SMC occurring at the end of their proliferation phase (41).

In a study by Frank Sims in 1989, the structural features of coronary arteries of 10 different species were compared (18). The study pertained to the structure of the IEL, and suggested that discontinuities or disruptions of the IEL were structural abnormalities that were present at birth and progressed throughout life. Animal models were found to repair such irregularities of the IEL, while humans did not, and this forms the basis of intimal thickening due to an increase of SMC in the intimal compartment. The internal mammary artery (IMA), also known as the internal thoracic artery (ITA), in humans appears to be the ideal vessel, since it does not have these disruptions in the IEL, and does not develop significant atherosclerosis. It also has endothelial cells closely associated with the IEL that forms a continuous inner lining for the arterial wall. In contrast to animal models, Sims found that human coronary arteries showed substantial intimal thickening with an incomplete endothelialized luminal surface. Their findings suggest that the structural differences in arterial walls among different species, could explain the variations of advanced coronary disease. Animal models compared were baboon, pig, sheep cattle, rabbit and rat coronary arteries (18).

IH is formed over a period of days following injury in animals and over six months in humans. Virmani et al. described this variable vascular response in rabbit and porcine models compared to human. In animal models, the first 24-hour period involved platelet and neutrophil migration to site of injury. After three days, neutrophils and macrophages were evident. By day seven, SMC proliferation and migration had occurred, and by day twenty-eight, foreign body giant cells and SMC in a PG, collagenous matrix were present. In humans granulation tissue occurred by day 14, with an

inflammatory process evident from day 1-30. At six months the presence of SMC within a matrix was visible (42).

The delayed healing that occurs in human arteries can be explained by the fact that there is an underlying diseased state of atherosclerosis whereas the experimental balloon injury done on animals, is typically done on young healthy animals, without an existing inflammatory state (42).

1.2.2 The Role of the ECM

The ECM plays a critical role in the development of IH. It is made up of PG (versican, biglycan, decorin), HA and collagen types I and III. PG and HA are synthesized by SMC and are involved in regulation of vascular permeability, lipid metabolism and thrombosis. During the formation of the neointima, in response to balloon injury, the ECM modulates cell proliferation and migration, growth factor expression and remodeling. In spite of the fact that the ECM constitutes 50% of the volume of restenosis lesions, SMC proliferation and neointimal inflammation have been in the forefront of research into the development of IH (43).

In human coronary arteries that have undergone endovascular stenting, neointimal versican and HA stain strongly positive, co-localizing with smooth muscle actin (SMA) in SMC. In stents implanted for longer than 18 months, decorin has been reported to stain strongly. SMC density and restenosis is reduced in stents implanted for longer than 18 months. Scott et al. suggested that the later stages of in-stent restenosis are caused by enhanced ECM rather than by SMC proliferation (44).

The pattern of wound healing follows a path very similar to restenosis, which is a re-occurrence of intimal thickening following vascular intervention. Initially there is a thrombotic and acute inflammatory reaction, followed by a granulation phase, which involves macrophage infiltration, myofibroblast ingrowth and angiogenesis. An early ECM begins to form, composed of fibrin, fibronectin, HA and versican. HA provides the matrix for mesenchymal cells to migrate and promotes cell proliferation. It also supplies feedback regulation to growth factor synthesis. Versican binds to HA and creates viscoelasticity to healing tissues (45). HA then begins to degrade with reabsorbtion of a portion of collagen III, while synthesis of collagen I, decorin and biglycan takes place. This is followed by wound contraction and healing within two weeks. The response to a coronary stent in humans, does not show complete healing until 18 months after deployment (43). The importance of the ECM in the development of IH, is not clearly understood, however research in the past decade has unraveled the role played by the endothelial glycocalyx and its associated PG, and shown them to play a critical role in maintaining endothelial cell integrity and it's part in mechanotransduction. The PG in the ECM appear to play an important role in the control and development of IH (46).

1.2.3 The Endothelium

The endothelium is a single cell layer lining the entire vascular system, with a multitude of dynamic functions that impact on the behavior of the adjacent cells in the vessel wall. It is involved in vasoconstriction and dilation, thrombosis and fibrinolysis, inflammation and production of cytokines,

production and secretion of growth factors, and mechanotransduction by sensing changes in blood flow and shear stress. It is involved in the production of NO, essential to the proper functioning of the endothelium. EC are sensitive to the formation of ROS, which, in excess, can cause dysfunction of the EC (21). Disruption of the EC membrane by mechanical or biological damage, or endothelial dysfunction in CVD associated with diabetes or atherosclerosis, triggers a chain of inflammatory events in an attempt to promote healing (47).

1.2.4 Shear Stress and the Endothelium

Shear stress (SS) is the force that is exerted when the blood flow acts on the endothelial surface, and is frequently referred to as FSS or wall shear stress (WSS). The endothelial functions are mediated by blood flow, which acts via endothelial mechanotransduction (48). The mean WSS varies across species, between different arteries as well as along the arterial tree. In humans WSS varies between (0.3-1.3 Pa) compared to that in rats of between (5 and 10 Pa) (49). The glycocalyx is part of the mechanism of sensing and transducing shear stress (50), and it is of interest that the atherosclerotic prone regions have a reduced glycocalyx layer (51). Gouverneur et al. showed that shear stress actually stimulates endothelial glycocalyx production, which could explain the thinner EGL at arterial bifurcations exposed to low FSS (50), and therefore play a critical role in determining where vascular pathology originates (48).

High SS is beneficial in structural remodeling of the artery wall. It stimulates the release of NO, which is necessary for endothelial function. Davies et al have ascertained that endothelial mechanotransduction is unlikely to be the only mechanism of mechanotransduction (48). Normalizing SS at sites of vascular intervention would be a logical approach.

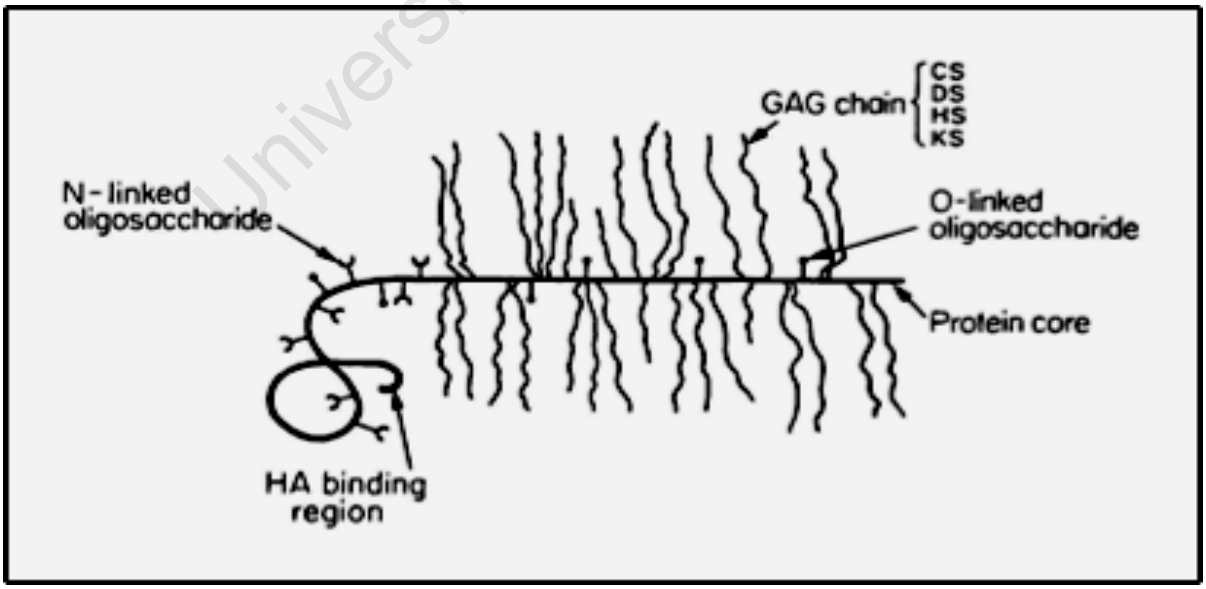

Figure 8 Schematic image of a PG monomer, consisting of a core protein and GAG side chains. (57)

Proteoglycans and IH play an integral role in vascular repair of the arterial wall following injury by PCI and have been shown to accumulate in atherosclerotic lesions. They have been targeted in many studies in attempts to reduce the formation of IH, and their distribution throughout the artery wall has

been well described (17, 52-54). PG are composed of a protein core with one or more glycosaminoglycan (GAG) side chains. There are five types of GAG chains, chondroitin sulfate (CS), heparan sulfate (HS), dermatan sulfate (DS), keratan sulfate (KS) and HA. HA is the exception of the GAG family in that it is not bound to a protein core (22). The basic structure of a PG can be seen below and variations in side chains give them their individual characters *(Fig-8)*.

The distribution of matrix PG is a determinant of intimal structure and patency in atherosclerosis and restenosis (55). Merrilees et al. compared the distribution of PG distribution in the intimas of coronary arteries (CA), saphenous veins (SV), internal ITA and radial arteries (RA). Results showed that the SV and CA were very similar in their PG profiles, with high levels of sub-endothelial versican and biglycan, but low levels of decorin. The ITA displayed high levels of decorin and this vessel gave better long-term patency. The radial artery, which is predicted to have better patency than the SV, has an even distribution of all three PG, versican, biglycan and decorin, does not the accumulate in the sub-endothelial layer. The differences in PG distribution in the intima, correlate strongly to established differences in patency between the SV and the ITA (55).

The IH region consists of ECM components including PG, elastin and collagen of which PG make up 80% of the IH within 3 months of injury. These components modify the biological functions of, and in the artery wall, such as viscoelasticity, lipid metabolism, permeability and thrombosis (56). The key PG are discussed below together with their importance and role in neointimal formation.

1.2.4.1 Perlecan

Perlecan is a PG that contains both HS and CS side chains. It is found in the basement membrane of several cell types and is critical for vascular repair and a regulator of homeostasis (53). Secreted by vascular smooth muscle cells (VSMC), perlecan is a potent inhibitor of SMC proliferation due to its capacity to bind FGF-2. As one of the prominent PG, perlecan is part of the regulation of IH and an absolute necessity to the prevention of occlusive thrombosis with its ability to bind to anti-thrombin III. The removal of perlecan has been shown to cause a decrease in the ability of EC to reduce intimal thickening. The HSPG are also involved in lipid metabolism, as lipoprotein-lipase interacts with EC in a HS dependent fashion as well as, possibly by modulating the charge density of the lipid as it passes through the EC barrier (53). In the rat model, there is a 2-fold increase in perlecan transcription within 2-4 weeks of balloon injury (40).

1.2.4.2 Versican

Versican is composed of CSPG. The synthesis and secretion of CS is carried out by SMC, and it is a major arterial PG (56). The prominence of CS containing versican in primary, restenotic and atherosclerotic lesions is evidence of its importance as a matrix PG. It accumulates in intimal lesions where it is involved in trapping of LDL (40). The proliferation and migration of SMC is facilitated in the ECM by sub-endothelial versican and HA (55).

1.2.4.3 Biglycan

Biglycan, composed of DSPG and CSPG, is one of the three matrix PG (together with versican and decorin) that are important determinants of the vessel wall structure and pathology. They are small leucine rich PG associated with restenotic lesions (55). Biglycan is found in the intimal and medial regions of such lesions and is present after 9 months to 18 months following stenting (43). Its function is not yet well understood.

1.2.4.4 Decorin

Decorin is a small collagen-associated PG made up of CS and DS, both synthesized primarily by SMC (56). It presents in a more fibrous intima or fibrous caps of atherosclerosis. It has been found in the intima of the ITA and the RA correlating to improved patency following artery grafting, and could have a protective role against the build up of IH (55).

1.2.4.5 Hyaluronan

Hyaluronan, also referred to as HA, is the exception of the PG, as it does not contain a protein core and it is non-sulfated. It is strongly demonstrated in vessels with vascular disease and only weakly in normal vessels (57). HA forms the basis of the pericellular matrix, and is anchored to the cell surface by the CD44 receptor *(Fig-9)*. PG attach themselves to the HA structure thereby increasing its stiffness. It is substantially reduced in atherosclerotic lesions of diabetics, while in non-atherosclerosed arteries it is increased. SC and DS in contrast are increased in diabetics. This suggests a different pathological process in the macro vascular disease in diabetes to that of atherosclerosis (58). HA is involved in cell adhesion, proliferation and migration and possibly in inflammatory processes (3).

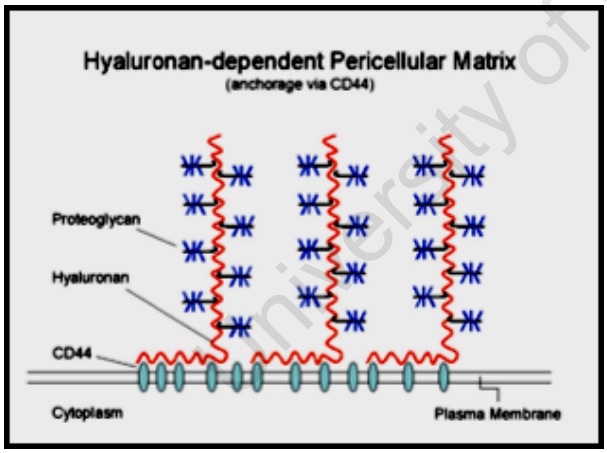

Figure 9 Hyaluronan chains attached to the cell surface via CD 44 & associated proteoglycans. (3)

Versican & HA are present in high amounts in the restenotic arterial tissue after balloon injury, and their synthesis is modulated by growth factors PDFG and TGF-beta (57). This combination of PG and collagen matrix enables tissue to resist shear deformation (3). The matrix into which mesenchymal cells migrate is provided by HA, which promotes proliferation and supplies feed back regulation of growth factors. It is still present after 18 months following stent deployment (59).

The Endothelial Glycocalyx and Intimal Hyperplasia

The entire vascular endothelial surface is lined with a fine, carbohydrate-rich layer, approximately 20 nm-5 µm in thickness, made up of PG and glycoproteins, the EGL. GAG side chains are covalently attached to a core protein *(Fig-10)*. The PG are said to be the "backbone", connecting the glycocalyx to the endothelium (22). Although, first discovered some 40 years ago by Luft, with the use of electron

microscopy, its composition and function still remain unclear. Much research has been done in the last 10 years, as its importance in vascular pathology has become appreciated (22). As a major component of vascular tissue, PG are involved in lipid metabolism, vascular permeability, homeostasis and thrombosis. Wight et al. stated that "the accumulation of PG in intimal lesions is a hallmark of early and late atherosclerosis" (60). The glycocalyx thus forms an integral part of the vasculature and the loss or reduction of this delicate structure must have detrimental effects on the functions of the endothelium. PG are synthesized by both EC and SMC, and play an important role in migration, adhesion, and proliferation of SMC.

The polyanionic nature of the components of the gylcocalyx, result in a net negatively surface charge. HS, CS and DS are amongst these PG, as well as HA. HS comprises 50-90% of the EGL in the vasculature, and contains anti-coagulative species thus preventing thrombus formation (60, 61). The three main protein core families of HSPG found on EC are transmembrane syndecans, membrane bound glypicans and basement matrix associated perlecans (61). In addition to glycoproteins & PG soluble proteins, originating from the bloodstream or the endothelium, may give added stability to the mesh like glycocalyx, particularly HA. It is known that the glycocalyx layer is very delicate and its properties are affected by enzymatic removal of any components (22).

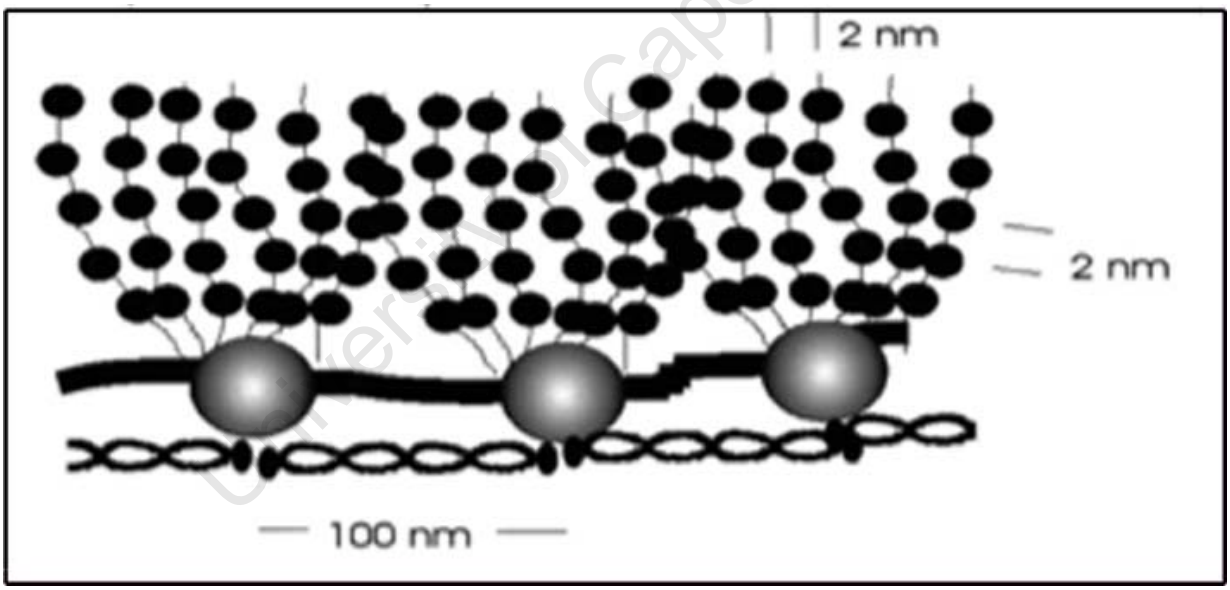

Figure 10 Schematic representation of the Glycocalyx Structure, consisting of a core protein with GAG side chains attached (64).

Van den Berg et al. suggested that damage to the glycocalyx layer played an important role in atherosclerosis and demonstrated that the carotid arteries in mice, which are prone to atherosclerosis, have a reduced glycocalyx, and therefore a disturbed flow pattern (51). Noble et al hypothesize that the disruption of the glycocalyx is the first step prior to atherothrombotic disease (32) and suggest that disturbed blood flow manifests itself as "shear stress", first detected by the glycocalyx which then signals the underlying endothelial cells to release NO, an anti-atherogenic factor. They further

proposed that the damage to the lumenal area results in changes such as exposure of the EC to thrombus and inflammation, leading to atheroma.

In a study by Yao et al. on the effect of SS on the endothelium, it was shown that the glycocalyx was necessary for the alignment of SMC and their response to SS. It is known that after 24 hrs of laminar flow, EC will align in the direction of flow with reduced proliferation. In this study, the removal of HS GAG from the cell surface using the enzyme heparinase III, revealed that EC were unable to align under laminar flow conditions and proliferated as if there was no flow present. It was demonstrated that HSPG establish themselves in a peripheral pattern and accumulate above cell-cell junctions, which could reduce the shear gradient that cells undergo during conditions of flow (54).

The Starling principle can be described as the balance of hydraulic and colloidal osmotic forces across the capillary wall. Hydraulic conductivity is a measure of the ease with which water flows through a micro-vessel wall (62). The fluid exchange across micro-vessels is driven by the plasma protein concentration gradient between the lumen and the tissues. The Starling Principle, which was challenged in 1996 and subsequently Michel & Weinbaum et al. proposed that the osmotic barrier was not represented by the whole capillary wall, but in fact the endothelial glycocalyx which acts as a sieve for molecular proteins (61).

The past ten years of research in this field have revealed the important role the EGL plays in this interaction and its function as a primary mechanotransducer to FSS, its interactions with white blood cells (WBC) and red blood cells (RBC) as well as its response to physical disruption have been described (61).

Nieuwdorp et al. showed that loss of the glycocalyx coincides with acute hyperglycemia in patients with diabetes mellitus, who already have a propensity for increased vascular episodes (21). The resulting disturbance of flow is accompanied by activation of the coagulation system leading to a build-up of thrombosis. In their experiments, hyperglycemic clamping resulted in reduction of glycocalyx volume and increased plasma levels of glycocalyx components such as HA. With the addition of N-acytylcysteine (NAC), an anti-oxidant, the disruption of the glycocalyx could be prevented. This suggests that ROS contributes to glycocalyx damage in the presence of excess blood sugar. Nieuwdorp also suggested that HS is vital to NO signaling and the decrease of HS resulted in loss of the EC super oxide dismutase (SOD) enzyme that catalyses ROS to oxygen, noting the important role of the EGL in removing free radicals from the blood stream. Perrin et al.

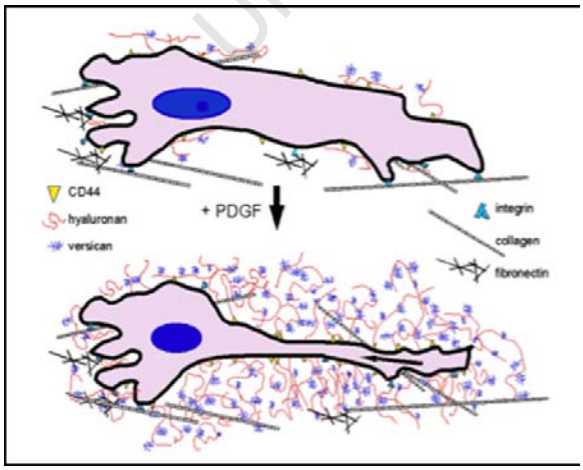

Figure 11 Stimulation of SMC with PDGF induces shape change and elevated HA and versican PG (3)

did an extensive study in 2007 on the effect of excess glucose on hydraulic conductivity and the reflection coefficient as well as on compliance. They conclude that the increase in blood glucose alone caused an increased micro-vessel permeability in the rat and frog and suggest that understanding the mechanisms of this micro-vascular permeability to water may be a target for therapeutic intervention in diabetic vascular disease (62).

The proliferation of cells within the intimal area comprises a collection of SMC, fibroblasts, myofibroblasts as well as collagen and PG, together with cytokines, immunoglobulins and other factors.

Endothelial injury is implicated in every aspect of atherosclerosis. It is involved in vasoconstriction and vasodilatation, controlling blood pressure, thrombosis and fibrinolysis with secretion of Von Willebrand Factor (VWF), NO, thrombomodulin and prostacyclin, inflammation and edema, in its production of IL-1, IL-6 and IL-8. The endothelium also produces basic fibroblast growth factor (BFGF) and FGF as well as PG, HS, CS and DS. It is involved in filtering functions such as the blood/brain barrier and controls transit of white WBC in and out of the bloodstream (61).

Loss of the endothelium is the hallmark of vascular disease, while damage to the endothelium, results in platelet accumulation, and fibrin deposition, leading also eventually to the development of IH. PG have been implicated in the formation of IH (53, 55, 63), as well as in association with atherosclerosis and the formation of plaque build-up within the artery (61, 64). Perlecan, is an especially important EC derived regulator of vascular homeostasis. It has been found to be a regulator of NIH and thrombosis and critical for vascular repair, following vascular intervention (53). HA and versican play an important role following balloon injury, as they are present in increased amounts in the vascular wall, surrounding the proliferating SMC. Evanko et al. showed that stimulation of SMC with PDGF resulted in an increase in the pericelluar matrix particularly HA and versican (3) *(Fig-11)*.

Fischer & Wight et al. showed that the administration of bovine decorin at the site of balloon injury reduced SMC proliferation with the use of cell mediated gene transfer. Results showed a 35% reduction of NIH over 4 weeks, following cell-mediated transfer of bovine decorin, compared to untreated balloon injured tissue. They conclude that over expression of decorin to the injured area causes reduced ECM volume and changes to ECM composition (63). Nigro et al. found that modification of PG by shortening of the length of GAG chains caused less binding to LDL. Few studies have investigated the targeting of GAG chain composition through pharmacological drugs, and they suggest that this may be a step to decreasing atherosclerosis and CVD in diabetic patients (17).

EC secrete and synthesize collagen IV and V, PDGF, vascular endothelial growth factor (VEGF), inflammatory cytokines together with PG. Research has better elucidated the role of the glycocalyx in the build up to atherosclerotic lesions and the effect of flow mediated shear stress on the endothelium, and therefore the EC role in mechanotransduction (65, 66).

Understanding the role of the glycocalyx has been limited due to poor visualization techniques. Currently it is only visible histologically through the use of transmission electron microscopy (TEM) following perfusion fixation and staining of the vessel wall (67). In-vivo techniques using fluorescent tracers have been successful in evaluating the thickness within a vessel though.

Restenosis can be defined as the re-narrowing of dilated lesions following PCI. This process is complex and only partially understood, but is initiated by balloon angioplasty or stent implantation, as treatments for CVD. Acute vessel wall injury results in the denudation of the endothelium from the intimal surface, followed by platelet adhesion and monocyte recruitment. The first response is of an inflammatory nature, followed by the proliferation and migration of SMC into the intimal region (68). This IH layer is a major limiting factor of balloon angioplasty and stent deployment.

PCI by balloon angioplasty, was first introduced in 1977 by Andes Gruntzig, as treatment for restenosis in coronary artery disease (69). The limitations of this procedure became clear with a high restenosis rate due to elastic recoil and negative remodeling, while intimal thickening occurred secondary to smooth muscle cell proliferation and migration (70). Today, twice the amount of PCI procedures are performed compared to coronary bypass surgery. Restenosis occurs in 20-50% of patients after balloon angioplasty and in 10-30% of those receiving a stent, but this prevalence is increased in patients with diabetes. Drug eluting stents (DES) have exhibited a high potential for reducing restenosis, but recently presented with the risk of late thrombosis and a stroke.

Rabbits, porcine and non-human primate models show a strong inflammatory response, in comparison to human studies that show acute, long lasting inflammation of stented arteries especially when medial injury or lipid core penetration occurs (71). Renu Virmani et al. confirmed in a review article in 2007 that in humans, peak neointimal thickness occurs between 6 months to 1 year with 22% regression of neointimal growth after a year. Healing after bare metal stent (BMS) placement in the human coronary artery take five to six times longer than in porcine or rabbit models. This finding is critical when evaluating the healing pattern of DES, while this could be explained by the fact that there is an atherosclerotic process presenting in the fifth to sixth decade of life, compared to research carried out on younger, adult animals where stents are placed into normal arteries without an existing inflammatory process (42). The molecular mechanisms and patho-physiology of restenosis is incompletely understood, but extensive research on several animal models continues, in an effort to establish safety and efficacy of vascular devices and therapeutic pharmacology. Despite their limitations, animal data goes a long way to developing a better understanding of the complex morphological changes induced by PCI and response to treatment.

1.3 Therapy

The use of PCI has provided a feasible alternative to CABG for the treatment of coronary artery disease, however the need for reintervention due to restenosis remains (72). A multifaceted approach to the treatment of CVD and restenosis is necessary.

Table 5 Possibilities for the development of therapeutic drug prevention. Research for most of these conditions is performed in animal models.

Clinical Condition	Treatment
Hypertension, Hypercholesterolemia, Obesity	Statins and Fibrates
SMC proliferation and development of IH	Anti-proliferative drugs
Thrombus formation	Anti-coagulative drugs

1.3.1 Percutaneous Coronary Intervention (PCI)

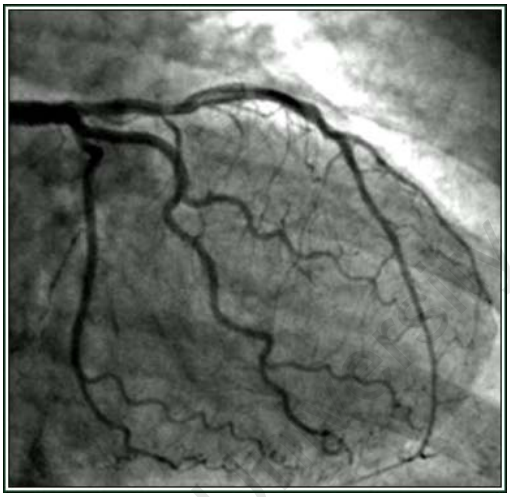

Figure 12 Angiogram indicating the coronary arteries

The procedure for dilating narrowed coronary arteries is known as coronary angioplasty or PCI. This is carried out by a cardiologist, and has revolutionized the method of treatment for coronary stenosis, previously requiring open chest coronary artery bypass graft (CABG). Angioplasty is facilitated by injection of a radio-opaque contrast agent, during X-ray, to visualize the stenosed area throughout the procedure.

Balloon angioplasty involves positioning of balloon catheter into the coronary artery via the femoral artery through an incision in the groin. It is positioned before being fully expanded with water pressure, followed by deflation of the balloon and withdrawal of the catheter.

1.3.2Coronary Artery Bypass Grafting (CABG)

The surgical procedure of CABG involves open-heart surgery with or without extracorporeal circulation to allow work on the non-beating heart *(Fig-12)*. Diseased coronary arteries are bypassed with veins or arteries from elsewhere in the body, which are sutured into position. In some instances, synthetic expanded polytetrafluoroethylene (ePTFE) vascular grafts may be used.

1.3.3 Statins

Statins are LDL lowering drugs. They also have a vascular protective role due to their ability to decrease oxidative stress. They reduce proliferation and migration of SMC and also lower plasma cholesterol levels. Together with a decrease in oxidative stress, there is an increase in NO availability and therefore improvement in endothelial function (16). In support of this, Schaefer et al. described a study in which statins block EC proliferation due to hypoxia by preventing ROS and calcium formation in response to oxidative stress (73).

1.3.4 Fibrates

Peroxisome proliferators activated receptor (PPAR-y) agonists, like Fenofibrate, bind to a family of nuclear receptor comprising three sub-types, α, δ and γ. Fibrates are primarily involved in lipid metabolism but also have many effects on the vasculature. PPAR agonists are expressed in all the major cells in the vessel wall, EC, SMC, and macrophages. They are known to reduce LDL and TG, increase HDL and VLDL, as well as have beneficial effects on insulin resistance (39). PPAR-γ appears to be the "good guy" in the vessel wall, as it is known to reduce inflammation (74). They are also able to detect fatty acids and mediate glucose and lipid metabolism thereby making them ideal treatments for MS and DM (75).

The FIELD study (Fenofibrate Intervention & Event Lowering in Diabetes) found a decrease in cardiac events but no improvement to individuals who already had atherosclerosis. Zhao et al. showed that the anti-inflammatory Thiazolidinediones, which bind to PPARs and inhibit TNF-α, IL-6 and IL-1, as well as reduce blood glucose levels, are mediated through nuclear kappa B ($NF\text{-}_k ß$) pathways (76). The effects of PPAR-α and γ were tested by Desouza et al. and found that PPAR-γ reduced IH in rats, but not PPAR-α (77).

Dietary supplementation with fish oils, which are natural agonists of PPAR, has been shown to be beneficial in the rat model by restoring adiponectin levels and PPAR-α expression in the liver and visceral fat. (78).

1.3.5 Drug Elutin gStents

The use of DES, affords us a combination of mechanical and biological strategies to combat the effects of angioplasty or vascular stenting procedures. The most commonly used anti-mitotic drugs for stent-coatings, include Sirolimus (also known as Rapamycin) and Paclitaxel.

Rapamycin is an antibiotic as well as a natural fungal fermentation product from Streptomyces hygroscopicus, originally found on Easter Island (Rapa Nui Island). It has potent anti-inflammatory and immunosuppressant properties. The RAVEL and SIRIUS trials confirmed the reduction of IH in humans using sirolimus-eluting stents (79). Paclitaxel is an anti-neoplastic agent, commonly used for anti cancer treatment. Kolodgie et al. showed inhibition of proliferation and migration of cultured VSMC reduction in restenosis in in-vivo studies (80). The FDA has conducted several human drug

trials to establish these drugs as pharmacological treatments and which have received approval. DES were initially considered the answer to restenosis, however thrombosis related cardiac events have led to controversial opinions relating to the benefit of DES over BMS (81). Long-term follow-up of DES and BMS interestingly show no difference in mortality rate (82).

More recently coating of stents with glycocalyx components has been introduced. Synthetic glycocalyx is covalently bonded onto the stent surface, which promotes the healing process through its biocompatible, anti-thrombogenic nature. These stents are made in Germany by Eucatech, and have highly polished metal surfaces. They are registered under the trade name "Camoflage", and the coating is composed of N-and O-desulfated, N-reacetyl, which is a modified heparin. This coating prevents platelet deposition on the inner-stent surface and reduces the release of growth factors and cytokines in the injured area (83).

1.3.6 Brachytherapy

Brachytherapy is a form of radiation using a radioactive source, which is placed close to the target area. It is currently one of the most successful forms of treatment for restenosis, but not the most economical. It has been shown to decrease angiographic and clinical restenosis in new disease and in stent restenosis (ISR). The SCRIPPS study (Schripps Coronary Radiation to Inhibit Proliferation Post Stenting), showed encouraging results of intravascular radiation for treatment of restenosis. This has been confirmed by the WRIST study (Washington Radiation for IN Stent Restenosis Trial), as well as by the ARTISTIC (Angiorad Radiation Technology for In Stent Restenosis Trial in Native Coronaries). Overall it has been shown that there is a 10% decrease in restenosis with the use of brachytherapy (81)

1.3.7 High Speed Rotational Atherectomy (rotablation)

Mechanical debulking or rotablation prior to PCI should minimize IH compared with percutaneous translumenal coronary angioplasty (PTCI) alone, however these results are debatable.

1.3.8 Incretins

Incretins are gut hormones that control insulin release after meals even prior to blood glucose elevation, for example Glucagon-like peptide (GLP-1). Exenatide is an example of a synthetic analogue to GLP-1, known as an incretin mimic. GLP-1 can be inactivated by agonists like the enzyme Dipeptydal pepsidase (DDP-4), however not much is known regarding the effect of either DDP-4 inhibitors or incretin mimics on IH following PCI. Diabetic patients on exenatide show improved glycemic control but incretins need to be administered continuously by i.m injection. (39).

1.4 Hypothesis

The following hypotheses are proposed:

- The effect of obesity has a significant impact on the pathology in the neointima, more specifically to the development of IH following balloon angioplasty and vascular stenting in lean, obese and pre-diabetic rats.
- The pro-inflammatory nature of obesity results in an increased inflammatory response and this may contribute to increased stenosis following PCI.
- The impact of vascular stenting has the potential for decreased IH and that the inflammatory response to injury together with the response to foreign material within the vessel, may increase the rate of IH in lean, obese and diabetic animals.

Chapter 2
Intimal Hyperplasia in Animal Models

2.1 Histological Variations of Vascular Arteries in Different Species

Animal models have been successfully used for the investigation into the effects of balloon angioplasty and stenting, primarily rodent, porcine, canine and primate models (71, 84-90).

These studies have proved invaluable to understanding the mechanisms and pathology of artery disease and restenosis. There is, however, a wide diversity of pathophysiology observed in the various animal models used in the investigation of type II diabetes, as well as in their individual histopathology.

Rabbit models though have frequently been used for understanding restenosis therapies and show stenosis similar to that of humans. Anti-platelet drugs were also shown to reduce IH in this model (87).

Bergman et al. (90) performed a canine study in 2007, describing the role of obesity in cardiovascular risk and in the pathophysiology of MS. Their results support the idea that FFA in visceral fat enters the liver where they have detrimental effects on insulin resistance. They suggested that excess FFA are released due to SNS hyperactivity in obesity, together with the compounding effects of insulin resistance and hypertension, also associated with obesity. The fact that dogs have a significantly different coagulation system from humans together with the fact that they produce a very thin neoinitma, however, makes them a poor model for restenosis (71).

The mouse model is not necessarily a practical one due to the size of the animal, wound healing has been shown to be similar to that of other models, allowing us a better understanding of SMC proliferation and migration and vascular remodeling. The availability of transgenic and knockout mouse strains also hold much promise in elucidating molecular mechanisms associated with the hyperplastic response as well as in determining the contributions of the immune and inflammatory host response.

Pasa et al. conducted a study on porcine carotid arteries, due to the fact that porcine arteries are similar in size and anatomical structure as those of humans. They also noted that pigs raised in pastures developed atherosclerotic lesions only after 4-8 years in comparison to those fed on cholesterol rich diets, where the changes were seen to be more rapid. In their evaluation of stented and non-stented (balloon injury only) arteries, they demonstrated significant IH in the latter, suggesting that balloon injury alone was capable of exerting sufficient damage to stimulate intimal cell proliferation (88). Spurlock et al. similarly found the pig to be an exceptional restenosis model, with particular regard to the involvement of adipose tissue and adipokines in obesity and MS (85). The porcine model also exhibits the greatest similarity of neointimal response to humans, with a thick neointima occurring 28

days after injury. The degree of IH in the porcine model has also been shown to be proportional to the extent of medial damage and IEL rupture (87).

In the 1960's the rat carotid artery was established as model for the study of balloon angioplasty, and has laid the foundations for an understanding of vascular biology (87, 91, 92). The Zucker rat has been previously described as the ideal model for the study of the effects of balloon angioplasty and stenting using the carotid artery (93-95).

Finn et al. established the Wistar rat model for the deployment of stents into the carotid artery, which was previously thought to be too small, but highlighted the need for validating the findings of this model into larger animals and humans (89).

The rat model nevertheless offers several areas of study including toxicity, as in DES and margin of safety (84). Other parameters include histopathology with assessment of inflammation, incomplete endothelialization, adverse effects of drug delivery, molecular biology, medial necrosis, intimal fibrin, thrombus formation and PG all of which, cannot be determined by IVUS (intravascular ultrasonography) in humans (86, 87), but have been reported in other animal models such as canine, porcine and non-human primate models (90, 96, 97).

Table 6 Characteristics of rodent models used for the study of vascular injury (38)

Rodent models of type 2 diabetes commonly used to study vascular injury.

Model	Hyper triglyceridemia	Hyperglycemia	Hyper-lipidemia	Hyper insulinemia	Obesity	Insulin resistance	Nephropathy	Leptin	Clinical diabetes	Islet β cells
Rat										
OLETF[a]	+	Late onset[b]	+	+	Mild[c]	+	+	–	Chronic course	3 stages: a. Inflammatory b. Hyperplastic c. Atrophic
ZF[d]	+	Early chronic progressive	+	Early but fails[e]	+	+	+	+	+	Late nonfunctional
Goto–Kakizaki[f]	-	Early	+	–	Early	+	–	Mild		Decreased cell mass
Mouse										
db/db[g]	+	+	+	+	Progres-sive	+	+	+		Necrosis
ob/ob[g]	+	+	+	+	+	+	–	+		Necrosis

Note: OLETF, Otsuka Long Evans Tokushima fatty; ZF, Zucker fatty; *db*, diabetes and *ob*, obese gene mutations; GLUT4, insulin-regulated glucose transporter.

[a]Cholecystokinin A gene deficient.
[b]Distribution of GLUT4 similar to human diabetes.
[c]Reduced ability to attain satiety.
[d]Reduced GLUT4
[e]Reported to be mediated by NO.
[f]An initial or late phase retinopathy model.
[g]Decreased neuropeptide Y.

The interpolation of results from animal studies should of course be carefully undertaken. Several factors need to be considered, namely the nature and extent of injury, the state of the arteries being injured (non-diseased), the healing response and the variations in the pathology as well as mechanisms of each animal model, the variations in inflammatory response etc (98).

Virmani et al. described changes in the vascular healing patterns between human and animal studies, and demonstrated that the time course of healing was more prolonged in human clinical studies. In addition, long-term data on animal studies is rare, with most implants extending to only 21-28 days. Animal studies are nevertheless critical for the understanding of safety factors of PCI devices, and for the cellular response of arteries in response to injury (42).

2.2 The Zucker Rat – Model of Choice

The Zucker rat model is well established as a model for the study of balloon injury and stenting (89, 99). The strain was developed in the 1980's at Indiana University. Following incorporation of a colony from Eli Lilly, the strain was then licensed to Genetic Models Inc. in 1991. Ten years later they were transferred to Charles River Laboratories (100, 101). The obese rat model offers an opportunity for improved understanding of the pathophysiology associated with IH and the impact thereon of obesity and MS.

The rat circulatory system is almost identical to that of humans *(Fig-14)*, but there is substantial variation between data obtained from different species and direct extrapolation of findings into therapeutic options for patients must be done with caution.

The Zucker rat has the advantage of three separate phenotypes, allowing for the determination of the neointimal response to balloon angioplasty relative to obesity and diabetes as risk factors *(Fig 13)*. The Zucker diabetic fat (ZDF) rat is a useful model for the study of type II diabetes, with the male rat often becoming spontaneously hyperglycemic, and the female while fed on a recommended high fat diet (Purina 5008) (100, 101). ZDF rats display progressive glucose intolerance and hyperinsulinemia and like humans, also develop hyperglycemia, hyperlipidemia, nephropathy, impaired wound healing and cardiovascular disorders (102). The female Zucker rat is hyperinsulinemic, insulin resistant, normoglycemic and non-diabetic, but when fed on a high fat diet, Purina (C13004) containing high levels of pork fat) converts to a state of frank diabetes. The lean Zucker rat (ZFR-L) has normal metabolic parameters and serves as a useful control (91). A significant difference between male and female ZDF rats is that females become glucose intolerant after a longer period of time, and this can be useful when testing drugs that depend on the ability to produce insulin (100, 101)

In contrast to human arteries, there is no vasa vasorum in the rat carotid and it contains a substantially thinner sub-intimal layer with less elastin content (103). The homozygous Zucker rat has a deficient leptin receptor in the brain, preventing post-prandial satiety. The mutation of the leptin receptor is frequently referred to as [Lepr^{fa} (fa)]. The homozygous form of the Zucker fatty rat (ZFR-F) Lepr^{fa} (fa) results in hyperphagia, leading to morbid obesity and IR. Leptin is a small molecule that binds to receptors in the hypothalamus, signaling a feeling of satiety. In addition, the Zucker rat has an impaired mechanism of insulin release in response to glucose, resulting in hyperinsulinemia. (104)The Zucker rat model has been used in many diabetic studies in spite of the leptin receptor defect [Lepr^{fa} (fa)].

GENOTYPE	PHENOTYPE	
	Obese/Lean	Diabetic
ZFR$^{fa/fa}$	Obese	No
ZFR$^{fa/fa}$ ZFR$^{fa/fa}$	lean	No
ZDF$^{fa/fa}$	Obese	Male-yes Female-(yes if fed high fat diet)
ZDF$^{fa/fa}$ ZDF$^{fa/fa}$	Lean	No

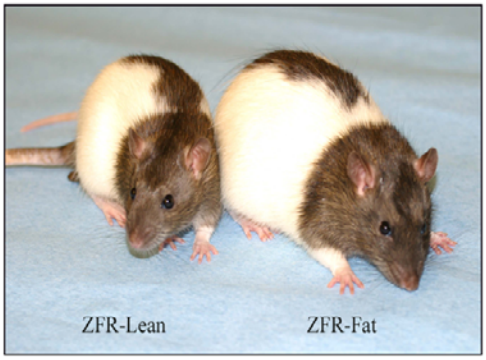

Figure 14 Zucker rat genotypes and phenotypes.

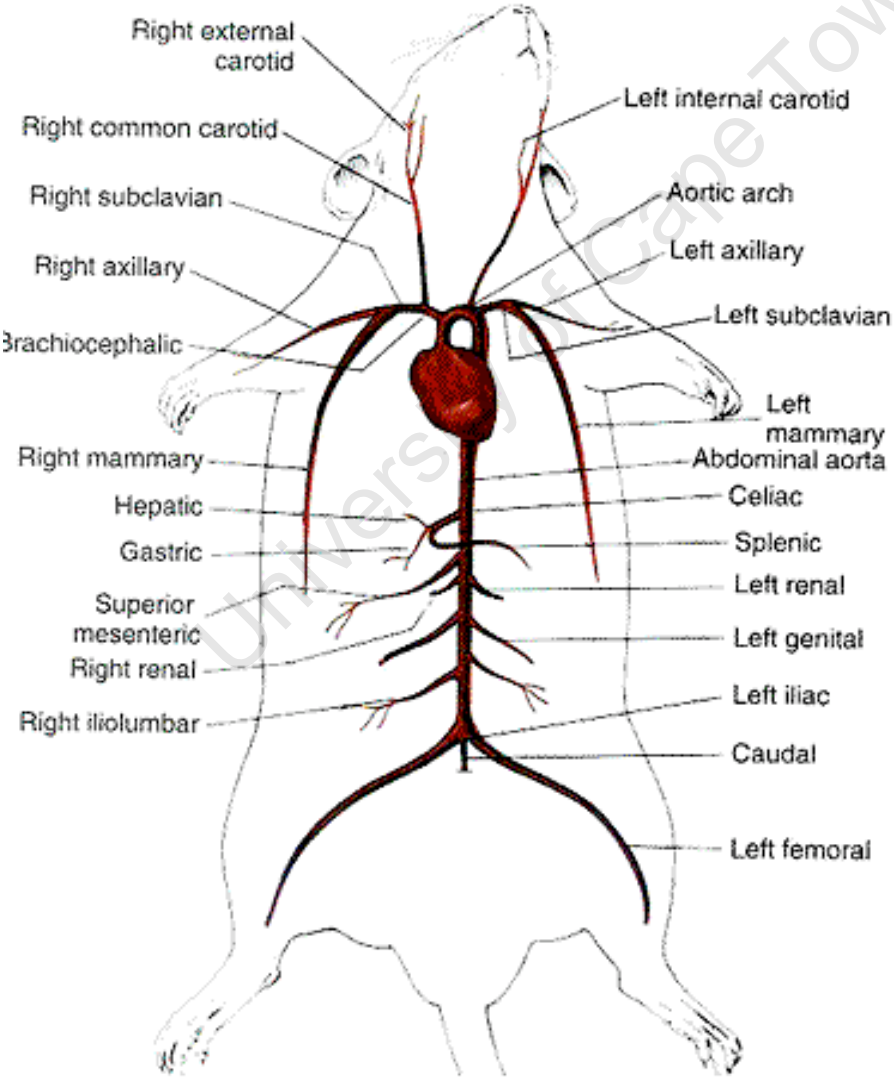

Figure 15 The Schematic Vasculature of the Rat (104)

2.2.1 Anatomical Comparisons of Carotid Ateries of different species

The structure of arteries varies significantly in their morphological composition and more notably their elastin content both within a species and from one species to another. Response to injury, as studied in many models also varies considerably. In a comparison by Frank Sims (18) in 1989, the intima of human arteries was seen to differ from those of animal models, since they developed intimal thickening from a young age. Human coronary arteries with substantial intimal thickening had an incomplete endothelium, whereas animal models showed EC closely associated with the IEL. In contrast to human arteries, the IEL of animal vessels was observed to be capable of repair.

In a study by Gabeler et al. the response to injury in three different rat arteries, namely the common carotid artery (CCA), the iliac artery (CIA) and the abdominal aorta (AA) were compared. Results showed that the decrease in lumen diameter was higher in the CCA and CIA compared to that of the AA. Possible explanations for this are the healing response of different arteries, the elastic composition, the vessel diameter and the absence of a vasa vasorum in the tunica adventitia of CCA (103). Porcine, rabbit and human arteries all have vasa vasorum in the tunica adventitia, and Gabeler et al. suggest that the CIA and AA in the rat perhaps more closely represent the response in larger animal models than does the CCA.

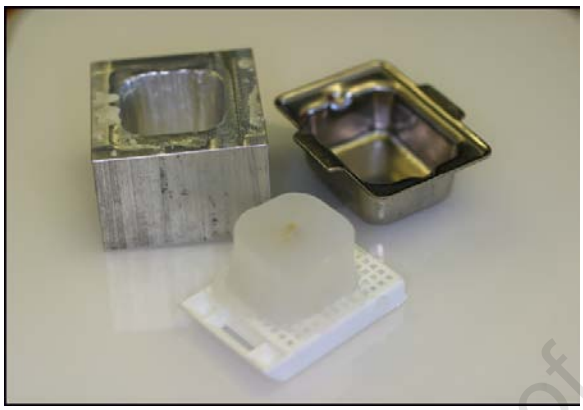

Figure 16 The modified, deeper embedding cassette used for embedding longer arteries and the Zucker Rats.

To compare the physiological differences between various arteries, we excised and analyzed the histology of the carotid, femoral, axillary and mammary arteries of a Zucker rat

2.2.2 Materials And Methods

For the analysis of arterial structure, a ZFR-L rat was anaesthetized with ketamine/xylazine and perfusion fixed using 4% PFA in phosphate buffered saline (PBS) following an antegrade heparin PBS pre-flush. The four arteries to be studied were located using a stereomicroscope (Nikon-SMZ 800) and excised and stored in 4% PFA overnight at room temperature. Existing baboon and procine artery control samples were used as comparisons. Samples were dehydrated through graded alcohol solutions into xylene and paraffin wax using a Tissue-Tek II tissue processor (see Appendix for methodology). Standard embedding procedures were used, except that, due to the length of the samples, a deeper embedding cassette was required *(Fig 16)*. This was hand made in our laboratory from Aluminum, making it possible to embed a section of approximately 20mm long in one block.

Sections (3µm) were cut on a rotary microtome (Microm HM 360) and mounted on slides and stained. To assess the physiological consistency through the length of the vessel, sections were taken at 280µm

intervals and stained with an Elastic Masons trichrome to differentiate between collagen, muscle fibres and elastin *(Appendix-A-5)*. The Zucker rat common CCA, axillary, mammary, and femoral arteries were analyzed. In addition stock porcine and baboon coronary and carotid arteries, were analyzed, for comparison of morphological structures.

Images were captured on a Nikon 90i microscope. In order to view the complete cross-section of a vessel in a single frame, images taken at 10x magnification were automatically aligned and tiled into one single composite image. These images were analyzed to compare differences in morphology between the various arteries, as well as between different species.

2.3 Results

There was considerable variation between the species studied. The most characteristic differences of these various arteries was their elastin content as well as the extent of the medial/muscular layer, which varied not only within the rat but from one species to another.

The rat carotid has 3-5 solid bands of elastin interrupted by layers of smooth muscle cells. The baboon carotid presented with several finer layers of elastin in a significantly thicker arterial wall, while the porcine carotid artery was seen to have a dense muscular wall containing fine strands of elastin at irregular intervals and a solid, undulated internal elastic lamina *(Fig 17)*.

The mammary and axillary arteries of the Zucker rat had a similar morphology with a dense internal elastic lamina and a deep band of SMC with intermittent elastic layers surrounded by a collagen-rich ECM *(Fig 18)*.

The femoral artery resembled the carotid artery, with a thinner wall containing 3-4 thick elastin bands with smooth muscle between them. There was very little variation throughout the length of each artery.

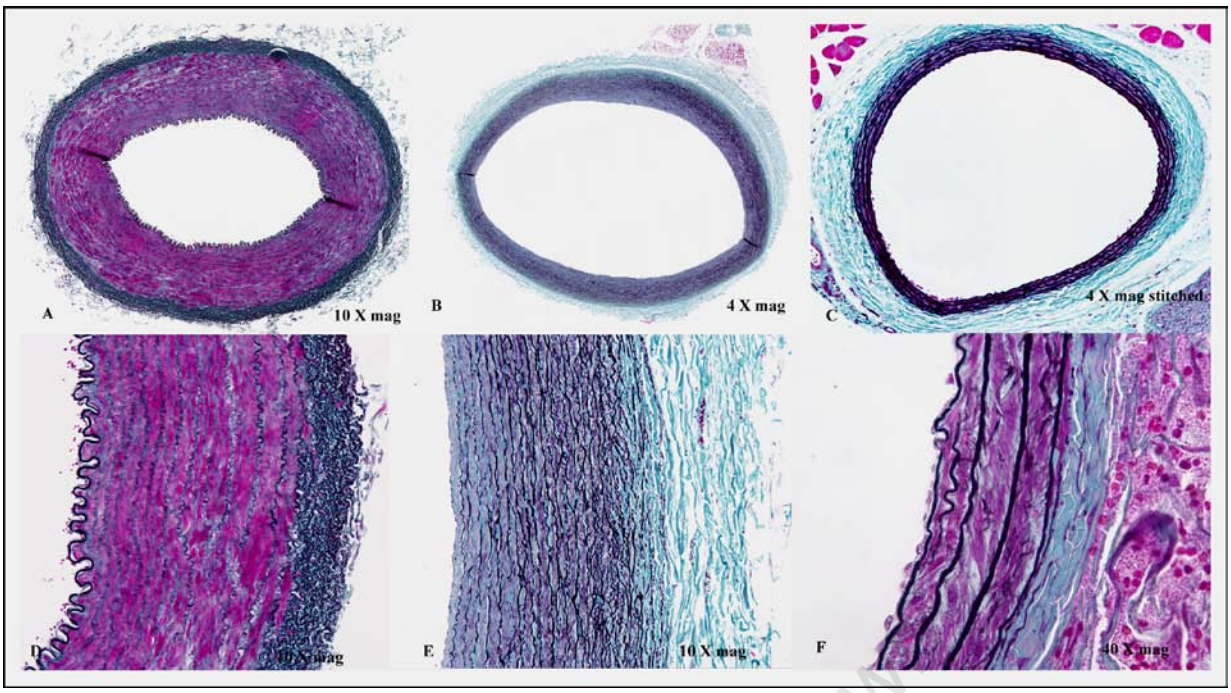

Figure 17 Morphological variations between (A) porcine, (B) baboon and (C) rat carotid arteries, together with high magnification images D, E and F, stained with elastic Masson's trichrome

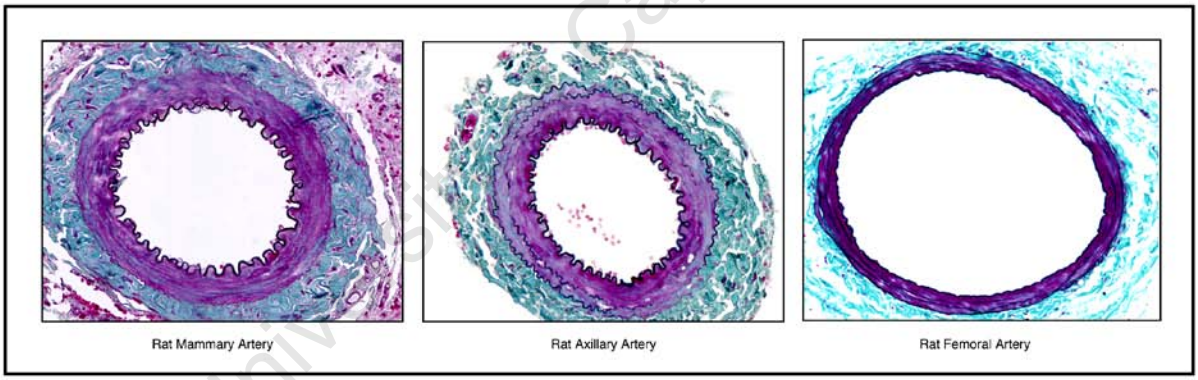

Figure 18 Morphological variations between rat mammary, rat axillary and rat femoral arteries, stained with elastic Masson's stain

2.4 Discussion

It has been suggested that the well-formed IEL, closely associated to EC found in the human mammary artery, is not susceptible to intimal thickening or atherosclerosis (18). Sims suggested that this combination of IEL closely linked to EC forms a barrier or anchorage onto which endothelial cells can attach themselves. Coronary artery thickening which occurs in humans from a young age, most likely is not found in non-human primates due to the 'near perfect' arrangement of well-formed IEL in close contact with EC. The authors concluded that arterial wall structure in different species might account for the variations in coronary artery disease that is observed between humans and animal models. This is reinforced by the higher success rates seen with mammary (internal thoracic) arteries used as vein grafts compared to SV, both with regard to patency (80-90%) and neointimal formation (105).

The rat model offers a fair degree of IH in response to balloon injury as well as stenting, however it is not the most suitable model of inflammation, with maximal macrophage staining being seen at around 7 days. It does offer the evaluation of the temporal response to small vessel injury with particular regard to IH, SMC proliferation and migration, and formation of ECM components. The Wistar rat model, was established by Aloke Finn et al. in 2002 as a novel model for carotid artery stenting, and had a very similar time course of healing after stent deployment to that of porcine coronary and rabbit iliac arteries in spite of differences in elastic and muscular arteries as well as vessel size (89).

Si Hoon Park et al. conducted a balloon injury study on Zucker male rats in comparison with streptozotocin-induced diabetes in Sprague-Dawley rats, and found the Zucker model to be an appropriate insulin resistant model with a propensity for NIH (94).

While porcine and non-human primate models are the closest to human morphology, they are more difficult to handle and expensive to work with and not always available. These models do not offer the option of acquired or heritable metabolic disorders, such as DM and systemic hypertension. In contrast the rat provided a model of obese and/or diabetic with the advantage of being relatively inexpensive. Based on these findings the Zucker rat was selected for this study of the effects of obesity and IR on arterial injury.

Chapter 3
Balloon Angioplasty

3.1 ZFR-F (Fat) vs ZFR-L (Lean) vs Pre-Diabetic (ZDF) Zucker rats.

In order to evaluate the potential role of metabolic syndrome in the pathology associated with balloon angioplasty, the Zucker Fatty Rat (ZFR) and Zucker Fatty Diabetic Rat (ZDF) carotid artery balloon injury models were selected specifically to distinguish the risk associated with both an obese and insulin resistant state.

In addition to balloon angioplasty, a further objective of this study was to carry out stent deployment, according to the method of Aloke Finn (89). The first stent implants in rat carotid arteries were originally done in 2000 by Ciro Indolfi (106). Our preliminary stent work in setting up the model is shown in the next section, to compliment this parallel study involving balloon angioplasty and stent deployment in Zucker rats

3.1.1 Materials & Methods

The institutional animal care and use committee of the University of Cape Town approved all the procedures used in this study. Three distinct phenotypes of both male and female Zucker rats were used in this study for balloon angioplasty, ZFR-Lean (ZFR–L n=9), ZFR-Fat (ZFR–F n=8) and ZDF Fat (ZDF n=9). Rats were kept at 21-23°C, with a 12 hr day-night cycle, and were allowed water and standard rat chow, Ad libitum.

The rats were anaesthetized with ketamine/xylazine (200µl/400g; ratio 9:5ml; i.p.). Buprenorphine (0.05mg i.m.) was administered pre-operatively for prophylactic analgesia. Surgery was performed aseptically with the use of a Nikon-SMZ800 stereomicroscope *(Fig-19).*

Access to the carotid artery was gained via a mid-line neck incision. Heparin (100U/Kg) was administered into the jugular vein prior to arteriotomy. Following ligation of the distal left external carotid artery (ECA) and application of temporary vascular clamps to the left common carotid artery (CCA) and the left internal carotid artery (ICA), arteriotomy was performed proximal to the ECA ligation. A Fogarty embolectomy balloon catheter (Edwards 2F) was inserted via the arteriotomy and introduced into the CCA target area, inflated to 2 bars (atm) and withdrawn to a point proximal to the carotid bifurcation. This procedure was repeated a further 2 times. The effect was to both potentially cause endothelial denudation and damage to the elastic lamellae. Following final withdrawal of the catheter, air in the CCA was expelled with blood by brief release of the CCA vascular clamp and the ECA proximal to the arteriotomy was finally permanently ligated. Blood flow was restored via the ICA by removal of both the CCA and ICA vascular clamps, and the incision was closed once homeostasis was ensured.

3.1.2 Follow up

The rats were observed post-surgery for any complications. Body weight, food intake and blood glucose (in the case of the ZDF rats) were tested during a twenty-one day follow-up period. Post-surgical complications included transient Horner's Syndrome, most likely due to tissue swelling surrounding the sympathetic nerves. This caused ptosis of the eyelid (107). The surgical method was refined to further minimize trauma to the nerve tissue overlying the vessels in the operative site to avoid this complication.

3.1.3 Explant Procedure

Twenty-one days after balloon injury, the rats were anaesthetized as described before and the thoracic cavity exposed via a laparotomy extending through the diaphragm. A cannula was placed into the left ventricle and phosphate buffered saline (PBS, pH 7.4 containing heparin) was infused using a peristaltic pump. This was followed by infusion of Para formaldehyde (PFA; 4% w:v). The left and right CCA were finally dissected free, together with the aortic arch and immersed in PFA for 24 hrs *(Fig-19)*. The right CCA served as a non-injured control. Macro photographs were taken, using a Leica-stereo microscope (MZ75) and Leica (DFC 280) camera.

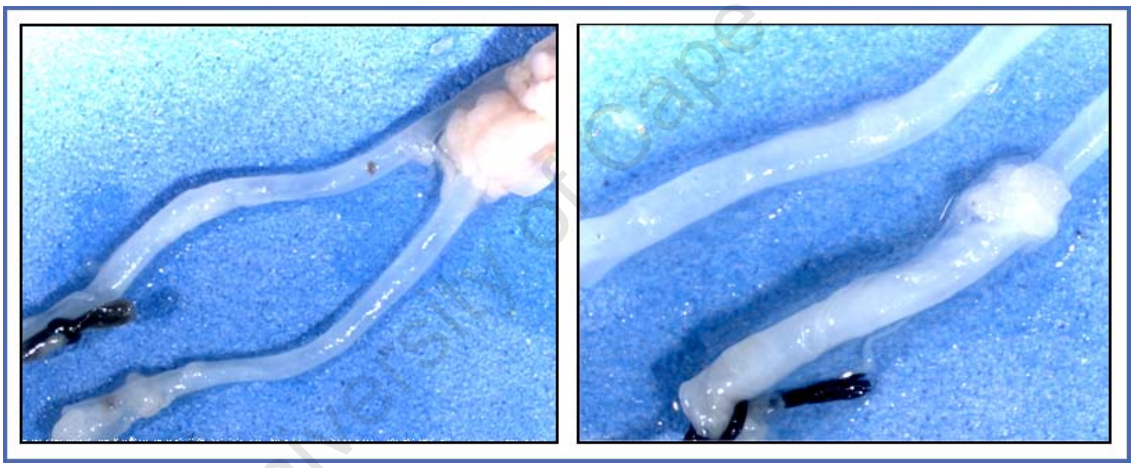

Figure 19 Explanted Left and Right CCA attached to Aortic Arch. The injured CCA is marked with a stitch. (Magnification 0.6 x3 and 1.0 x respectively).

3.2 Histology and Morphometric Analysis

The samples were processed overnight in a Shandon Tissue-Tek II processor, containing graded alcohol (70%, 90%, 100%), Xylene-100% and paraffin wax. The following day the samples were embedded in an upright position into a purpose made deep embedding tray. They were serially sectioned using a rotary microtome (Micron H360) from the bifurcation towards the aortic arch to evaluate the extent of intimal thickening. Five to ten sections were taken from a point where IH was visible and thereafter every 500µm (defined as a level), until there was no further evidence of hyperplasia. Each level was labeled accordingly and stored in slide boxes.

Once the levels were prepared for each explant, one slide from each level was stained with an Elastic Masson's trichrome stain, which differentiated collagen from SMC while staining elastic fibres black

(Appendix-A5). This stain allows easy visualization of the IH region and allows assessment of the extent of elastic lamellae damage.

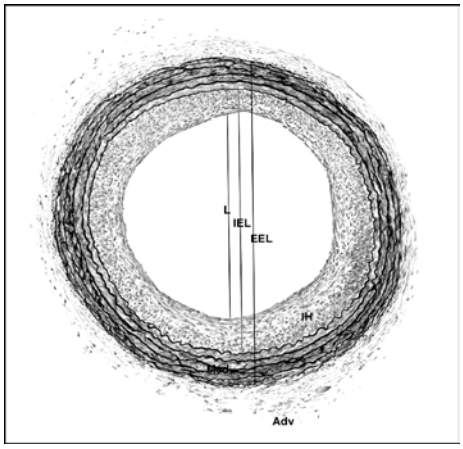

Figure 20 Lines representing the lumenal, IEL and EEL diameters, as well as IH, Media and Adventitial zones, demarcated by the elastic lamellae.

Stains were imaged using an automatic stage, at 10x magnification, on a light microscope (90i, Nikon) that allowed capture of the entire cross-section of the vessel into a single tiled image using Eclipse Net software (Laboratory Imaging, Prague, Czech Republic). Calibration grid images taken at 10x magnification were used to calibrate the image analysis (IA) software. IA was performed using Adobe Photoshop version 7.0 (San Jose, CA) and IPTK version 5 plug-ins (Reindeer Graphics, Asheville, NC).

The extent of the areas inscribed by the lumen and internal and external elastic lamellae were defined and measured *(Fig-19)*. From this data, the areas occupied by intima and media could be calculated. Equivalent thicknesses of lumen, intima and media were derived based on approximation of the areas to geometric circles:

The diameters (ø) of the areas occupied by lumen, internal and external elastic lamellae were derived as follows:

$$ø_{Lumen} = \sqrt{\frac{A_{Lumen}}{\pi}} * 2 \; ; \; ø_{IEL} = \sqrt{\frac{A_{IEL}}{\pi}} * 2 \; ; \; ø_{EEL} = \sqrt{\frac{A_{EEL}}{\pi}} * 2$$

where A = area inscribed by the lumen surface, IEL and EEL.

The equivalent thickness (d) of the intima and media were further derived as follows:

$$d_{Intima} = \frac{ø_{IEL} - ø_{Lumen}}{2}; \; d_{Media} = \frac{ø_{EEL} - ø_{IEL}}{2}$$

The Intima to Media ratio was calculated as follows:

$$I : M = \frac{d_{Intima}}{d_{Media}}$$

Within each animal, the mean for each parameter was obtained by selecting the level with maximal IH thickness, as well as its four adjacent levels. These levels were then used to report all other parameters.

3.2.1 Statistical Analysis

All data was expressed as means ± standard deviation. Inferential statistical analysis involved one-way analysis of variance testing with post-hoc Student's t-test (JMP version 6.02 software, SAS, Cary,

NC). A significance level of less than 0.05 (two-tailed, unless otherwise stipulated) was accepted as confirmation of statistical significance following Bonferoni correction for multiple comparisons *(Fig 20 & 21)*.

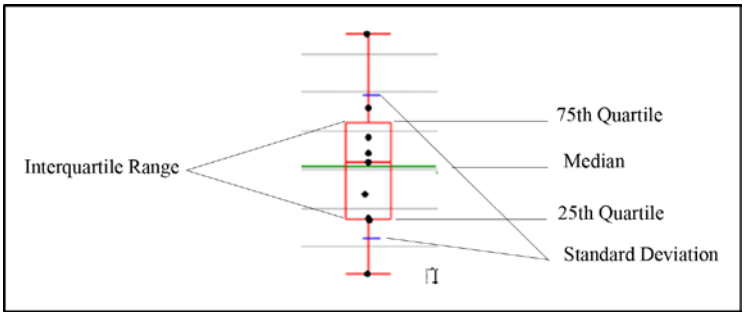

Figure 21 Box and whisker plot definitions used in figure 5

3.3 Results

3.3.1 Morphomtric Analysis

ZFR-F rats demonstrated extensive IH compared to the ZFR-L control group. The ZDF group exhibited a markedly reduced intimal area *(Fig-22)*. The ZFR-F group exhibited a significantly thicker intima compared to both the ZFR-L and ZDF groups (108.2 ± 25.7µm, 71.6µm ± 28.0, 36.4µm ± 21.2 for ZFR-F, ZFR-L and ZDF respectively; p<0.0001). Both mean stenosis (45.5% ± 9.1, 30.3% ± 10.7 and 16.8% ± 9.9 for ZFR-F, ZFR-L and ZDF respectively; p <0.0001) and intima:media ratio (1.42 ± 0.34, 1.01 ± 0.31 and 0.46 ± 0.26 for ZFR-F, ZFR-L and ZDF respectively; p<0.0001) were similarly higher in the ZFR-F and least in the ZDF group. The thickness of the media was not significantly distinct between the three groups (60.5µm ± 18.3, 59.0µm ± 8.2 and 69.1µm ± 10.3 for ZFR-F, ZFR-L and ZDF respectively; p = 0.23). *(Fig-23)*.

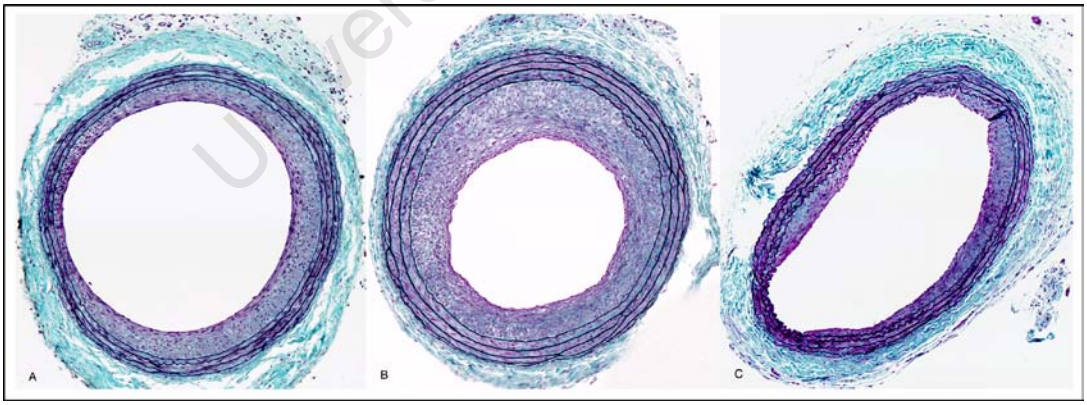

Figure 22 Elastic Masson's trichrome staining of carotid cross sections (3µm) 21 days post injury, demonstrating the elastic lamellae in black and the IH within the IEL, in (A) ZFR-L (B) ZFR-F, and (C) ZDF. Original magnification 10 x.

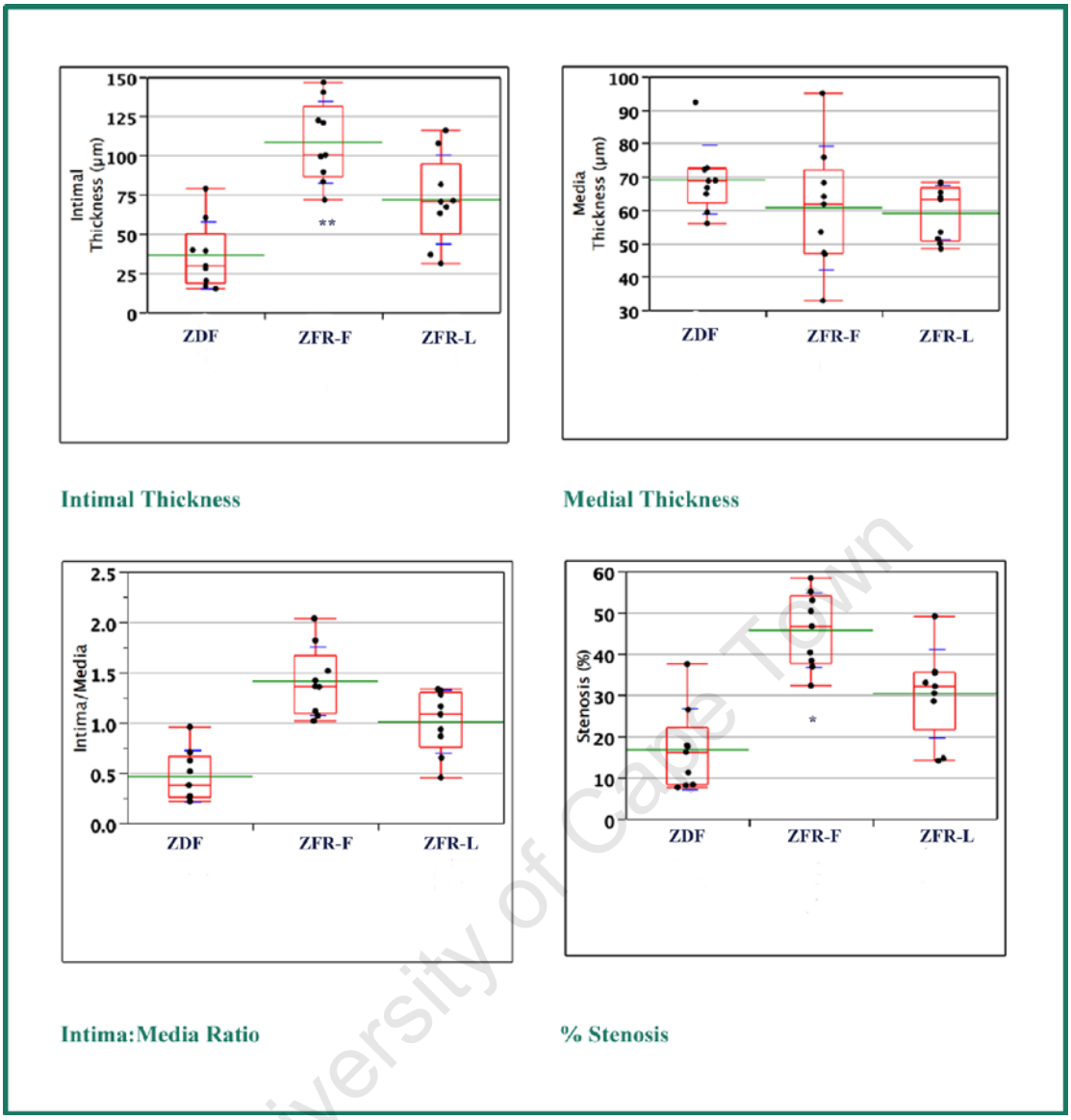

Figure 23 The intimal and medial equivalent thicknesses, intma/medial ratio and % stenosis .

***** Indicates the significantly increased intimal thickness in the ZFR-F group (p<0.0001)***

****** Indicates a significant difference in stenosis specifically in the ZFR-F group (p<0.0001)***

3.4 Inflammation

Obesity predisposes a patient to a pro-inflammatory state concomitant with elevated CRP and cytokine levels (108) and an increase in a risk for CVD. Excess adipose tissue translates into inflammatory mediator levels, which contributes to the underlying inflammation. Significant weight loss has resulted in decrease in CRP, IL-6 and IL-18 levels and raised adiponectin levels. This in turn serves to mitigate an otherwise pro-inflammatory state. Strong evidence suggests that inflammation correlates with the degree of injury, which varies depending on whether that injury is a result of balloon angioplasty or stent deployment (109, 110). An increase in plasma CRP levels is known to promote both inflammation and atherosclerosis and participates in restenosis following coronary intervention.

Elevated CRP plasma levels are also noted in diabetes. Increased CRP is also a common histological finding in atherosclerosis (98) and is associated with components of MS, such as hyperglycemia, hypertension, obesity, decreased HDL.

It was therefore important in this study to evaluate the inflammatory status by histological analysis of selected contributors to this process, namely CRP, macrophages, IL-6, adiponectin and immune complexes IgG and IgA.

3.4.1 Materials and Methods

3.4.2 Specific Markers

The following six markers were set up to assess the level of inflammation, and set up as follows:

- Polyclonal C-Reactive Protein (CRP) rabbit anti rat (Abcam: ab 47795)
- Polyclonal Rabbit anti rat IgG/ FITC Conjugated (Serotec: Star 17B).
- Polyclonal Goat anti rabbit IgA (Komabiotech: K0211684).
- Monoclonal mouse anti rat macrophage marker CD 68 (Clone ED-1) (Serotec: MCA341R).
- Polyclonal rabbit anti rat Adiponectin (Abcam: ab3455).
- Polyconal Goat anti rat IL-6 (Cedarlane: CL9571AP)

3.4.3 Immuno-Fluorescent Staining

All antibodies were diluted in 1% bovine serum albumin (BSA) in PBS to minimize background staining. The levels selected were with maximal IH from each rat explant, usually occurring at the mid point of the injured area. Since these were wax embedded tissues, serial sections, 500µm apart from each level were sectioned and stored for future use. Each slide included the corresponding, un-injured control artery from the same rat, which served as a control. The sections were de-waxed in xylene, and brought to water through graded alcohol. Antigen retrieval, using P XIV (Sigma) or proteinase K (Diagnostech) pre-treatment, to break down covalent bonds induced by formalin fixation, was performed where necessary depending on the primary antibody used. Standard immunohistochemistry for paraffin embedded tissue was done using appropriate primary antibody dilutions in 1% BSA *(Appendix A -7)*. The appropriate anti-mouse or anti-rabbit fluorescent secondary antibodies were applied and incubated in the dark (Donkey anti-mouse for monoclonal; and Donkey anti-rabbit/goat for polyclonal antibodies). All slides were mounted in DAPI nuclear mountant (Vector shield) to differentiate the nucleus, and protected from light to preserve fluorescence *(Appendix-A7.1)*. Images were taken immediately, to prevent photo bleaching of the fluorescent signal, using a fluorescent microscope (Nikon 90i). Appropriate filters for the various fluorochromes were selected (e.g. Alexa 488 and Cy 3).

A scoring system was used to assess the level of positive staining, individually for the intima, media and adventitial zones. Scores of +, ++ and +++ were arbitrarily defined for ED-1, CRP, IgG and IgA antibodies, negative controls were set up to ensure that positive staining was not due to non-specific antibody binding. This step involved sections without the addition of a primary antibody, but undergoing all the steps that the test slides went through, to rule out the possibility of secondary antibodies binding to immunoglobulins in the tissue.

3.4.4 Results

Very few macrophages stained positively within the intimal or medial areas in any of the three groups based on the monoclonal antibody (ED-1 Serotec-CD 68). Occasional macrophages were observed in the intimal zone and within the media but, more frequently, they were seen in the surrounding adventitial zone *(Fig-23)*.

IgG staining was largely absent in the intima of the diabetic group but strongly positive in the adventitia (p=0.025). In the ZFR-F and ZFR-L groups however, there was no statistically significant difference between the layers (N.S) *(Fig-24)*. The intima, media and adventitia of the ZFR-F group displayed staining for IgG but this was no different from the ZFR-L group *(Fig-25)*. Mild staining for IgA was found in the intima, media and adventitia of the obese and lean group, with strong staining in association with the endothelial cells in the ZFR-F group *(Fig-26)*. The diabetic group showed substantially reduced staining in comparison to the fat and lean, with no evidence of endothelial association, in spite of confirmation of the presence of an endothelial layer by VWF immunostaining. (Not shown).

C-Reactive protein showed variable staining within each group, but most notably it was intensely stained in the intima in all groups *(Fig-27)*. The majority of ZFR-L arteries displayed highly variable staining in the media, intima and adventitia, varying from severe to nil. The ZFR-F group displayed strong CRP staining in the intima only, and the ZDF group only displayed some strong staining in the intimal and some medial areas, as can be seen from the charts in *(Fig-26*). No statistical differences were discernable for this stain however.

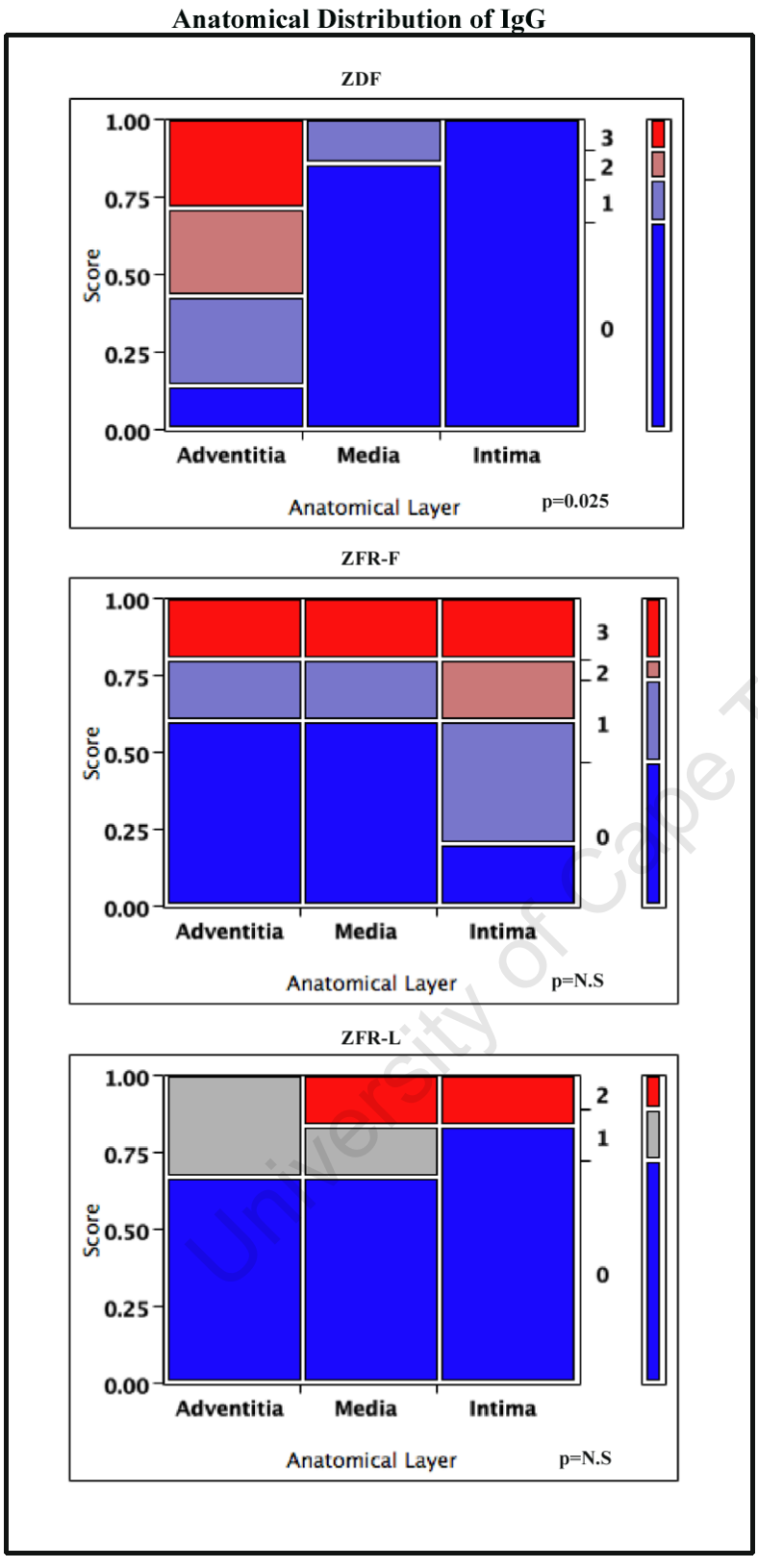

Figure 24 IgG comparative staining between ZFR-F and ZFR-L rats after balloon injury.

Adiponectin staining was strongly detected in the intima and media of the ZFR-L group, compared to the adventitia (N.S). The ZFR-F group showed a trend towards stronger staining in the intima compared to the media and adventitia. The ZDF group, however, stained strongly for adiponectin in all layers but this did not achieve statistical significance.

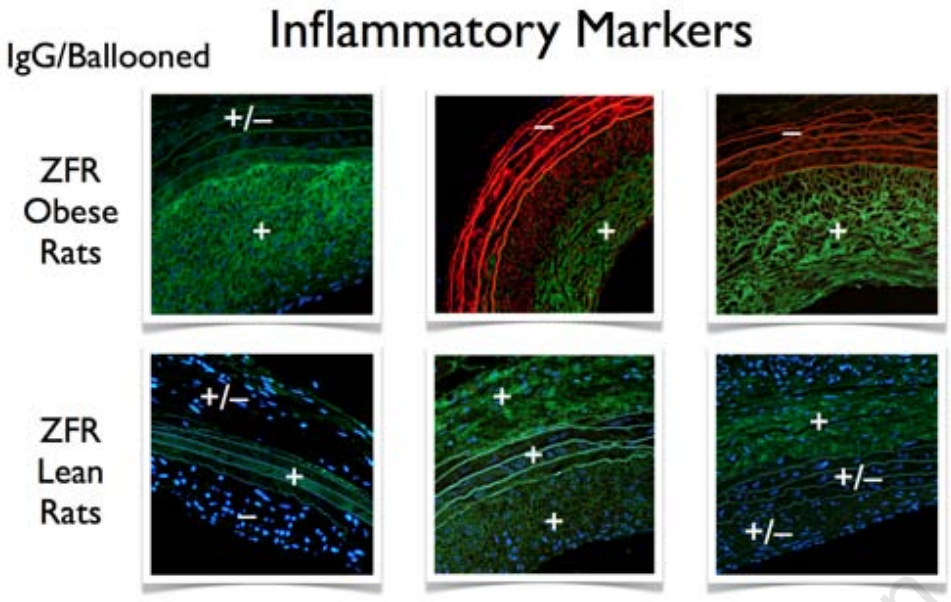

Figure 25 F Comparative values of IgG between the anatomical layers of ZDF; ZFR-L and ZFR-F.

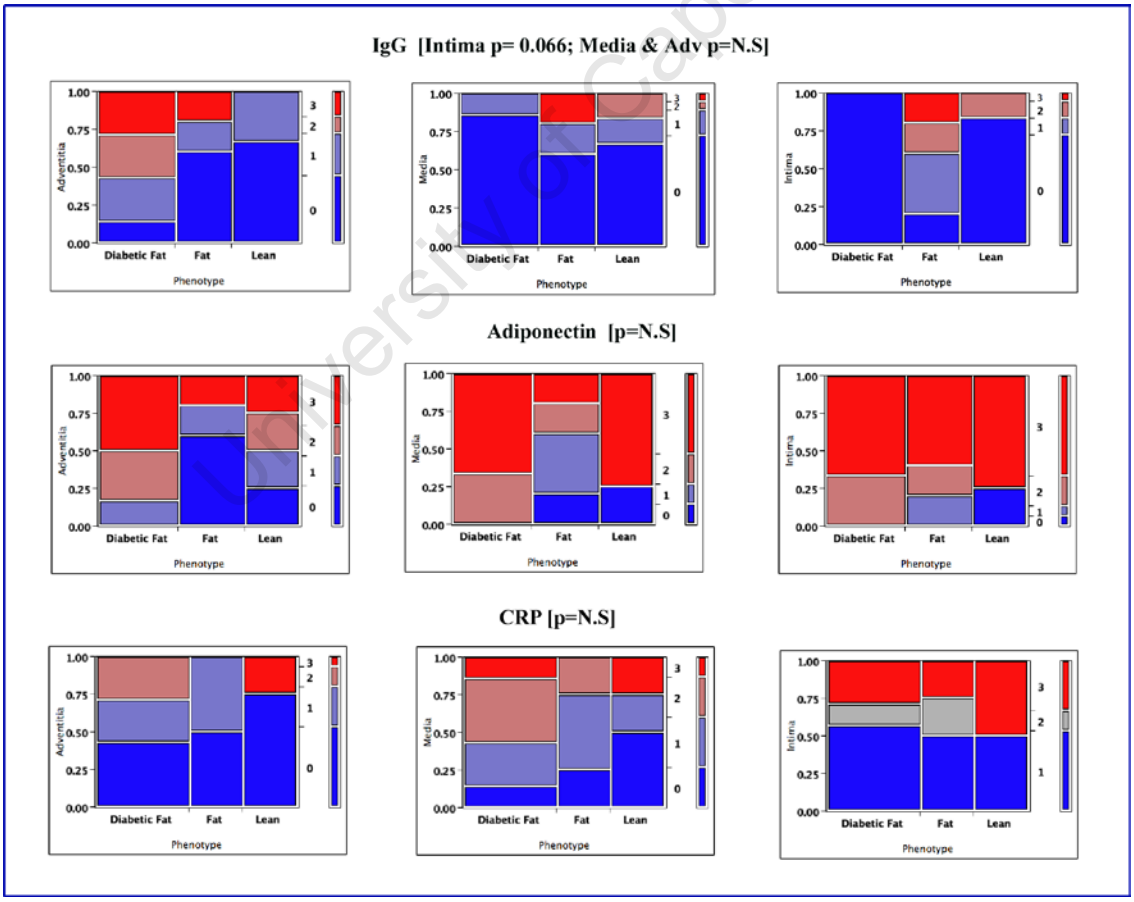

Figure 26 IgG, Adiponectin and mosaic plots for adventitial, medial and intimal layers.

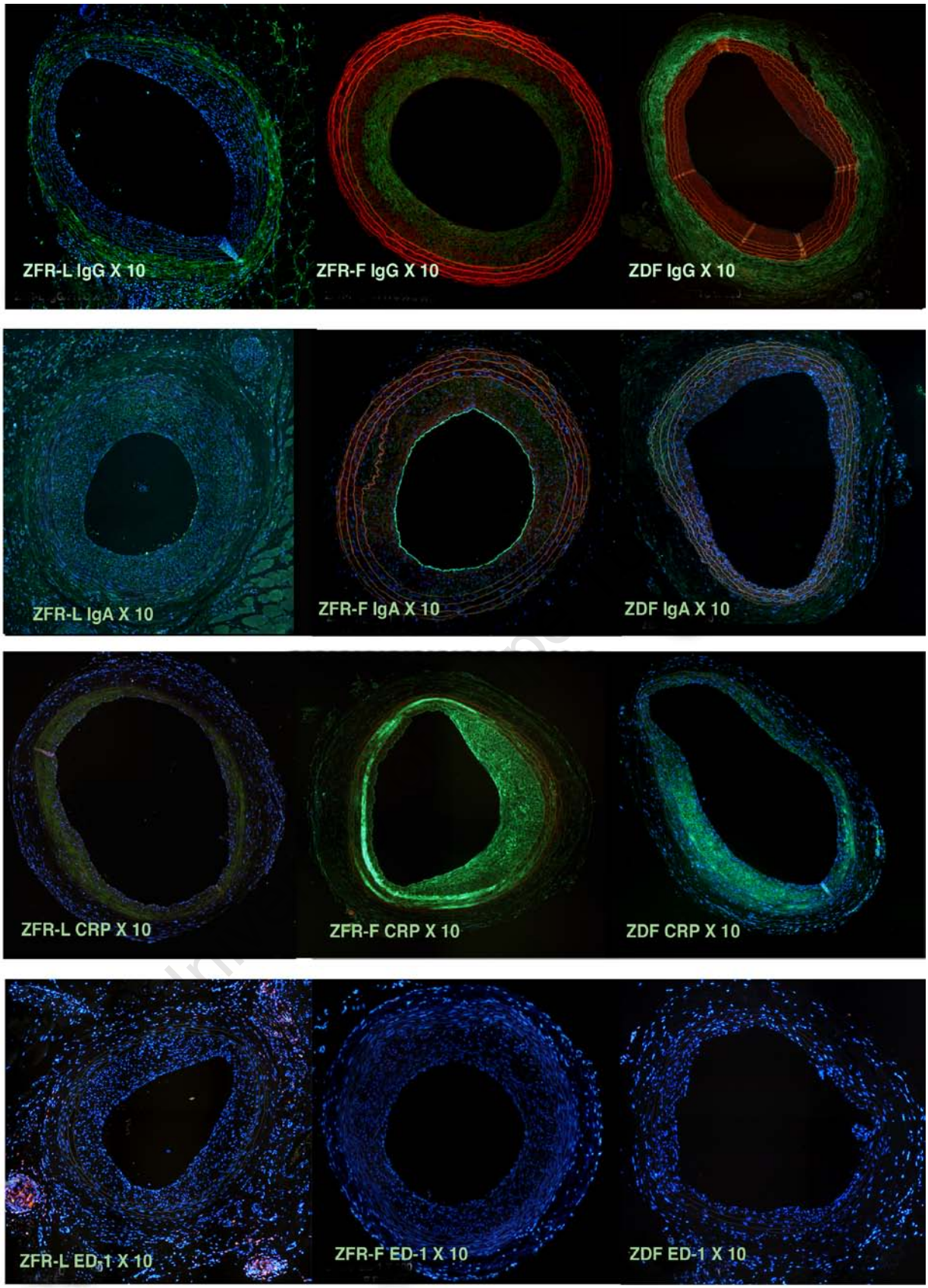

Figure 27 Immunohistochemical staining of IgG(FITC), IgA(Alexa 488), CRP(Alexa 488) and ED-1(Cy3) at 10 x magnification for each phenotype.

3.5 Staining of GAGS (PG) using a Modified-Movat stain

PG can be detected by individual immunohistochemical staining, but in general by histochemical staining using Movat stain. This stain is similar to that of a Masson's trichrome in being able to differentiate muscle, collagen and elastin, but additionally stains PG and GAGS in blue. In general the most prevalent PG detected by the Movat is CS.

3.5.1 Materials & Methods

Serial sections to area of maximal IH thickness from the balloon injured area were dewaxed through xylene and graded alcohol to water, and stained with a modified Movat stain *(Appendix A-6)*. The Verhoef's solution allowed visualization of the elastic fibres (black), with Van Gieson counterstain differentiating collagen from muscle. The PG components stained using Alcian Blue (1%). Sections were scored according to scoring system described previously

3.5.2 Results

The arterial wall of balloon injured carotid arteries consistently demonstrated very limited GAG staining as detected by the Movat stain *(Fig-29)*. Occasional clumps of blue PG staining were seen in the tunica media and tunica intima, in comparison to the un-injured control vessel that failed to show GAG staining. Positive PG staining was best viewed under high magnification, but there were no clear differences between the ZFR-F, ZFR-L and ZDF groups. *Figure-30(B)* shows a baboon coronary artery SV graft, 6 months after CABG, and a artery twenty one days post angioplasty rat carotid *Fig-30(A)*, modified Movat stain. This was to demonstrate the differences in PG content in the two species at different time points. It is important to note that Movat staining predominantly identifies the CSPG and not HSPG type (112).

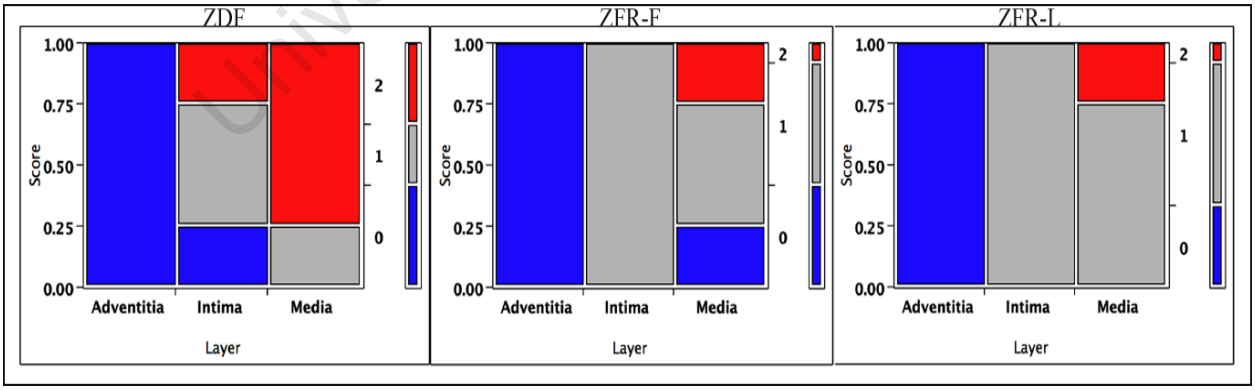

Figure 28 Numerical scoring of GAGs in anatomical layers in representative examples ZDF, ZFR-F and ZFR-L rats.

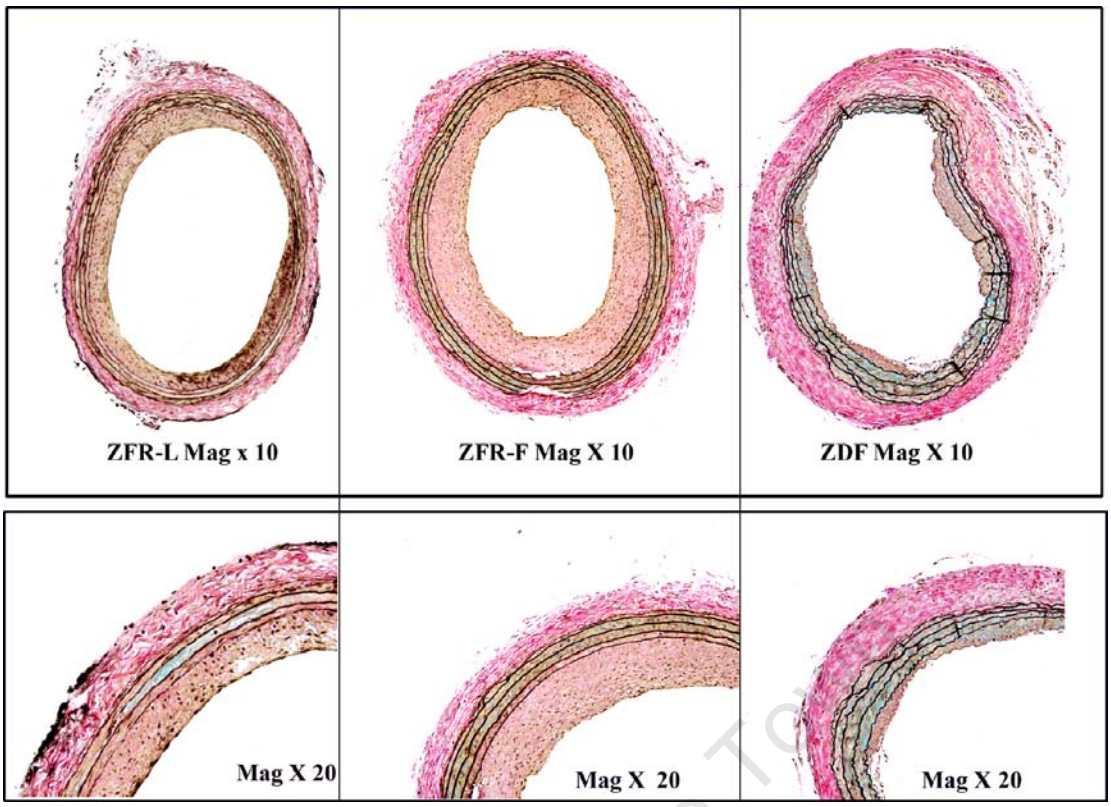

Figure 29 Modified Movat staining of a selection of ZFR-F, ZFR-L and ZDF Zucker rats. Images were taken at 10 x magnification. High magnification 20 x demonstrating the GAG components staining with Alcian blue.

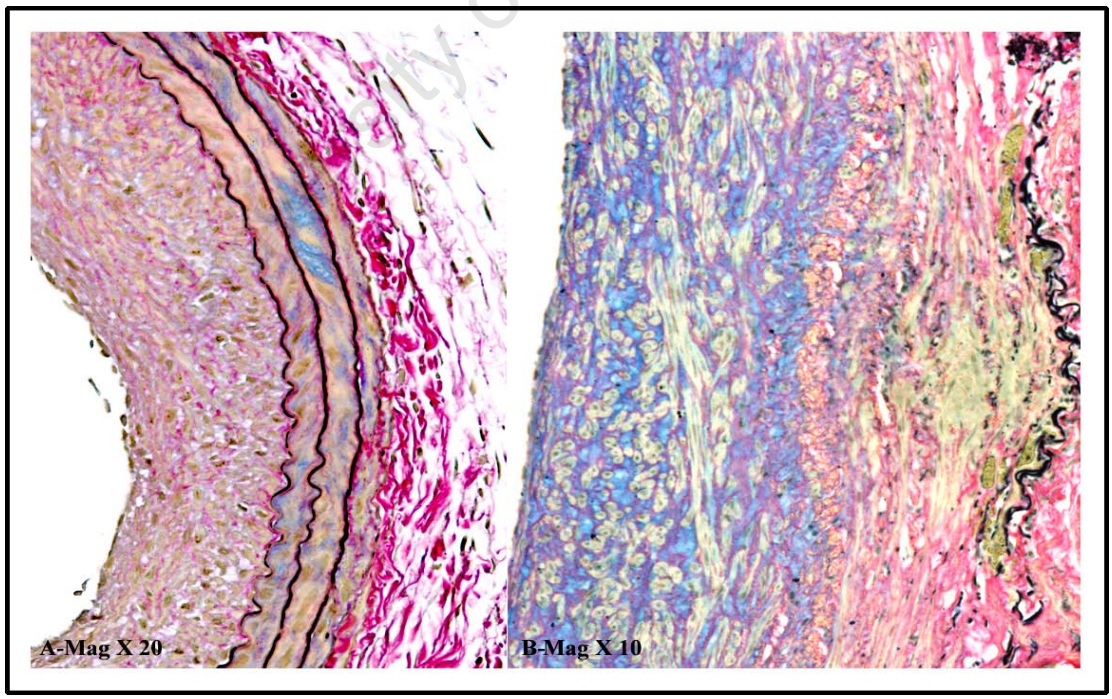

Figure 30 Rat carotid artery 21 days after angioplasty and stented baboon coronary artery 6 months after external stent deployment (Movat stain).

3.4 Glycocalyx Analysis

3.4. Introduction

The glycocalyx is made up of a network of PG and glycoproteins, predominantly of the HS variety. Although Movat staining did not show differences between the rat groups with respect to PG we decided to re-examine whether differences did exist with regard to specific PG (i.e. CS and HS) (56).

The critical role played by the endothelial glycocalyx has been acknowledged in recent years, however the challenge to determine if it could be a marker of cardiovascular disease remains. In addition, there is a need to assess whether restoring the glycocalyx would have an influence on the process of atherosclerosis and, therefore, how therapeutic intervention in this regard could be useful in the clinically (113).

The presence of Heparan Sulfate (HS), as a major component of the glycocalyx and that of the artery wall, has been demonstrated in the intima and media of vascular tissue (114). However, the evidence of HS, as part of the surface endothelial glycocalyx, using light microscope techniques, has not yet been published. All previous detection of the glycocalyx has been demonstrated by electron or confocal microscopy (22). The glycocalyx is destroyed during processing and paraffin embedding. The presence of the glycocalyx can be seen in the typical tuft-like formation described in previous studies using transition electron microscopy (TEM)(115).

Three techniques were set up to confirm the presence of the HSPG. Light microscopy immunohistochemistry; confocal immuno-fluorescent-histochemistry and TEM incorporating Alcian Blue staining.

3.4.2 Materials & Methods

3.4.2.1 HeparanSulfate (HSPG) Immunohistochemistry

The most prevalent PG component of the endothelial glycocalyx is HS and was therefore targeted to detect the presence of HS on the luminal surface, in the intimal area and throughout the arterial wall, using immunohistochemical techniques.

3.4.2.1.1 Light Microscopy

Cross sections of ballooned, right common carotid (RCC) artery at the maximal point of IH, together with control, left common carotid (LCC) artery from the same rat, were immunostained for Anti Heparan Sulfate (Abcam-ab2501). Sections were dewaxed and taken to water through xylene and graded alcohol solutions, as previously described. Blocking for endogenous staining was performed using hydrogen peroxide (3%) in methanol to prevent endogenous staining. Antigen retrieval using Proteinase-K, to better expose antigen sites obscured through the formation of covalent bonds during formalin fixation, was performed for 10 minutes prior to application of goat serum (1:20 in PBS for 20 minutes), to minimize background staining. Incubation with the primary antibody diluted 1:100 (in PBS + 1% BSA) was performed overnight @ 4°C. Sections were washed in tris-buffered saline (TBS), followed by incubation with biotinylated Goat anti-mouse IgG (Histomark: 71-00-18), followed by

Streptavidin-peroxidase (Histomark: 71-00-38). True Blue-HRP (Histomark: 71-00-68) was used as the chromogen due to its much higher sensitivity compared to diamonobenzidine (DAB). Colour development was maximal after 5 minutes, and sections were counterstained with Neutral Red (0.25% for 2 seconds). Slides were air dried and mounted in Entellan *(Appendix A-7.2)*. Negative controls excluded primary antibody to rule out non-specific secondary antibody binding. The un-injured left carotid vessel also served as a control.

3.4.2.1.2 Confocal Imaging

Confocal imaging is a method to visualize cellular components incorporating immunohistochemical techniques, in which whole mount samples can be viewed using optical scanning. This method does not require tissue fixation and therefore causes less structural damage and dehydration to the tissue by solvents and alcohol solutions, resulting in better preservation of the glycocalyx components in the lumenal area

To demonstrate the presence of Factor VIII containing endothelial cells adjacent to HSPG at the EC surface, double immuno-fluorescence staining was performed on freshly explanted, un-fixed carotid artery. The carotid artery was harvested as previously described but without fixation. The tissue was treated with HEPES buffer, before being stained with a cocktail of two antibodies, namely HS (ab2501) and von Willebrand factor (VWF- M0616 Diagnostech] *(Appendix A-7.3)* to allow visualization of the endothelium, stained with VWF/Cy 3 (red) and HS stained with Alexa 488 (green) on the luminal surface. Visualization was effected on a Zeiss confocal microscope and images captured in two separate channels and combined into a Z-stack *(See Fig-15)*.

3.4.2.1.3 Transmission Electron Microscopy

Transmission electron microscopy, for very high magnification visualization, was used as a third technique, to demonstrate the presence of the endothelial glycocalyx. A special process of fixation and staining was performed, according to a protocol obtained from a research group in Maastricht, and which utilized Alcian Blue staining.

Carotid arteries harvested 21 days after balloon injury, were used. The arteries were initially perfused for 5 minutes with HEPES buffered salt solution, followed by 30 minute of perfusion with a fixative/staining solution containing 1% Alcian Blue and Magnesium Chloride ($MgCl_2$) at a flow rate of 8ml/min. The Alcian Blue solution required continuous agitation to keep it in solution. Thereafter, carotid arteries were explanted according to the procedure previously described and placed in McDowell's fixative overnight. This was followed by post-fixation and en bloc counter staining with Osmium and Uranyl Acetate (*Appendix A-9)*.

Samples were dehydrated and embedded in Spurrs resin, and polymerized at 60°C overnight. A Leica-Ultracut microtome was used to cut thin (100-200nm) sections using a glass knife *(Appendix-A-9.11)*. Sections were picked up and placed onto grids for staining and viewing on the electron microscope. A

Phillips EM420 electron microscope was used to visualize sections, and images were captured using an AnalySIS program *(Appendix A-9.12)*.

3.4.3 Results

Light microscopy demonstrated the presence and extent of the EGL. Both the lean and the fat ZFR groups showed variations in HS staining, with several displaying a substantial endothelial glycocalyx. The ZDF group showed occasional presence of a glycocalyx, with positive HS staining in the IH region as well as patches in the media *(Fig-31C)*. There was no evidence of an endothelial glycocalyx in the control vessels, but they had positive staining for HS in the media and/or adventitia *(Fig-31B)*.

A scoring system was used to quantify the findings. The thickness of glycocalyx was scored from 1-4, and the % coverage was estimated *(Fig-32)*.

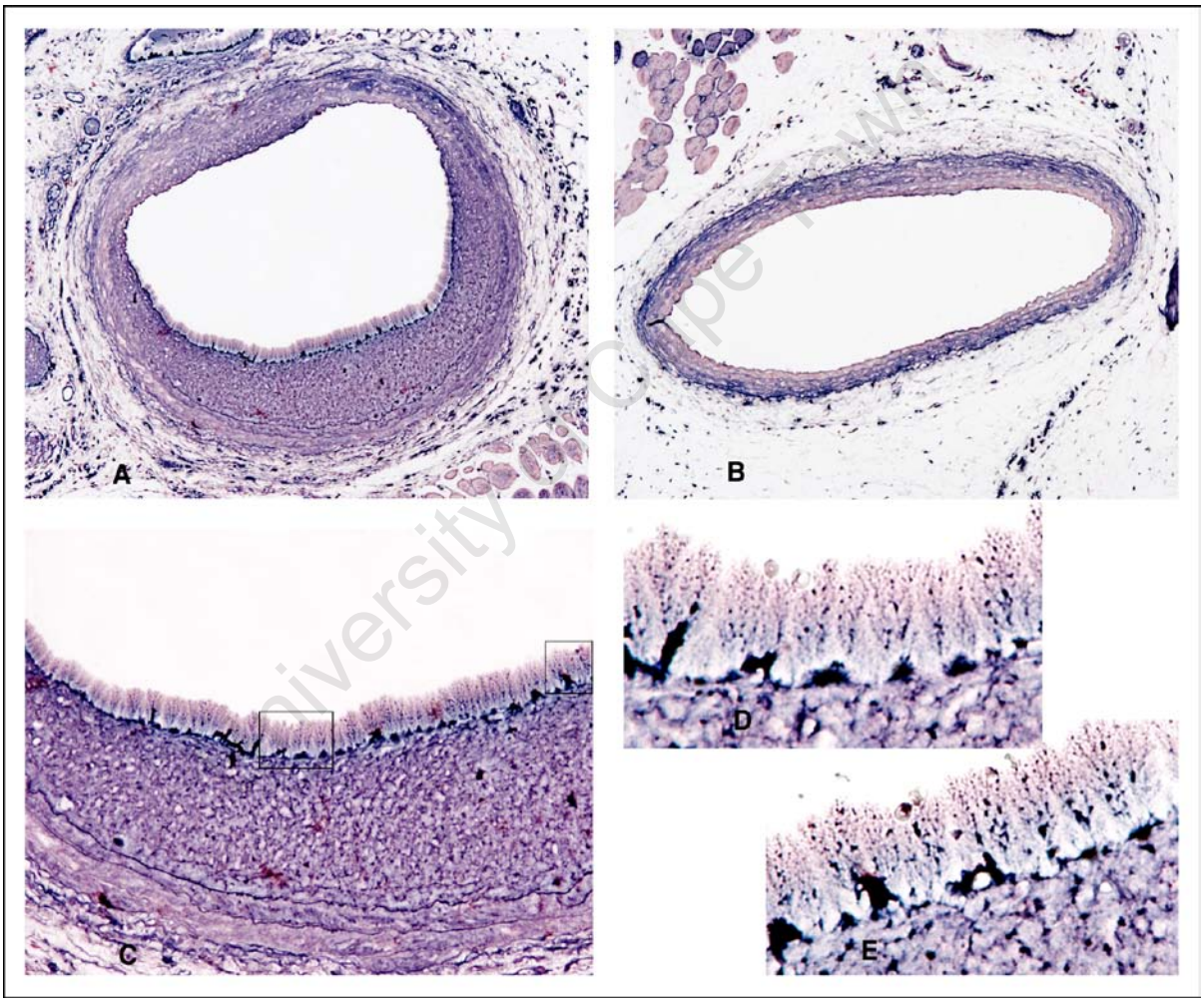

Figure 31 Heparan Sulfate Immuno-staining of A - Balloon injured right carotid artery showing IH and the presence of glycocalyx; B - Control left carotid artery of the same rat, showing no IH or Glycocalyx, but positive HS staining in the media; C - High Magnification (x 20) of HS staining of the intma, media and glycocalyx on the endothelial surface; D + E (x 60) magnification of erythrocytes present on top of the glycocalyx

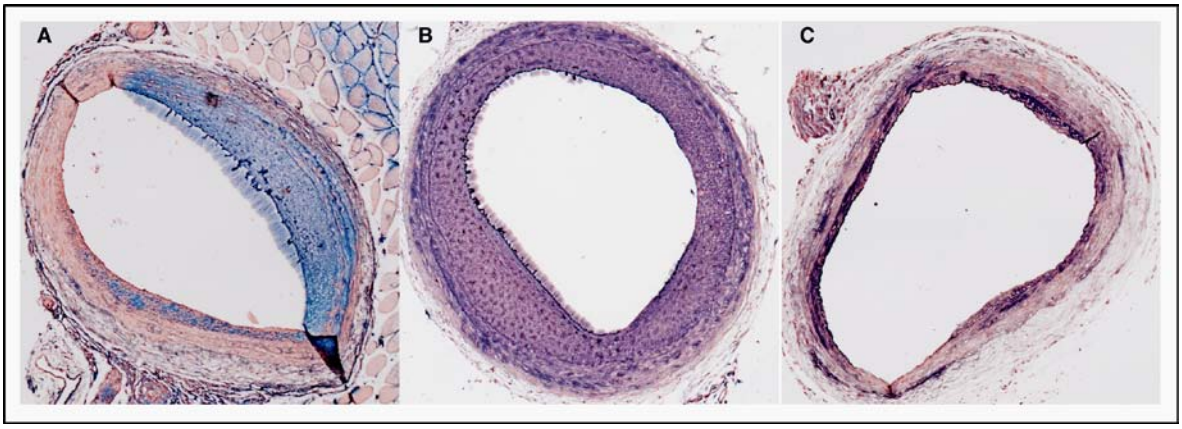

Figure 32 Anti-Heparan Sulfate/True Blue Immunostaining of (A) ZFR-L; (B) ZFR-F and (C) ZDF showing Glycocalyx, intimal and medial staining of HS. Original magnification 10 x).

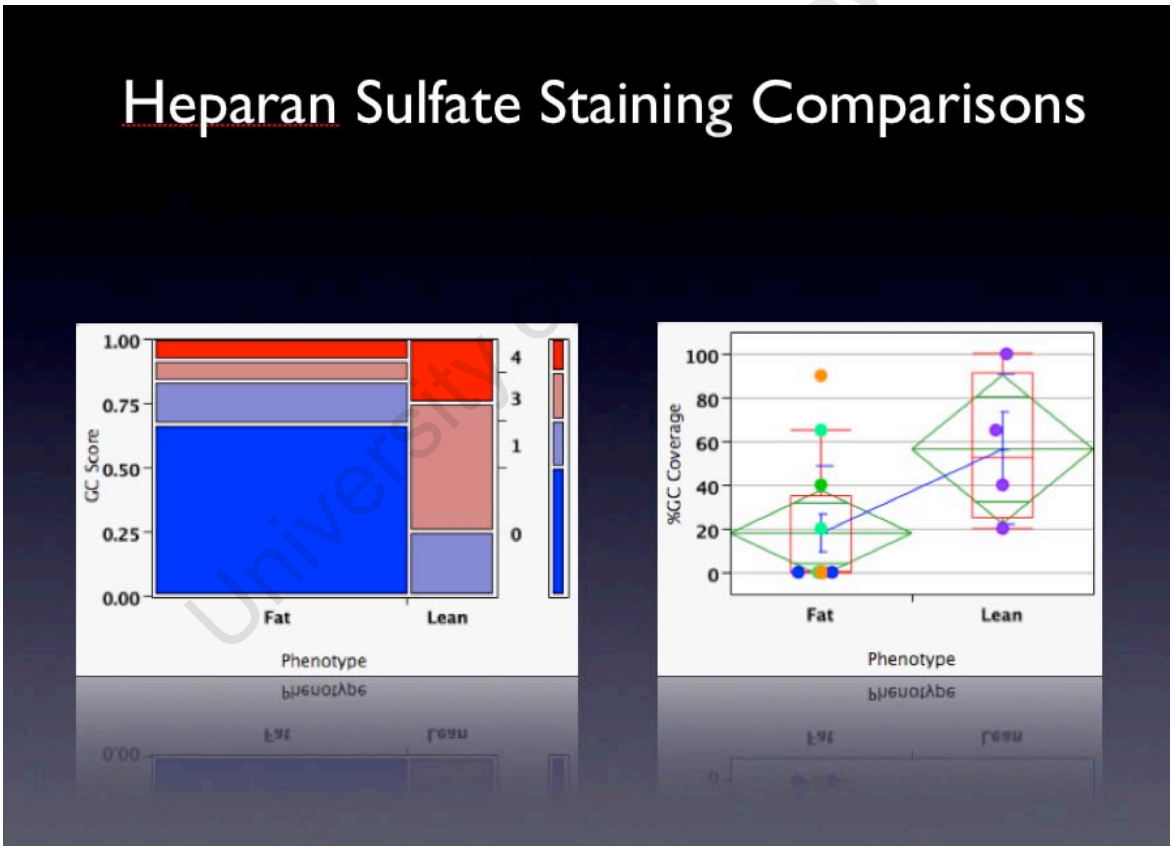

Figure 33 The glycocalyx thickness score in relation to fat (ZFR-F) vs lean (ZFR-L) on the left, and the percentage of luminal coverage on the right, extrapolated from manual scoring

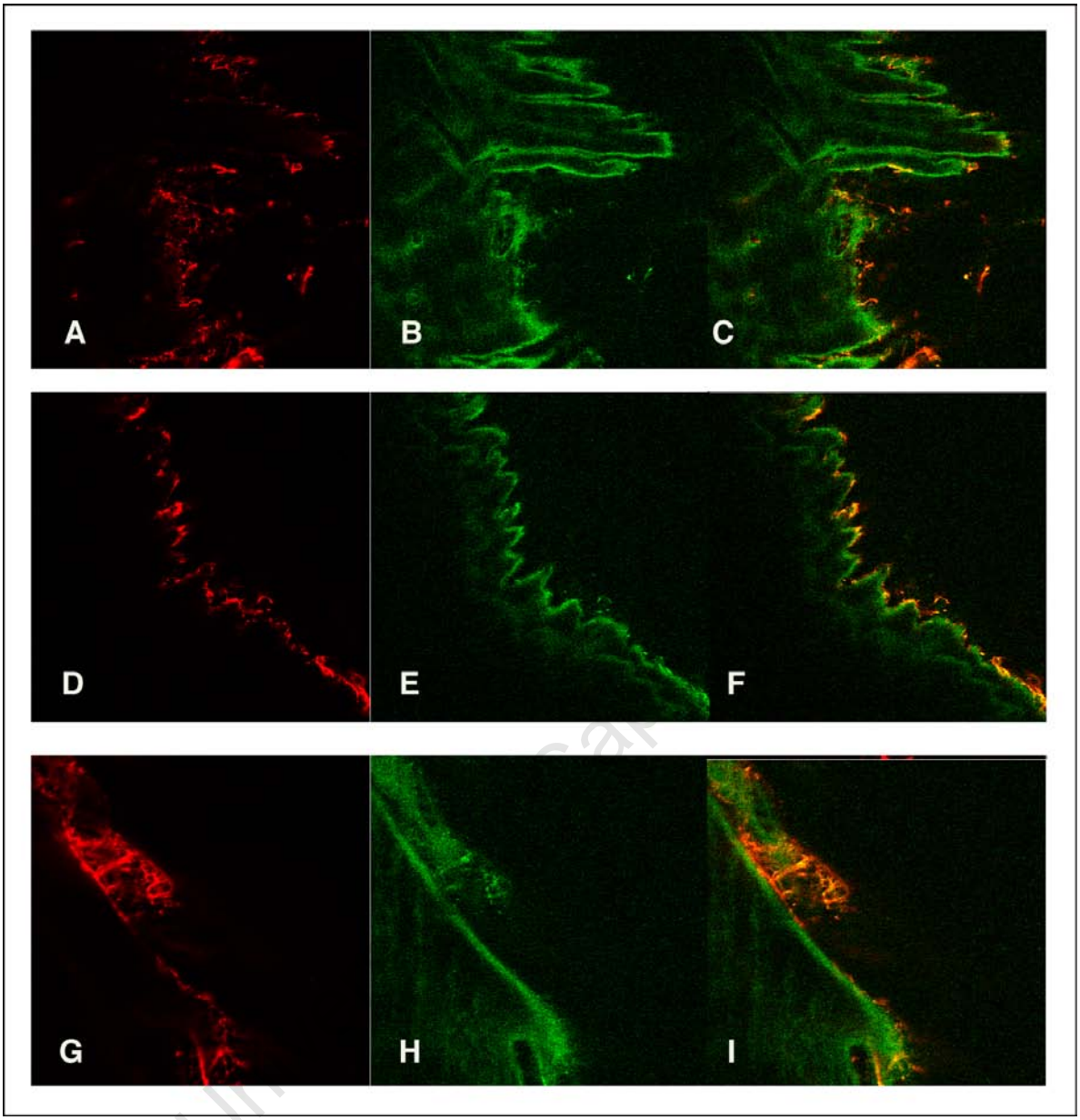

Figure 34 Confocal Imaging on fresh Carotid Artery double stained with Anti-HS/Alexa 488 and Anti-VWF/Cy 3. A-C View from above of EC surface; D-F Endothelial Edge; G-I High Magnification of Endothelial Edge.

Confocal imaging showed double staining in spite of high background in the green channel. Results indicated the presence of HS on the lumenal surface in green, closely associated with the endothelial cells containing VWF, in red *(Fig-34)*.

Transmission electron microscopy confirmed the presence of a glycocalyx on endothelium of the balloon injured carotid artery *(Fig 35)*. Although the structure appeared slightly clumped in comparison to published images, this was attributed to the fact that the perfusion pump flow rate was not high enough.

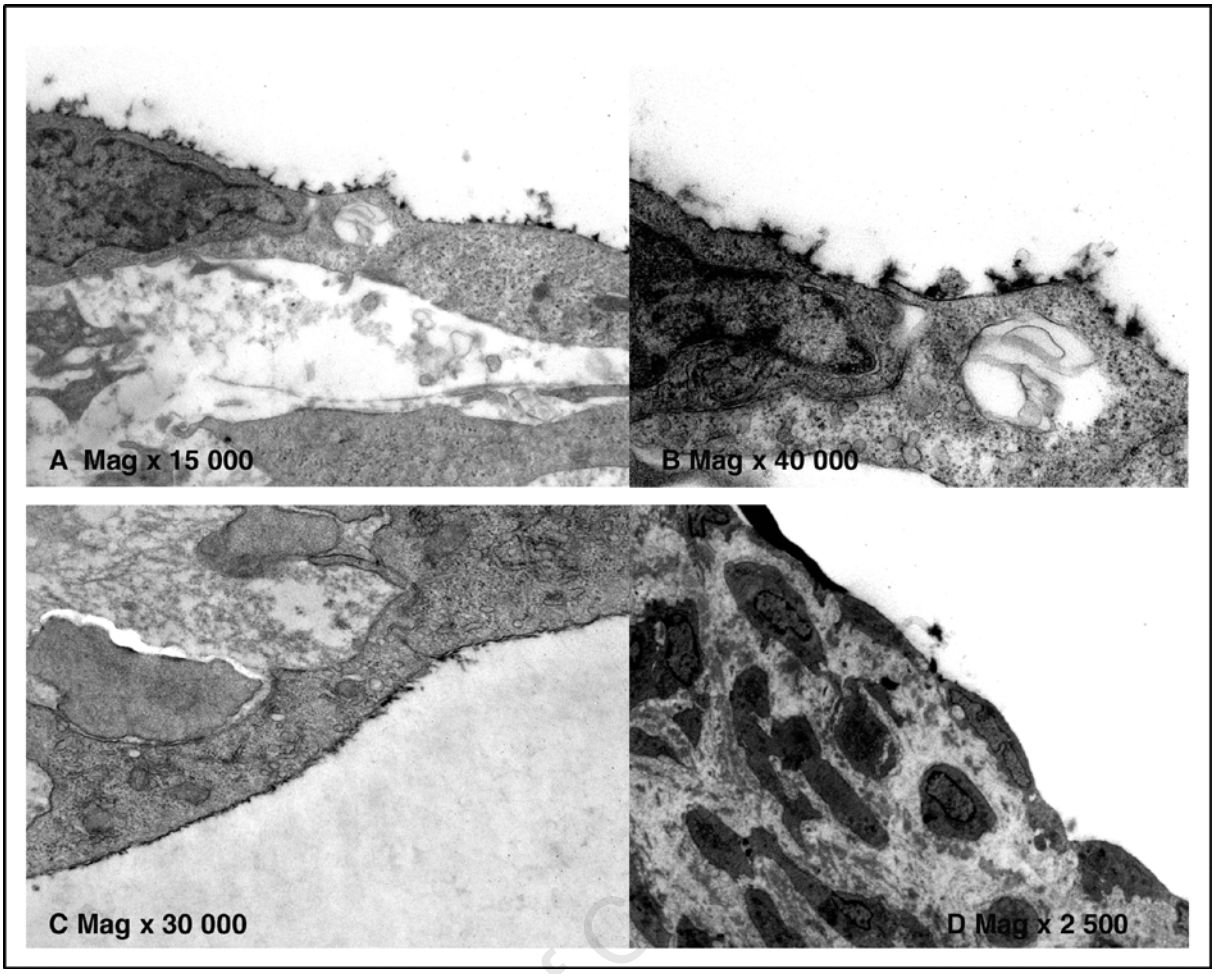

Figure 35 TEM on balloon injured carotid artery using Alcian Blue staining to demonstrate the presence of glycocalyx on the surface of the endothelium (A, B & C) although this was not consistent in all areas D.

3.5 Pathological Changes

Morphological changes to peripheral organs, such as the pancreas and the kidney are not uncommon in association with DM2. Its association with intimal hyperplasia is less well documented. We performed histology on both organs to assess their pathological state and determine if there was any correlation with the extent of IH.

3.5.1 Hydronephrosis

Pathological changes observed in the kidneys of Zucker rats have been well documented (116-119). This phenomenon, first described by Vora et al in 1996, can be detected in obese and diabetic Zucker breeds, and to a lesser degree in lean rats.

3.5.1.1 Materials & Methods

To ascertain the extent of renal damage in the zucker rat model, the kidneys were excised at explant. Left and right kidneys were cut in half and embedded in wax. Comparative histological evaluation was conducted on lean, obese and diabetic models, with the damage being scored according to severity. Assessment of immune complexes was demonstrated by immunofluorescent Anti-Rat-IgG staining in

the kidney, while macrophage accumulation was determined by ED-1 fluorescent staining. As a measure of the extent of interstitial and glomerular fibrosis and an early indicator of nephropathy, smooth muscle actin was done by immunofluorescent techniques.

3.5.1.2 Results

Severe hydronephrosis is evident in virtually all of the ZFR-F rat kidneys, bilaterally in many cases, while three out of ten ZFR-L showed mild hydronephrosis *(Fig 36)*, as stained with Haematoxylin and Eosin *(Appendix A-4)*. ZDF showed hydronephrosis in some cases, however many unilaterally, and some not at all. This is determined by dilation of the renal pelvis, occasionally presenting as complete hollow areas in the medulla, extending to the cortex. The glomeruli of the lean rats appear fairly normal with no evidence of glomerulosclerosis. The squamous cells lining the Bowman's capsule are in tact, and there is no tubular dilation in the medulla or cortical region. There was no sign of ascending infection, which is a cause of hydronephrosis. There was no correlation of kidney damage to changes in IH.

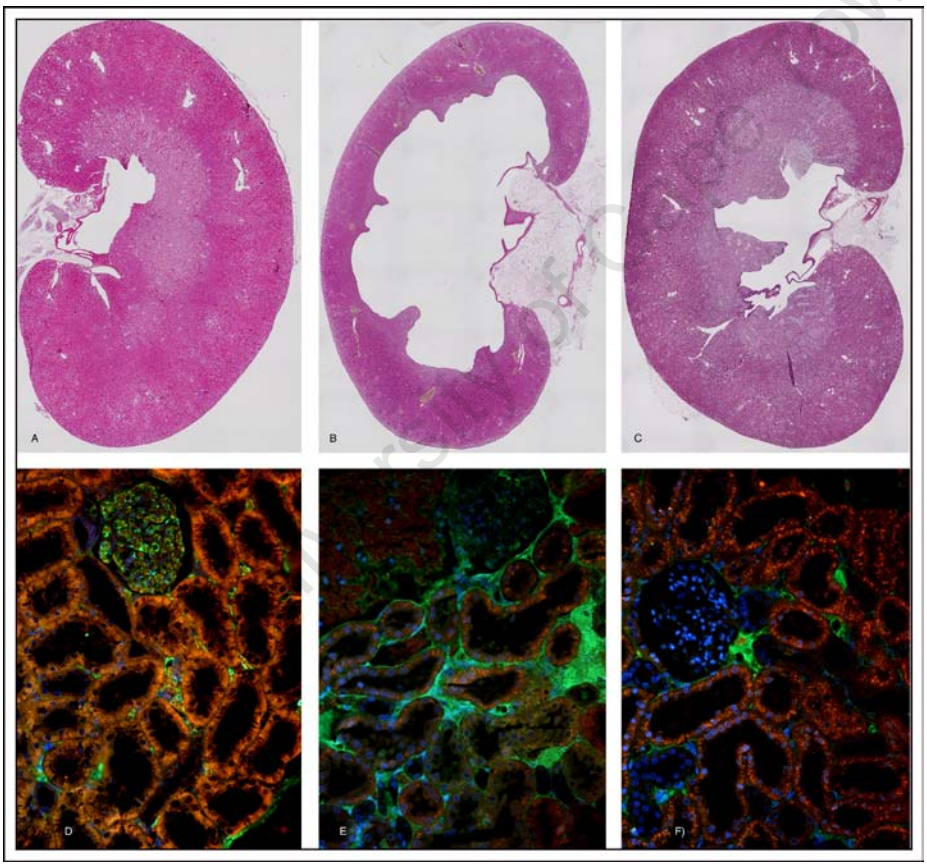

Figure 36 Histological Changes in the Kidneys of Zucker Rats; A - C Hematoxylin & Eosin on ZFR-L, ZFR-F and ZDF (Magnification 2 x tiled images). D - F Immunofluorescent Staining for IgG/FITC (Magnification 20 x).

3.5.2 Pancreatic Islet Morphological Changes

In the course of our study, we looked at the morphological changes that occurred in the pancreas within the 3 groups, with regard to islet morphology and insulin expression.

3.5.2.1 Materials & Methods (Pancreas)

The pancreas was harvested from ZDF- F, ZDF- L and ZDF - F rats and processed according to standard wax embedding procedures. Sections (3µm) were cut on a rotary microtome as previously described and stained for Haematoxylin and Eosin *(Appendix A-4),* modified Masson's trichrome *(Appendix-5)* and immunohistochemical *(Appendix A-7.4)* staining of Insulin, to determine morphological changes of the islets of Langerhans, beta cells and the surrounding acinar tissue. Image analysis data of the islet morphology was compared between the three groups with regard to the size of individual islets and the total islet area (JMP version 6.02 software, SAS, Cary, NC).

Results

The mean cross sectional area of islets in the ZDF obese rats was markedly higher than either the ZFR-F of ZFR-L rats (112493±35013µm^2 versus 44767±39001; p=0.024 and 23463±894; p=0.005respectively; Dunnett's t-test). The ZFR-L rats exhibited not only smaller, but also rounder, more uniform islets with defined boundaries compared to the ZFR-F and ZDF obese rats *(Fig-38).*

Positive immunohistochemical staining for insulin confirmed ongoing production in the beta cells of the ZDF group despite the abnormal morphology observed *(Fig 37).*

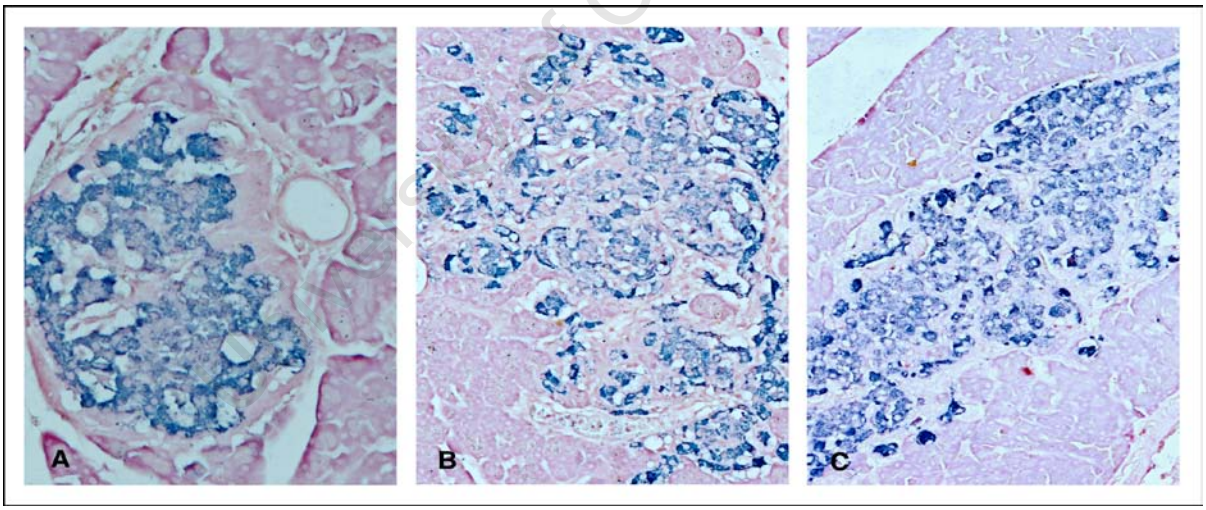

Figure 37 Insulin Immuno-staining of A: ZFR-Lean; B: ZFR-Fat and C: ZDF. Magnification 10x.

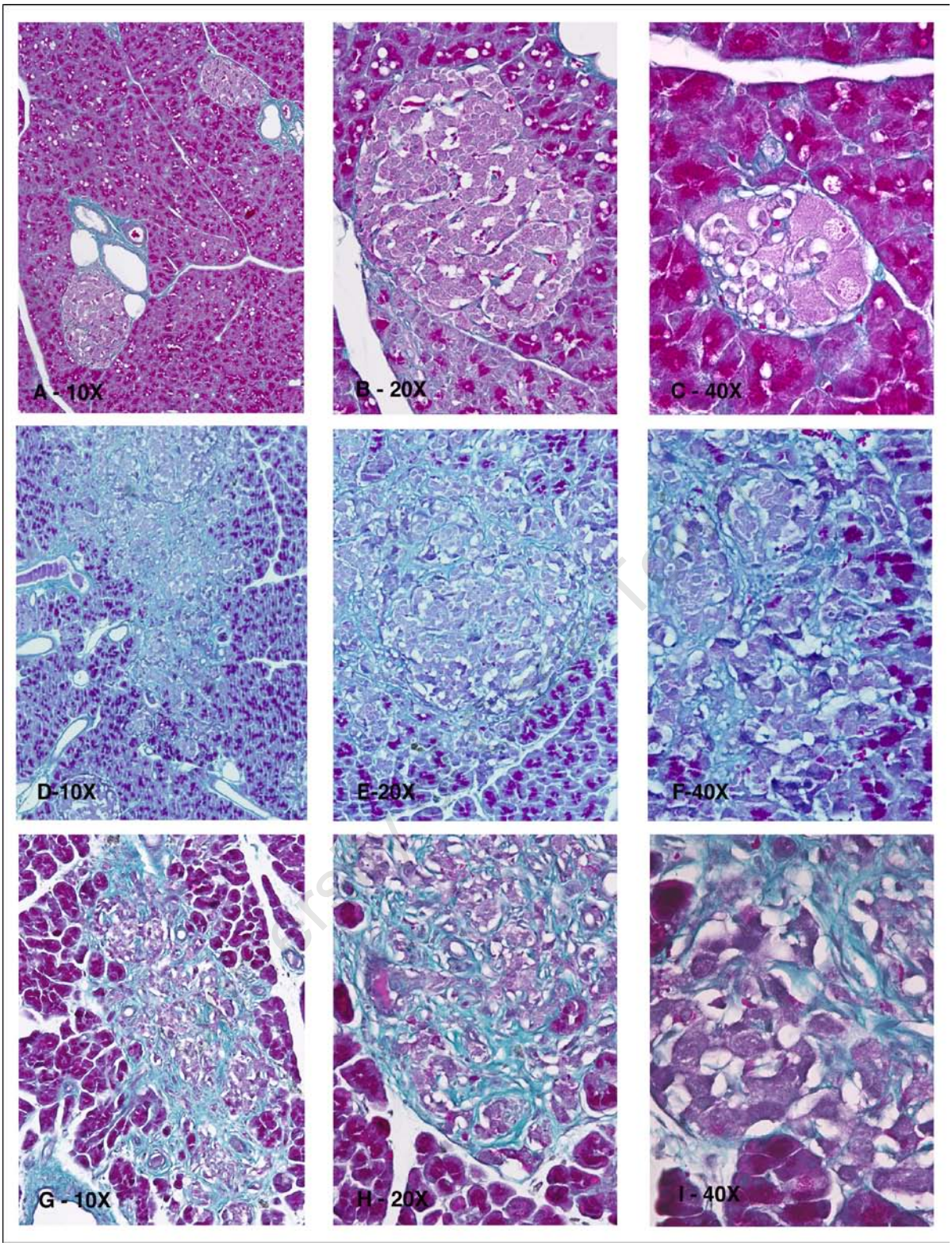

Figure 38 Histology of the pancreas: A-C Zucker Lean; D-F Zucker Fat; G-I Zucker Diabetic, stained with a modified Masson's trichrome. Magnification 10 x (tiled images); 20 x and 40 x.

3.6 Discussion

The restenosis in arteries following balloon angioplasty remains a major cause for concern. The role of obesity and MS in this pathological response, are not fully understood, however the phenomenon is believed to be exacerbated by hyperglycemia and IR. Obesity plays a role in the resultant EC dysfunction and development of IH and this is aggravated by, but not dependent on, hyperglycemia (120). This study of vascular morphology following injury has shed some light on the formation of IH, the components thereof within the intima, the effect on the endothelial glycocalyx layer and the effect of obesity on vascular pathology that follows.

The initial surgical intervention, which balloon angioplasty and stenting, represents, in itself elicits a response-to-injury, in the form of an inflammatory response and proliferation of SMC to the intimal area. The extent of the injury is determined by denudation of the endothelial surface, with or without rupture of the internal and even the second or more layers of elastic lamellae in the tunica media. The mechanical damage caused by intervention is variable and dependent on pressure applied during angioplasty as well as surgical isolation of the artery (in the case of animal models), and the effect of moving the balloon backwards and forwards within the vessel. This could be an external factor that may be seen as a limitation in the analysis of the response to IH, since the degree of IH is directly linked to the degree of endothelial denudation (121). The extent of the development of IH can be seen on the histology of the vessel through cross section, with obese animals displaying a greater level of IH than the lean controls. The ZDF group had a significantly lower level of IH, against our expectations, in spite of being overtly obese, with glucose levels higher than the normal range. This finding raises further questions with regard to obesity as a risk factor for IH, since the ZFR-F and ZDF groups were both overtly obese, but displayed such contradicting IH values.

In the stented groups, there was little variation in the degree of IH between all three groups. The pre-diabetic (ZDF) group displayed less IH than the ZFR-F group, in spite of being overtly obese. The mechanism for this is not clearly understood, but was previously documented by Jonas et al (2005) in a study on vascular response to stenting. Their finding was that the ZDF group displayed a similar degree of IH to that of the ZFR-L control group. Their suggestion is that the reduced IH is due to the weight loss incurred by diabetic rats in response to a hyperglycemic state, confirmed by previous studies (94, 106) and thereby creating a catabolic state. This highlights the role of hyperinsulinemia and IR as opposed to hyperglycemia as the driving force behind increased neointimal response (99). This was not confirmed by our study, as our animals were not yet hyperglycemic.

The presence of a stent significantly reduces the development of IH, within the stent area. Interestingly the area immediately beyond the stent showed a greater IH in the fat group, compared to the lean, and the ZDF group with a relatively high level of IH.

The majority of cellular material in the IH zone appears to be of ECM (60-80%) and SMC (20%) origin. The latter may be of the contractile (actin and myosin positive with a low proliferation rate or synthetic (myosin negative with a 10% increase in proliferation rate) phenotype, but producing four to five times more ECM deposition than the normal contractile phenotype. In IH there is an increase in the synthetic phenotype at the expense of contractile phenotype (122).

The intimal region of ballooned and stented vessels contained substantial amounts of elastin in this 21 day period, coinciding with the decreased secretion of PG (40).

The EC layer and the glycocalyx are critical to the normal functioning of the endothelial surface and play a vital role in the development of IH. EC dysfunction through mechanical trauma and a compromised glycocalyx affect the events leading to cell proliferation. The presence of endothelium was visualized by immunofluorescent VWF staining, and evidence of a glycocalyx was demonstrated by light microscopy, confocal and TEM. The discovery of the functions of the EGL in the past decade has brought to light the fact that this is a highly active layer constituting modulators in the formation of the NIH following vascular injury after PCI. Electron microscopy has been the only method of visualization of the glycocalyx since its discovery in 1962 (123). Ruthenium red or Alcian blue were used in the staining procedures, which have been refined sufficiently to enable the visualization of the glycocalyx. By 1979 the role of the glycocalyx was still unclear until Klitzman and Duling suggested that the vascular glycocalyx takes up a large proportion of capillaries causing limited capillary filling and low capillary haematocrits (32). In 1996 Vink et al reported that there was a “gap” between flowing red cells and the endothelium using intravital microscopy, suggesting that the glycocalyx measured approximately 0.4 - 0.5µm in thickness (124). Subsequently, much research has been done on the physiological role of the glycocalyx and to establish its thickness. This has been hampered by a lack of good visualization techniques. During histological preparation of samples, the glycocalyx is vulnerable to structural damage or dehydration, and therefore the method of TEM pre-preparation of tissue is critical for successful visualization.

The study of the EGL has revealed that it is not simply a bystander in the development of IH, as it is involved in shear stress changes that act as a mechanotransducer to the vascular wall. It possesses both anti-inflammatory and anti-thrombotic effects, it has an influence on the production of elastin, and it regulates SMC proliferation, and is known to be compromised in patients with DM2 who are prone to increased rates of NIH. The finding that HS stains the glycocalyx of balloon injured arteries could suggest that up-regulation of HS that occurs following injury may result in the expression of a much broader glycocalyx layer that then becomes detectable by light microscopy. Substantially increased glycocalyx on thickened IH may be a protective mechanism to deal with changes in FSS caused by luminal narrowing. Importantly, Bakker et al indicates that CSPG are increased in DM2 at the expense of HS. This may explain why ZDF display the EGL, as detected by HS staining.

Hydronephrosis is a pathology that occurs in Zucker obese and pre-diabetic rats but less so in lean Zucker rats (117). Morphological changes occurred in the kidneys of ZFR-F and ZDF rats, bilaterally in some cases. This was very rarely seen in the ZFR-L rats, and where present, was mild.

Hydronephrosis is the distention and dilation of the renal pelvis and calyces caused by obstruction of the free flow of urine from the kidney. This in turn leads to atrophy of the kidney. Renal complications include tubular dilation, necrotizing granulomas, inflammatory changes and pyelonephritis. Their findings suggested that the Zucker diabetic fatty rat (ZDF/Drt-fa) rat model closely mimicked the metabolic status of humans in NIDDM, and therefore offered a suitable model for research pertaining to this disorder (116). In 2007 Marsh et al completed a study on ZFR-F, ZFR-L and ZDF rats with relation to cardiovascular dysfunction and found that hydronephrosis was indeed a limiting factor for studies on renal or cardiovascular function, since both systolic and diastolic dysfunction was noted. Moderate to severe renal dysfunction was observed independently of obesity or diabetes in ZDF and ZFR-F rats, compared to mild dysfunction in ZFR-L and Sprague-Dawley rats. The combination of hydronephrosis and hyperglycemia, was confirmed as representing an adverse effect with respect to cardiac function. The presence of a low angiotensin II level in ZDF rats together with left ventricular dysfunction and increased norepinephrine levels, suggests a blunted rennin-angiotensin system (117). Chow et al conducted a study on mice in 2004, with regard to macrophage accumulation in the kidney, contributing to type II diabetic nephropathy, and concluded that macrophage-mediated injury to the kidney was associated with increased chemokine production and glomerular immune complexes (119). Nakagawa et al did a study on VEGF in relation to diabetic nephropathy, since decreased VEGF levels are associated with renal dysfunction. However in diabetics, renal dysfunction occurred in spite of high VEGF levels. The authors suggest that, since the protective role of VEGF could be due to it's ability to produce NO, and since NO is depleted in diabetics, perhaps the uncoupling of VEGF with endothelial NO was the mechanism by which VEGF caused diabetic nephropathy (118). A study by Erdely in 2004, found that obese hyperglycemic, hyperlipdiaemic zucker rats develop severe kidney disease due to a reduction in renal eNOS activity and nNOS protein abundance, which do not resemble human diabetic nephropathy (125).

Two possible methods of improving renal complications include the use of troglitazone, to correct IR and PPARy agonists that normalizes plasma glucose (126, 127). Hayashi et al demonstrated that the correction of IR with troglitazone restored the vasodilator action in micro vessels of Zucker obese rats, and was therefore a useful strategy for prevention of glomerular sclerosis in IR conditions. Baylis et al found that PPARy agonist was a potent protective component of chronic renal disease in the Zucker rat. Nevertheless, in our study, it did not appear to influence the extent of NIH, and the time-point studied here did not allow for catastrophic renal failure to develop.

The histology of the pancreas confirmed that obesity appears to have a direct effect on beta cell dysplasia. This takes place before the onset of hyperglycemia. This finding alone supports the argument for treatment of obesity ahead of that of atherosclerosis in an attempt to prevent vascular

disease. Obesity is clearly a risk factor for an enhanced intimal response to injury. This response is independent of glycemic levels, since the ZFR obese group was normoglycaemic as was the ZDF group. This suggests that hyperglycemia alone was not responsible for IH development.

The morphological dysplasia shown in the islet histology of the pancreas, indicate that metabolic changes or beta cell changes, occur early in the course of DM2 and that these changes are a result of abdominal obesity with excess FFA in the circulation which have an impact on IR. Histological confirmation of significant islet hyperplasia noted in the obese and diabetic rats, in comparison to the lean controls, may suggest that future treatment should be aimed at control of obesity before IR or hyperglycemia. Our data confirms the findings of Tokuyama et al in that the ZDF-F group had not yet become hyperglycemic, yet already presented with changes in islet morphology. Islets of diabetic rats become hypertophic and dysmorphic with several irregular projections into the surrounding exocrine pancreas (24).

The pancreas of obese and diabetic rats has displayed changes in islet morphology (24, 128, 129). Beta cells found within the Islets of Langerhans, make up 65-80% of cells in the islets. These cells produce and release the hormone insulin, which controls glucose metabolism. They also secrete C-peptide, involved in prevention of neuropathy, as well as amylin for glycemic control. Weir et al proposed that there are five stages of beta cell dysfunction with changes in beta cell mass, phenotype and function at each stage (130).

Beta cell dysfunction occurs long before hyperglycemia manifests itself (24) and patients presenting with diabetes type II have lost 50% of their beta cell function already (128). Holst et al, in an endocrinology review, suggested that incretins might be an exciting future target for treatment of type II diabetes. They reported that animal studies which had shown that the incretin (GLP-1) as well as inhibitors, DPP-4 (dipeptidylpeptidase) responsible for the degradation of GLP-1, lead to beta cell proliferation and cytoprotection. GLP-1 protects the ischemic and re-perfused myocardium in rats by a mechanism independent of insulin. GLP-1 is also known to improve endothelial cell dysfunction as well as increase left ventricular pressure (129). Inhibition of DDP-4 enzyme,T cell antigen could be a potential mechanism for preventing DM2, by enhancing circulatory levels of GLP-1. DPP-4 is currently on the market by Merck as Sitagliptin or Novartis as Viblagliptin. Holst conclude that incretin based therapy may halt progression of DM through their protective and perhaps trophic effect on beta cells (129).

In a review by Frode on drug testing using animal models with respect to their potential anti-diabetic activity, they highlight the importance of controlled food intake in determining the severity of the diabetic phenotype on the ability of beta cells to produce sufficient insulin. They also conclude, even as recently as 2008, that a standard model of experimental diabetes to study drug efficacy, has yet to be established (128). In his review, Frode lists natural products with anti-diabetic properties, and stresses the need to focus on other targets of pancreatic islet dysfunction in new models to determine the effects of medicinal plants for treatment of DM.

A large component of atherosclerosis and the higher post-percutaneous coronary intervention (post-PCI) risk for restenosis, associated with metabolic syndrome and DM2, involve an inflammatory response. This risk often translates into the requirement for vascular intervention or reintervention. This commonly involves either balloon angioplasty alone or together with stent deployment. PCI involves mechanical injury to the vascular wall in the form of endothelial denudation and disruption of the internal elastic lamella, but often extending to the external elastic lamella as well as trauma to the smooth muscle cells of the tunica media. This triggers an inflammatory response with migration and proliferation of SMC to the intimal area, together with T and B cell recruitment, in the formation of an intermediate lesion (93). In the complex inflammatory process following injury there is a release of cytokines, adipokines and proteins like adiponectin, MCP-1 and CRP as well as anti-inflammatory cytokines like TGF-beta and IL-10, which inhibit T cell mediated immunity (5).

The state of obesity commonly found in diabetic subjects, contributes to their pro-inflammatory condition. Adipose tissue is characterized by an abundance of macrophages that are a source of adipokines including CRP, IL-6, IL-8 and TNF-alpha (131). Yudkin et al. suggested that adipose tissue is associated with a chronic inflammatory state and that this may induce the IR and EC dysfunction that is associated with obesity and CVD (132).

CRP is synthesized in the liver in response to inflammation and adipose cells stimulate its production. The elevation of CRP levels, is a predictive marker for heart disease in healthy individuals and has been found to be elevated in the presence of obesity (132). The term hs-CRP refers to high sensitivity-CRP, which is an ultra sensitive laboratory test used for the detection of the protein, CRP. CRP levels are increased during systemic inflammation and this is implicated in increased risk of restenosis following balloon injury (33).

The recruitment of macrophages to the site of injury is part of the inflammatory response generated by balloon angioplasty. A 2006 study on the chronology of macrophage infiltration post injury, noted that macrophages infiltrate the area within 3 days following angioplasty, are still present at 14 days (133). Thereafter they begin to decline. Immunoglobulin G is produced by B cells as a secondary antibody immune response following activation by pro-inflammatory cytokines notably the interleukins. We assessed the degree of immune response following injury, using selected inflammatory markers. At the time point defined by our study, there was a distinct absence of inflammatory cells but a significant expression of inflammatory mediators such as CRP and IgG.

The complex mechanism of restenosis has confounded investigators for many years, and clearly targeting of individual role players has not achieved the desired mitigation of this process. Inflammation is a driving force, however, several other vitally important factors are required to alleviate this pathology.

Chapter 4
Carotid Artery Stenting in ZFR-L, ZFR-F and ZDF Rats.

The treatment of atherosclerotic lesions, typically involves the use of balloon angioplasty in combination with stent deployment to the stenosed area. In order to additionally assess the interaction of stenting with the effects of obesity and IR on IH development, we conducted a parallel study on three similar groups of rats; ZFR-F, ZFR-L and ZDF by performing angioplasty with the addition of stent deployment into the carotid artery.

4.1 Bare Metal Stents

Andreas Gruntzig first introduced stent implantation in 1977(69). This was a major breakthrough in the treatment of vascular stenosis, replacing coronary bypass surgery. Initial success rates were high, but in time, restenosis rates became unacceptably high. Intra-coronary stenting has to some extent addressed elastic recoil, but restenosis levels are in the region of 15-30% (81). Risk factors contributing to IH in stented arteries include lesion length, cross-section lumen area following stenting, atherosclerotic plaque, number & length of stents used, as well as clinical factors such as MS and DM2. The process of neointimal formation in stents following arterial injury primarily comprises thrombus formation, leukocyte activation and migration, SMC proliferation and migration and, finally, ECM formation. With thrombus formation, there is a release of cytokines and, therefore, stimulation of SMC proliferation. There is also an increase in matrix metalloproteinases (MMPs) that facilitates the proliferation of SMC and an early macrophage response, which give rise to PDGF, TNF-alpha, IL-1 and FGF. These cytokines play an important role in SMC proliferation. The anti-inflammatory marker CRP is increased after balloon injury and stenting. BMS have shown higher levels of CRP than DES following implantation when tested prior to, at 48 hr, at 72 hr and at two-weeks. Inflammatory reactions have been shown to increase with increasing medial damage or lipid core penetration by the stent, with the amount of restenosis being proportional to the extent of vascular damage and the extent of the inflammatory response. Gaspardone et al. also noted that higher CRP levels were associated with higher major adverse cardiac events (MACE), and persistent CRP levels after 48 hrs are associated with a greater incidence of restenosis (134). Subsequently, late thrombus formation following stent deployment, has led to MI, which has resulted in a loss of confidence in the long-term success of vascular stenting (135).

Animal studies have demonstrated that stent design has an impact on the degree of IH (136), while human studies had not been studied in this regard prior to by 2001. Hoffmann et al. conducted a human study in 2001, and suggested that the stent design had a significant impact on the development of IH. The corrugated ring Multi-link showed less IH than the Palmaz-Schatz and InFlow stents. This

is controlled by minimizing endothelial denudation during stent expansion and avoiding stent strut penetration of the vessel wall at deployment (137).

In diabetics, there is an increase in restenosis following PCI (138). Piatti et al. showed that IR and endothelial dysfunction together with stenting are early predictors of increased restenosis (139). The difference in morphological changes occurring during balloon injury as opposed to stenting includes the fact that, when using a stent, one avoids elastic recoil, vessel shrinkage and constriction, but sees rather vessel remodeling, increased SMC proliferation and increased NI formation (42).

The technical aspects of histological analysis of stented vessels have been challenging in the past, and limiting factors in the evaluation of restenosis. The development of the technique for resin embedding prior to this thesis involved traveling to the UK and USA in order to acquire the skills required. This also involved years of research into several different resin formulations that could accommodate our histological requirements. This culminated in a publication in collaboration with colleagues in Ottawa as a result of the research and development conducted as a preliminary to this study on comparative methods of sectioning methodologies of stented material (140) (see attached publication). The success in this technical field has made histological analysis of nitinol or stainless steel containing metal explants possible. There are two techniques currently in place for this procedure, namely sectioning with a tungsten blade on a rotary microtome or using a high-speed saw and grinding technique. Minimal damage to the tissue-stent interface occurs using a high-speed precision saw and grinding technique, but which is time consuming and results in substantial loss of tissue. Stent struts remain in place and undistorted. The bladed technique offers a wider range of special staining due to the fact that the resin is removed prior to staining. Occasional scoring or tearing of sections, together with stent distortion and displacement, can however occur. This technique results in minimal loss of tissue though, and it is possible to do serial sections and, in some instances, Immunohistochemistry.

4.2 Drug Eluting Stents (DES)

The DES was introduced in 2001 to address the problem of thrombosis, and for many years, they had a significant impact on the reduction of restenosis (141). Late thrombosis represents a major safety concern of stenting with at least 10% of BMS cases leading to MI. Studies comparing DES with BMS have been controversial, but seem to reflect similar success rates (142).

DES, containing coatings of Sirolimus or Paclitaxel, have been passed by the federal drug association (FDA) after undergoing clinical trials in 2001 *(Fig-39)*. Sirolimus, or Rapamycin, was originally an anti-fungal agent discovered in a soil sample on Easter Island (Rapa Nui) (143). It contains potent anti-inflammatory and immunosuppressive properties. Paclitaxel, in contrast, is a mitotic inhibitor, originally used for the treatment of cancer and now marketed under the name of Taxus (144).

In 2000 bioabsorbable stents, created from poly-L-lactic acid were used in a human study of 15 patients. The stent was self-expanding at 37°C. Restenosis rate and target lesion revascularization

(TLR) were only 10%, making them safe and feasible. There have been and continue to be a multitude of DES and dual DES under investigation in an effort to reduce NIH (145).

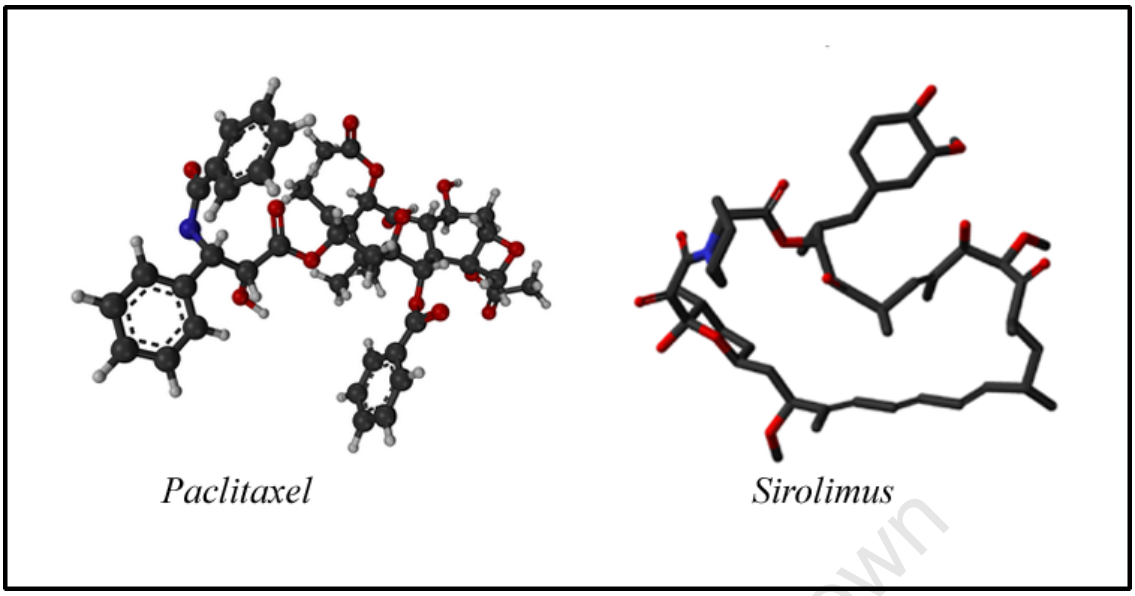

Figure 39 The structure of Paclitaxel and Sirolimus

4.3. Materials & Methods

As in the case of non-stented animals, three groups of Zucker rats chosen for stenting were ZFR-F, ZFR-L and ZDF. All the rats that underwent stent implantation were followed up for a 21day period. In the ZDF rats, glucose levels were monitored until they reached a level of 10mM before being entered into the study.

The rats were anaesthetized with ketamine/xylazine (200µl/400g; ratio 9:5ml; i.p), together with administration of buprenorphine (0.05mg i.m) as a prophylactic analgesic. Heparin (100U/Kg) i.v. was administered prior to arteriotomy. Surgery was performed with the aid of a stereomicroscope Nikon (SMZ 800). A balloon injury was performed as described previously, and the stent deployed and expanded to 8 bar of pressure followed by withdrawal of the balloon catheter. The circulation was restored via the ICA by removal of both the CCA and ICA vascular clamps, and the incision was closed once homeostasis was ensured. Retrieval of stents took place 21 days post operatively. A cannula was placed into the left ventricle and phosphate buffered saline (PBS, pH 7.4 containing heparin) was infused using a peristaltic pump. Perfusion fixation was performed with PFA (4% w:v) followed by surgical removal of the left and right carotid arteries into 4% PFA for 24 hrs, as described in the previous section.

4.3.1 Resin Embedding & Processing

Following fixation, stented-carotid arteries were processed manually, through graded alcohols (70%-100%), toluene, toluene/resin (1:1) and infiltrated with three changes of resin (Resin Solution: 1, II and III: 100%) according to the method by Erben et al. (146) *(See Appendix A-8)*. The following resin solutions were used: Solution I – 60ml methyl methacrylate (MMA Sigma: M5,590-9); 35ml butyl

methacrylate (BMA Sigma: 235865); 5ml methylbenzoate (Sigma: M2,990-8); 1.2ml polyethylene glycol (Sigma: 20,239-8); Solution II – 100ml solution I plus 0.4g benzoyl peroxide (Sigma-Aldrich: 228877); Solution III – 100 ml solution I plus 0.8g benzoyl peroxide. Polymerization took place at -20ºC over 72 hrs to enable slow, cold curing in a solution of 100ml solution III plus 400µl N.N-dimethyl-P-toluidine (Sigma: D18,900-6). A double embedding procedure was used to ensure that the stent remained in a vertical or upright position. The first embedding was into a 1.5ml micro centrifuge tube. This was removed by cutting the plastic tube open and the block was re-embedded into a 5ml polypropylene tube with a screw cap lid *(Fig-41)*. Polymerization took place under anaerobic conditions at 4C°. The resin blocks were cut from the polypropylene tubes and prepared for both saw grinding and tungsten carbide blade techniques of sectioning. *(Appendix A-8)*.

Three cross sections were taken to determine the formation of IH in the centre and at both ends of the stent (level b; c & d). In addition to this, a section was taken just before and just after the stent in order to determine the extent of IH taking place beyond the stent (level a & e) *(Fig-40)*.

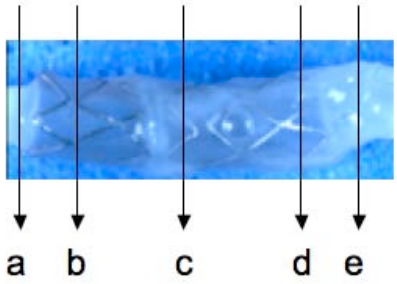

Figure 40 Schematic: Distribution of cross sections through the stent.

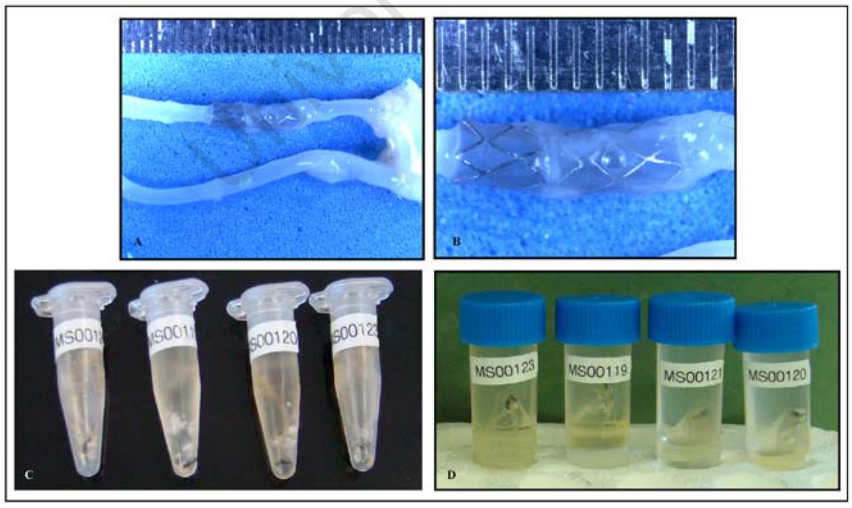

Figure 41 A: Macro-photograph of explanted right (stented) and left (control) carotid arteries together with the aortic arch. B: High magnification of expanded stent within the carotid artery. C: First resin embedding into 1.5ml micro-centrifuge tubes. D: Second embedding in 5 ml vials.

4.4 Histology

A Beuhler IsoMet 5000 high-speed precision saw [Dusseldorf; Germany] was used to cut sections (100µm) at a cutting speed of 3200 rpm with a feed advance of 12mm/min. A diamond-wafering blade (12.7mm x 0.4mm; Beuhler) was used. Continual water-cooling was employed throughout sectioning to reduce heat caused by friction. These sections were finely polished using a Beuhler Metaserve-2000 grinder [Dusseldorf; Germany] and two grades of sanding paper (600 & 800) grit to an approximate thickness of 8-10µm *(Fig-42 D-F).* This method of sectioning results in an intact, tissue-stent interface and undisturbed vascular wall. There is however substantial kerf loss (tissue depletion) due to the thick original section, and block preparation. Sections were stained for haematoxylin and eosin *(Appendix A-8.3.2)* and photographed on a Nikon 90i microscope. IA of IH was performed on these sections.

Thin sections using a tungsten blade were cut on a Leica SM 2500 sliding heavy-duty microtome to a thickness estimated to be between 5-10µm. Resin is removed using 2 methoxyethyl acetate and several special stains including selected immuno-fluorescent stains were performed. Sections were floated off onto 40% alcohol at 42°C, and bonded onto glass slides with Elmers glue (Cat No: 60308-Canada) and gently rolled with a rubber roller to flatten them *(Fig-42 A-C)*. They were clamped together and placed at 60°C overnight to ensure adherence of tissue sections to the slide (140).

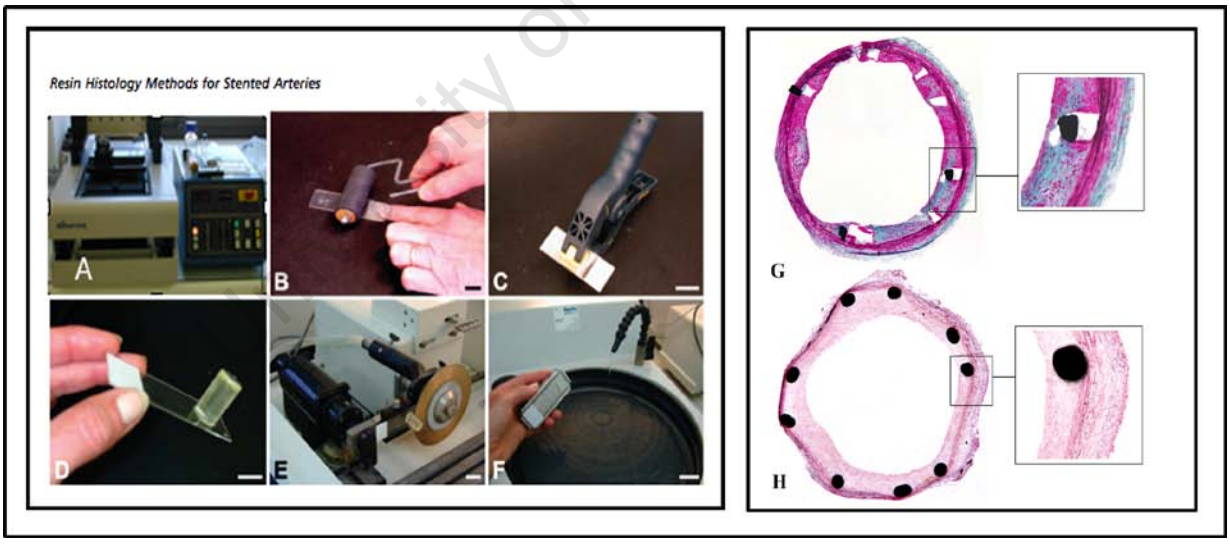

Figure 42 The Leica SM 2500, rolling and clamping technique in (A, B & C) and (G) the resulting bladed technique stained with Masson's trichrome. The precision high-speed saw and polishing technique (D, E & F) and (H) the resulting saw ground section.

Note the stent strut displacement & compression in the bladed section.

For the evaluation of elastin, SMC and collagen content, thin sections were cut on a heavy duty sliding microtome, the Leica SM 2500. This enables the removal of the resin and staining for Elastic

Masson's trichrome or modified Movat staining. Elastin is clearly stained in black up with Verhoef's elastin stain and muscle could be distinguished from collagen *(Appendix A-5).*

- ***4.4.1 Image Analysis:***

Image analysis was carried out using Adobe Photoshop 7.0, together with IPTK version 5 plug-ins (Reindeer graphics, Asheville, NC). The analysis was done on sections prepared using the saw & ground technique in order to preserve the tissue stent interface and avoid folding or scoring of the tissue.

The lumenal area (inside the hyperplasia) was measured, followed by the area inscribed by the IEL area and subsequently the EEL area. The areas occupied by stent wires was measured, and subtracted from the total IH area. Finally the intimal thickness was measured by finding the centroid of the luminal area and drawing perpendicular lines from this point to bisect the stent wires at their approximate mid point. Only the line from the stent wire to the edge of intimal hyperplasia was measured, reflecting the intimal thickness. This was performed again, now measuring the intimal thickness between the stent wires from the centroid of the lumen to the IEL *(Fig-43)*.

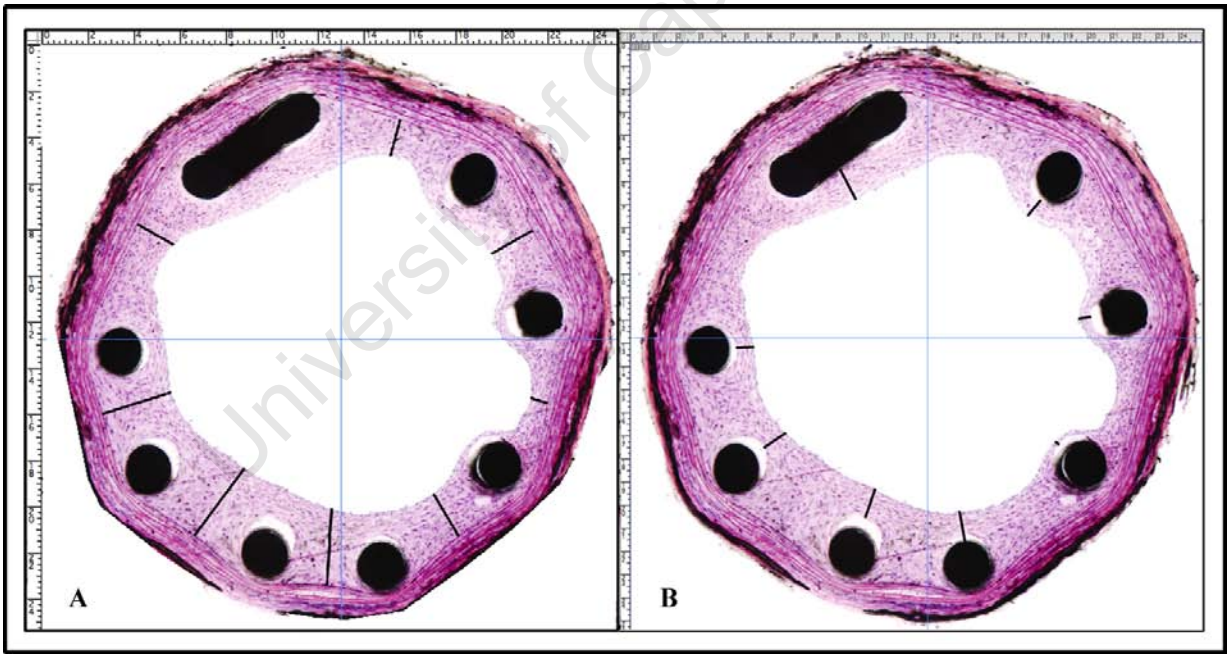

Figure 43 Image analysis: Measurement of IH area between the stent wires, from the lumen to the IEL in (A) and from the lumen to the stent in (B). The area taken up by the stent wires was subtracted from the total IH area.

Image analysis was also performed on sections of the arteries taken just beyond the limit of the stent. The luminal area, IEL area and EEL areas were measured and the thickness of IH calculated as described previously.

4.5 Results:

4.5.1 IH Comparison:

The presence of a stent reduced the IH quite considerably in all three groups, compared to the un-stented balloon injured experiments *(Fig 45*). The intimal thickness after 21 days following stent deployment over the three groups was non-significant. The mean intimal thickness between the wires (that is from the lumen to the IEL) was (129.8 ± 60.0µm, 120.3 ± 33.2µm and 141.4 ±100.8µm for the ZFR-F, ZFR-L and ZDF rats respectively; p=N.S). The intimal thickness over the wires (that is from the lumen to the stent wire, but excluding the stent area) was non-significant (79.5 ± 66.3µm, 96.4 ±58.3µm and 95.6 ± 97.6µm). Media thickness too was not significantly different between the groups (24.7±3µm, 32.4±5.9µm and 36.2±11.6µm for the ZFR-F, ZFR-L and ZDF rats respectively). The IM ratio in the ZFR-L group was significantly higher (5.8 ± 1.6µm) compared to the ZFR-F group (2.8 ± .02µm) and in the ZDF group (2.7 ± 1.3µm) (p=0.023). There was no significant difference in vessel stenosis between the three groups (35.8 ± 9.0%, 35.1 ± 8.1% and 43.8 ± 15.0%) for the ZFR-F, ZDF and ZFR-L rats respectively.

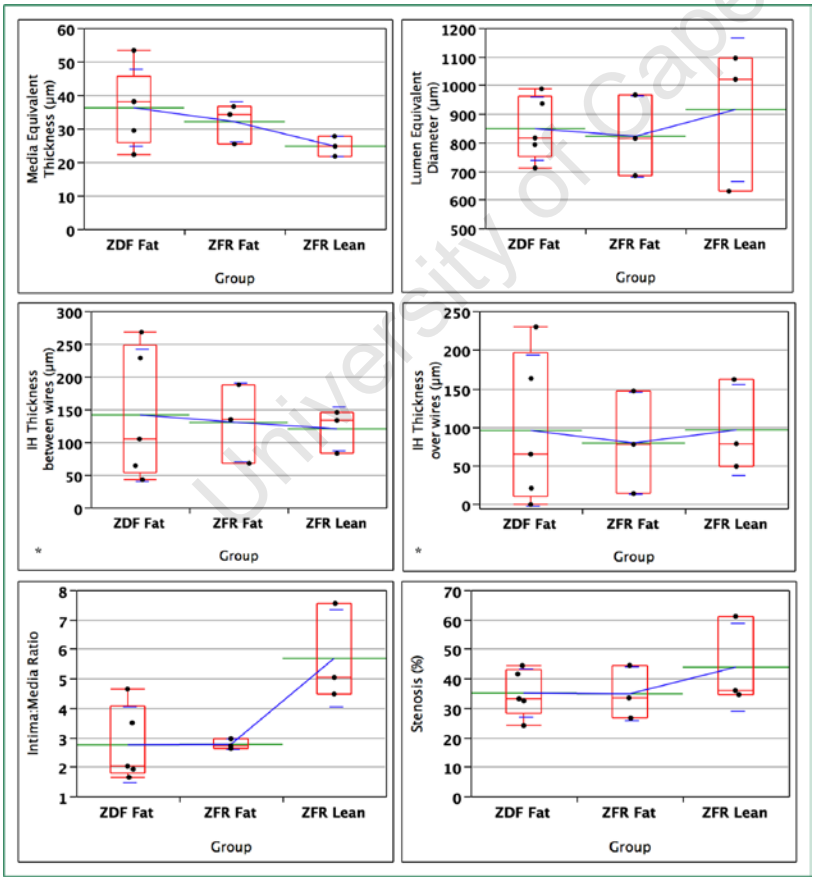

Figure 44 Graphs showing the medial thickness, lumen equivalent diameter, IM ratio and stenosis.

**** The intimal thickness between the wires indicates the thickness from the lumen up to the stent, and the intimal thickness over the wires indicates the thickness from the lumen to the IEL (excluding the area of the stent wires themselves).***

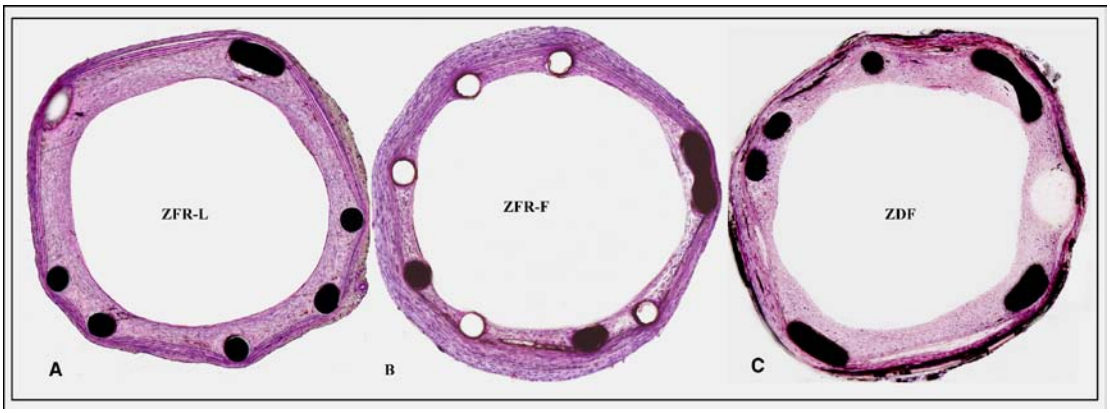

Figure 45 Stented Carotid artery in A-ZFR-Lean; B-ZFR-F and C-ZDF, sectioned on a high speed precision saw, ground and stained for Haematoxylin and Eosin. No damage to tissue-stent interface using this technique. (Original magnification 10 x)

4.5.2 Levels Beyond The Stent.

Sections were taken from the region beyond the stent from both proximal and distal ends, where there was sufficient tissue available, and stained in the same way as the stented sections. Image analysis was modified to exclude the presence of a stent. The parameters measured were lumen area, IEL area, EEL area and intimal thickness was calculated.

Comparison of ZFR-L, ZFR-F and ZDF beyond the stent showed a substantial increase in IH on either end of the stent *(Fig-46)*.

Medial thickness was 64.6 ± 10.6µm, 58.7 ± 11.3µm and 68.4 ±8.8µm for the ZFR-F, ZFR-L and ZDF rats respectively (p=N.S), a non-significant difference with (p=0.540). The I:M ratio was also similar in all groups 0.8 ±0.1, the 1.1 ± 0.7 and 0.6 ± 1 for the ZFR-F, ZFR-L and ZDF rats respectively. The extent of stenosis was also not distinguishable 17.3 ± 22.7%, 41.7 ± 14.5% and 30.2 ± 9.3% *(Fig-44)*.

The lumen equivalent diameter was also similar 821.3 ± 141.2µm, 914.9 ± 250.0µm and 848.2 ± 112.1µm for the ZFR-F, ZFR-L and ZDF rats respectively (p=N.S).

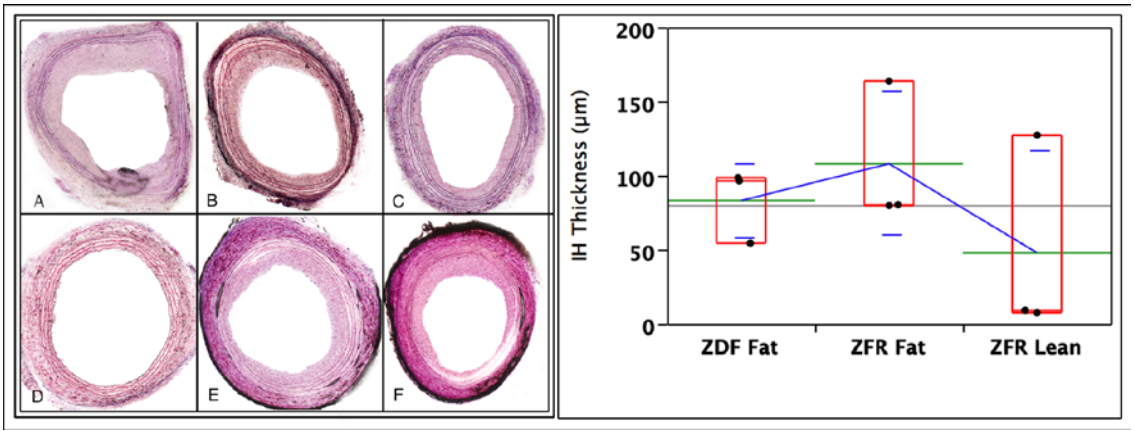

Figure 46 Levels beyond the stent: A&D - ZFR-L; B&E - ZFR-F; and C&F - ZDF-F Original magnification 10 x, as well as the results of the intimal thickness in the three groups (p=N.S).

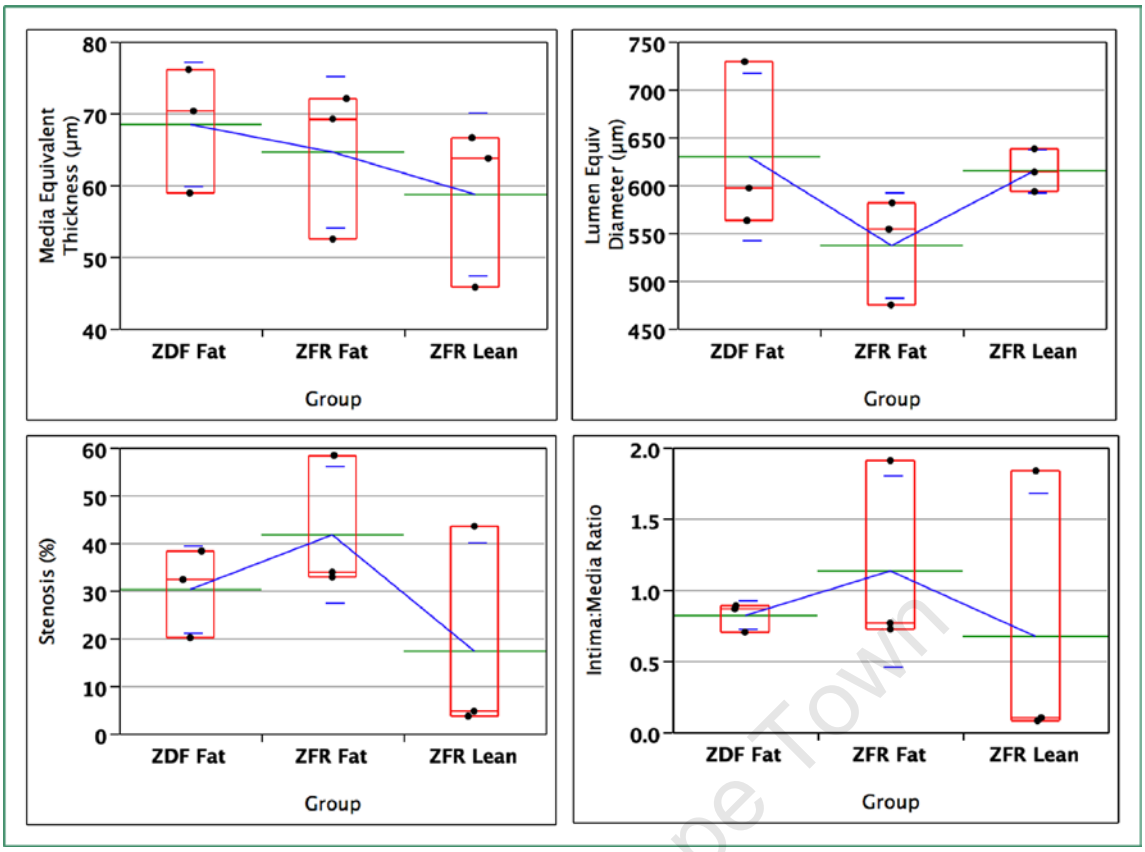

Figure 47 Media thickness, lumen equivalent diameter, % stenosis and I:M ratio graphs as measured on the levels beyond the stent.

4.5.3 Elastin In The Intimal Region: (Stented vs Ballooned)

In the stented vessels, elastin fibres stained clearly in the intimal region and had started forming dense bands of elastin around the SMC, as opposed to elastin fragments that could be seen at an earlier stage. This occurred inconsistently throughout the IH, and to varying degrees from one explant to another. There appeared to be a decrease in PG staining (in blue), while at the same time an increase in the presence of elastin. The balloon injured, non-stented explants also demonstrated the formation of dense elastin bands within the intimal region *(Fig-48)*. The extent of this varied between rats, even though all time points were kept the same.

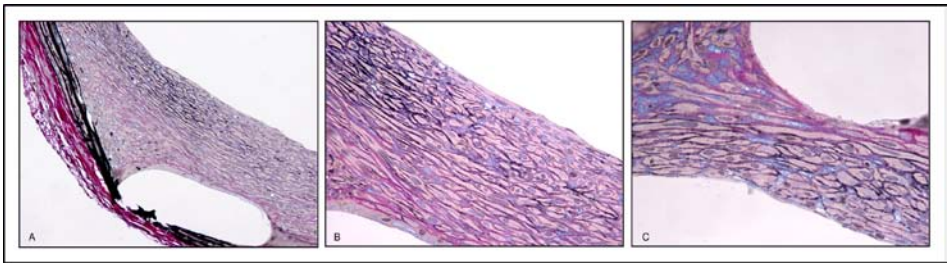

Figure 48 Resin embedded rat carotid artery 21 days after stenting showing the presence of elastin in between the SMC in the intimal hyperplasia region stained with modified Movat, on blade cut sections that the resin removed.

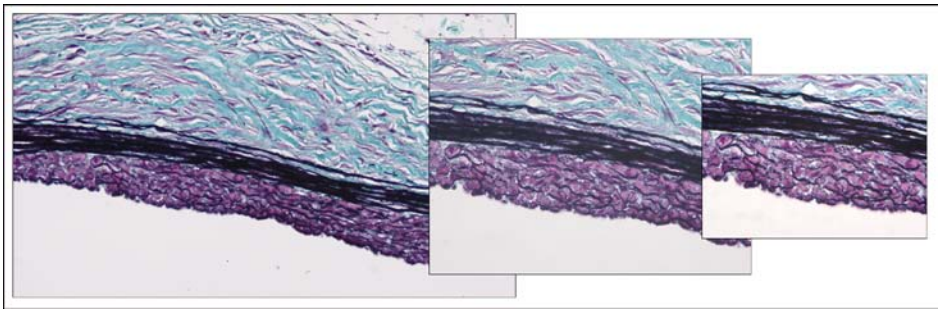

Figure 49 Wax embedded rat carotid artery (ZDF) 21 days after balloon injury showing elastin forming rows in the intimal region, stained with elastic Masson's trichrome .

4.5.4 Inflammation: (Auto fluorescence)

Macrophages were present 21 days following stent deployment, particularly concentrated around the stent strut region. Due to technical challenges relating to resin immunohistochemistry together with rat tissue, the rat specific ED 1 immuno stain was not successful on resin embedded rat tissue. Therefore polished, saw-ground images were subjected to UV light to visualize macrophages which auto-fluoresced and which were then assessed microscopically *(Fig-50)*. There were no significant differences between the three groups, but there were also no macrophages in the intima or media of the non-stented control vessel, in contrast to their stented counterparts.

Staining for inflammatory cytokines that were performed in the wax embedded balloon injured rats were unfortunately not possible on resin sections.

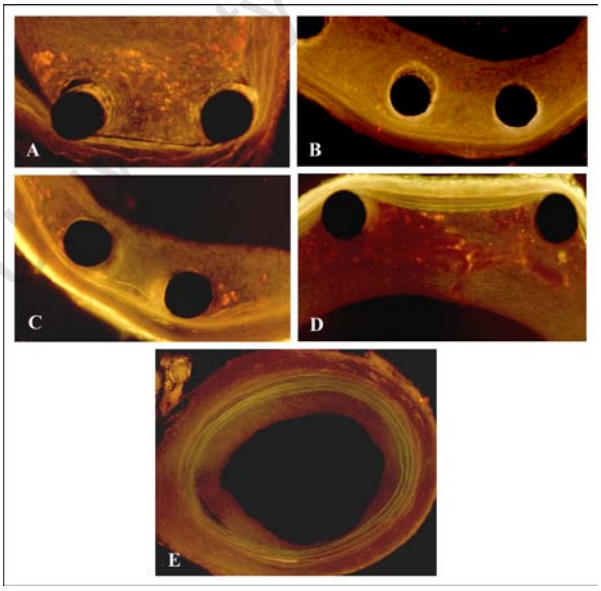

Figure 50 Auto fluorescent images of thick saw/ground sections showing macrophage auto-fluorescence

(A) ZFR-L; (B) ZDF; (C) ZFR-F and (D) ZFR-Lean), four different explants in comparison to that of a section just beyond the stent (E)-ZDF showing complete absence of macrophages.

4.6 Discussion

- 1977 - Andreas Gruntzig introduced PCI
- 1986 - Introduction of BMS
- 2001 - The development of DES
- 2009 - In – stent restenosis & thrombosis remains the confounding pathology of coronary intervention

The much needed stent industry has experienced many challenges since their inception, including late stent thrombosis and restenosis. They have revolutionized the management of CVD with a procedure that does not require a general anesthetic and is simple with a much reduced hospital stay. compared to CABG. Controversial data exists regarding the benefits of DES over BMS, and while the former may be found to lower rates of repeated revascularization, the risk of late thrombosis remains.

Our findings showed a definite reduction of intimal thickening in ZFR-L, ZFR-F and ZDF rats within the area of the stent. There were no consistent differences in the degree of IH between lean and obese groups. The expectations of an increase in restenosis previously described in diabetic subjects were also not confirmed by our experimental data. In accordance with Jonas et al, our ZDF group instead displayed less intimal thickening than the ZFR-L group in balloon injured animals. In the stented groups there was no significant difference in the extent of IH.

There continues to be a macrophage presence in the area adjacent to the stent struts after 21 days, presumably in reaction to the foreign material. In spite the ability to perform immunohistochemical stains on human and primate tissue using this resin formula, the combination of this resin and rat tissue unfortunately did not afford us the opportunity to perform in depth immunohistochemistry for inflammatory markers or HSPG.

The large amount of IH just beyond the stent was an interesting finding. Analysis confirmed that the ZFR-F group showed the greatest degree of intimal thickening beyond the stent, although this group was not statistically different from the ZFR-L or ZDF groups.

The sub-endothelial layer separating the endothelium from the IEL is an essential and complex layer without which, ECs cannot adequately attach themselves to form a confluent single cell layer. Elastin is a major component of the ECM, which is composed of ECM components providing cell with adhesive properties to enable adequate EC anchorage. Smooth muscle cell migration & proliferation together with ECM formation contribute to the development of intimal thickening. There is a substantial amount of elastin present in the intimal region of the artery following angioplasty as described by Aoyagi in 1996, when they linked the synthesis of elastin to proliferating smooth muscle cells and in the development of atherosclerosis (147). Strauss et al. suggested that elastin synthesis is

increased following arterial injury, while Nikkari et al. claimed that elastin synthesis was maximum at 2 weeks and decreased at 4 weeks after injury (40). Tropoelastin is a precursor protein of elastin, which is secreted by fibroblasts and SMCs and assembles to form mature elastin that is cross-linked by lysyl oxidase once excreted into extra cellular space. A 1998 study by Forough et al. demonstrated that tissue inhibitor metalloproteinase (TIMP-1) over expression in balloon injured arteries modulates proteolytic activity which assists in reducing IH. They deduced that MMP cause physical manipulation of the vascular wall, which increased elastin accumulation and that the injury to the intima of arteries accelerates elastogenesis (148).

The implications of having a well formed, stable IEL in order to have functional artery, have been stressed by Sims, however there are several contributing factors essential to this process, without which an injured vessel cannot execute repair and re-endothelialization.

The use of surface coatings with natural matrix components such as elastin or fibrillin-1 have showed that ECs attach poorly onto elastin coated PU or polycaprolactone (PCL) scaffolds, and displayed impaired functional properties. Fibrillin-1 coated surfaces had confluent EC monolayer coverage with stable functional characteristics, inhibiting SMC migration into vascular graft scaffolds (149). Thus it would appear that while a well-formed IEL is absolutely necessary to a healthy vessel, the sub-endothelial layer between elastin and the EC is of critical importance. This layer is a complex three-dimensional layer composed of PG and glycoproteins, laid down by the endothelium and is responsible for modulation of vascular tone and thrombogenicity, while providing an anchorage for cellular interactions. The IEL is composed of not only elastic fibres, but fibrillin microfibrils and PG as well. This would suggest that none of these components could operate individually to develop and sustain a healthy, functional and stable endothelium. The artery wall is dependent on an intact IEL, a confluent endothelium and the presence of a PG rich glycocalyx layer. Several studies have been done whereby vascular grafts have been coated with growth factors, heparin, elastin or PG etc in an attempt to stimulate development of an in-tact endothelium on the luminal surface, however, there is a need for further studies incorporating a combination of these components which are dependent on one another in order to endothelialize the inner surface of a vascular graft or stent (150).

Histologically, the arteries appeared to be well endothelialized and the tunica intima contained substantial amounts of elastin, SMC (Actin stain), collagen and PG (Movat Stain).

This year, 2009, has seen the promising two-year follow up report of the bioabsorbable everolimus-eluting stent in single de novo lesions (151). The elution of this drug restored the vasodilation and vasoconstriction in stented vessels in contrast to first generation stents that demonstrated vessel constriction during exercise. In addition this year has seen the development of a computer model by Elazer Edelman, a pioneer in drug delivery systems, used to predict stent performance under varying conditions. Through the use of computer modeling, this allows changes to stent configuration, materials, vessel wall shape and drug flow propulsion to evaluate the distribution of drug in different areas of the vessel wall. These developments offer promising future improvements to stent technology.

There is much work to be done on stent related complications, and DES are still associated with adverse vascular healing and endothelial dysfunction, as well as late thrombosis (142). Our data shows that there is clearly a benefit of reduced IH with the use of stenting as one of the treatments for vascular stenosis. Ongoing research in this area of technology together with pharmaceutical approaches, can only improve its current success in limiting SMC proliferation following coronary intervention.

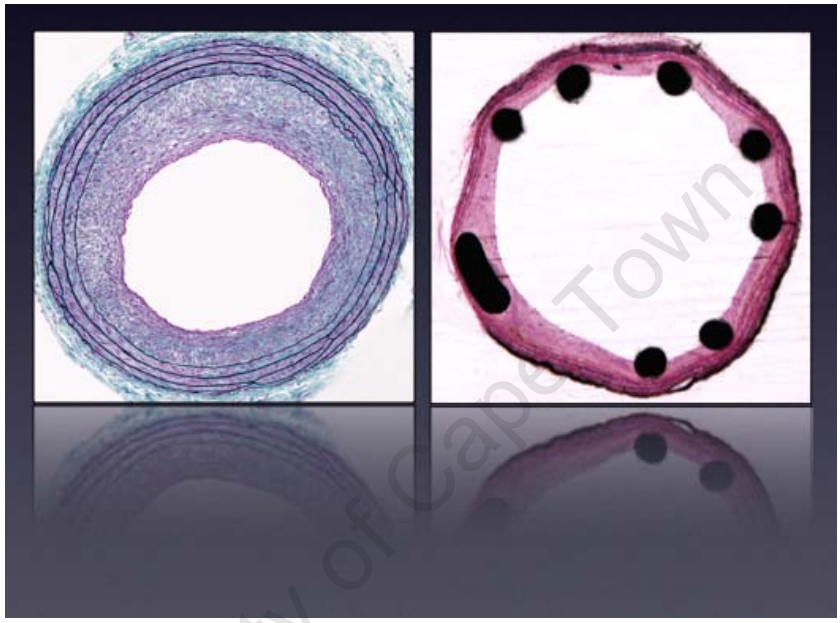

Chapter 5
Other Models of Intimal Hyperplasia

5.1 Introduction

Just as intimal hyperplasia as a consequence of PCI is analogous to the process of smooth muscle cell migration and proliferation in atherosclerotic disease, it is also a consequence of a variety of pathological situations. This includes CABG where the SV is used to bypass a diseased coronary artery feeding the heart muscle and vein grafting, in which the SV is placed into a peripheral artery for similar reasons, arterial stenting, be it endovascular, to relieve occlusion or extra vascular, as a means of support for a vein exposed to arterial pressures, likewise exacerbates this process. Trans-anastomotic ingrowth from the suture lines of a bioprosthetic graft is yet another form of IH, often referred to as pannus. Vascular grafting continues to be limited by the development of IH 100 years after it was first introduced (121, 122). The sequence of IH formation after balloon injury in PCI has similarities to the process that develops following vein grafting, however these two scenarios expose the grafted vessels to different haemodynamics and shear forces. Although a vascular graft does not undergo the endothelial denudation that occurs during balloon angioplasty, it has been shown to suffer a loss of EC within ? 24 hours following surgery (122). There is also a mismatch of elastic properties between the vascular graft and the native vessel. A vein that is placed into the arterial position becomes exposed to a change in arterial pressure from 0.2 dyne/cm^2 to 3-6 dyne/cm^2. The resulting neointima is composed of around 20% of proliferating SMC with its origin in the media, which in turn deposit ECM and which makes up 60-80% of the intima (122).

For the purpose of this thesis, a retrospective analysis of vascular grafts was performed in Chacma baboons in a comparable study using externally stented, SV grafts placed in the femoral as well as the coronary position in the same animal (152, 153). The extent of intimal hyperplasia was assessed in comparison to a non-stented control in the opposite femoral artery of the same animal (A).

A largely unrelated form of IH involving the proliferation and migration of SMC is that of trans-anastomotic ingrowth following implantation of bioprosthetic vascular grafts. This model also stimulates the use of bioprosthetic heart valves. This tissue needs to be stabilized with cross-linking agents and is devoid of an endothelium. Bioprosthetic tissue does not respond with sub-intimal SMC proliferation due to this cross linking but has the advantage of being immunogenic despite masking of the antigenic sites(154).

Once again in a retrospective study of the use of porcine bioprosthetic tissue implanted into the iliac position in baboons, the development of IH originating at the anastomosis through to the luminal surface was analyzed (B).

5.2 Coronary Artery Bypass Graft (CABG), Vein grafting & Extravascular stenting

In this analysis we compared the response to vascular grafting of the SV into the femoral position to the externally stented equivalent on the opposite side. The coronary artery underwent CABG using a SV with an external mesh support in the same animal. The mesh used in this study was nitinol, (a titanium and nickel alloy) 6 weeks and 12 weeks.

The graft was dissected with at least three representative mid-sections and a longitudinal section at each anastomoses as seen in *(Fig-51.)*. One of each stented sample was de-wired and embedded in wax and used for immunohistochemitry and one mid-section was embedded in resin and sectioned with a tungsten carbide blade. Blocks were already made and were just sectioned and stained as described below.

5.2.1 Material and Methods

5.2.1.1 Elastic Masson's Stain

To assess intimal thickening, 3µm sections were stained for Masson's trichrome stain to differentiate muscle from collagen as well as elastic fibres *(Appendix A-5*). Images were taken using a Nikon (90i) microscope at 4 x magnification, and tiled together to form one image *(Fig-51)*.

5.2.1.2 VWF

Section (3µm) were cut on a rotary microtome, Microm HM360 and mounted on coated slides. They were stained for Von Willebrand factor to detect endothelial cells, using immuno-fluorescent techniques *(Appendix A-7.1)*. Pre-treatment with proteinase K (*Diagnostech-S-302080 Denmark)* for 20 minutes was used as antigen retrieval followed by overnight incubation with rabbit anti-VWF *(*(ab6994 *Cambridge; UK)* diluted (1:400) in 1% BSA/PBS at 4°C. This was followed by washing in TBS and incubation with a Donkey anti-rabbit IgG/Cy 3 *(Jackson's Immunochem;Pennsylvania;USA)* secondary antibody for 2 hours. Sections were washed in TBS and mounted in Vector-shield DAPI mountant and photographed on the Nikon (90i) microscope.

5.2.1.3 Heparan Sulfate

Standard immunohistochemical staining for the presence of heparan sulfate (HS) was performed *(Appendix A-7.2)*. A monoclonal antibody rat anti-human HS Abcam (ab2501) *(Cambridge; UK)*. Proteinase K *(Diagnostech-S-302080 Denmark)* digestion for 10 minutes was performed to enhance antibody staining. Primary antibody incubation diluted in 1% BSA was performed overnight at 4°C. Goat anti-Mouse (HRP) bioyinylated secondary antibody (*Histomark 71-00-29 KPL-Gaithersburg; USA)* was used for detection, followed by Streptavidin peroxidase. *(Histomark-71-00-38 Gaithersburg; USA)* and Histomark True Blue *(Histomark-71-00-68 KPL-Gaithersburg; USA)* chromogen. Air-dried sections were dipped into xylene, and mounted in Entellan. Images were captured on a Nikon 90i microscope.

5.2.1.4 Macrophages (CD 68)

For the detection of macrophages 3µm sections were pre-treated with Proteinase K *(Diagnostech-S-302080 Denmark])* for 10 minutes, before incubation with the primary monoclonal antibody CD 68 (Diagnostech M0814) for 1 hour at room temperature *(Appendix A-7.1).* This was followed by washing in TBS and incubation with a secondary antibody, Donkey anti-mouse Cy3 *(JacksonsImmunochem; Pennsylvania; USA)* for 2 hours. Sections were washed in TBS and mounted in Vector-shield DAPI mountant.

5.2.2 Results

The control group showed a moderate formation of IH layer beneath the endothelium compared to the mesh reinforced groups. In the stented SV there was a significant degree of constriction of lumen diameter *(Fig51).*

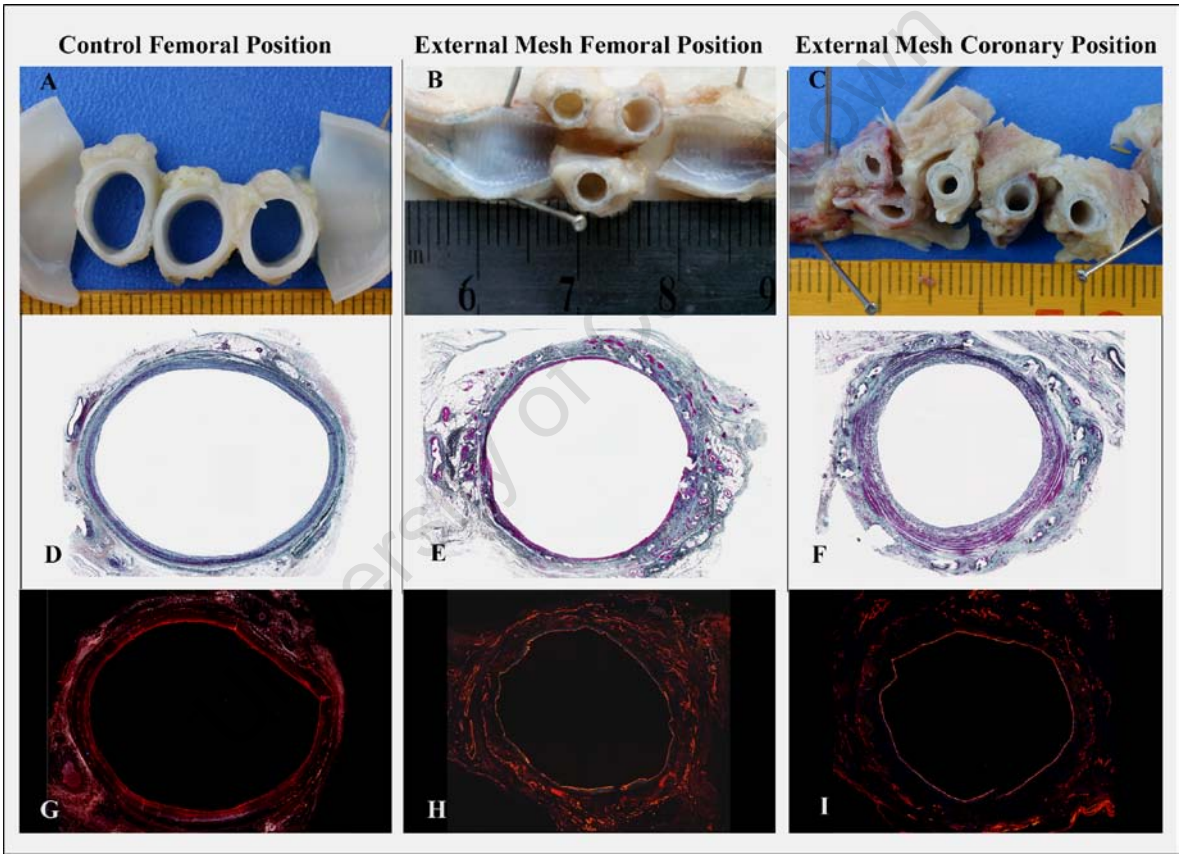

Figure 51 Microphotographs of (A) control SV, non-stented placed in the femoral position, (B) externally stented SV placed in the femoral position and (C) externally stented SV placed in the coronary position. (D-F) elastic Masson's staining of the same group respectively and (G-H) Von Willebrand Factor on equivalent sections with wires removed. Original magnification of microscopic images was 4x.

There was a distinct macrophage absence in the control vessel as well as in the externally stented arteries at both time points, as detected by CD 68 macrophage staining.

VWF staining confirmed full endothelialization in the control and mesh reinforced groups as well as the pre-implant samples. After both 6 week and 12 week time points *(Fig-51 and 52)*.

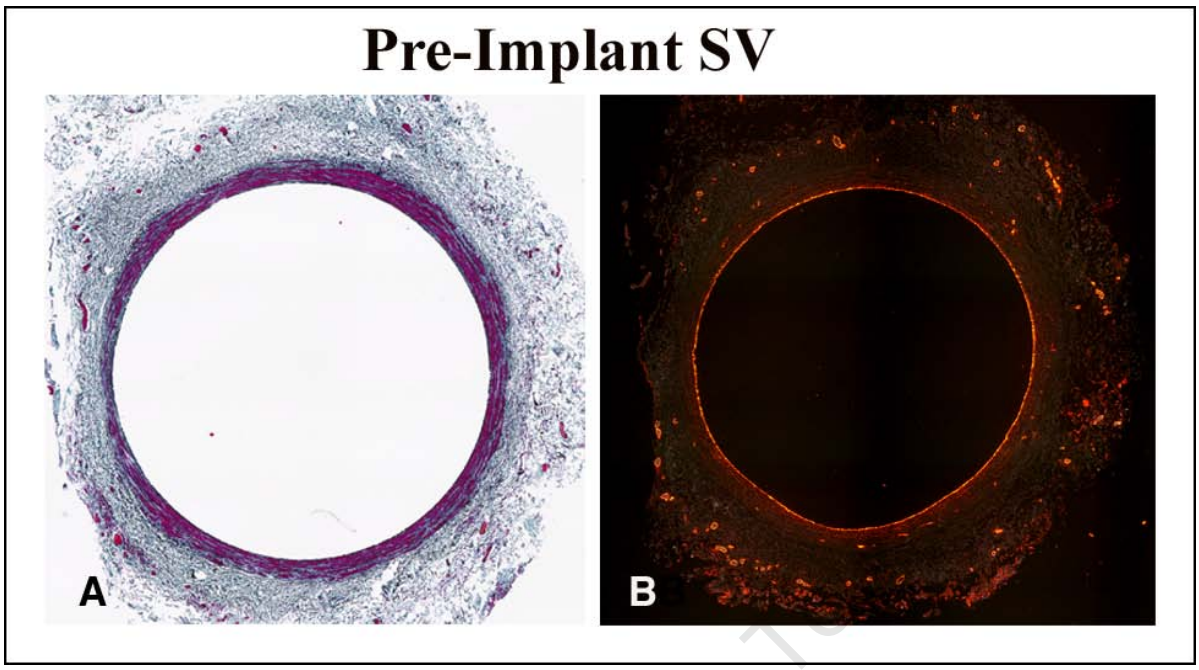

Figure 52 The pre-Implanted SV shown (A) elastic Masson's staining and (B) VWF fluorescent staining showing a full endothelium, as well as adventitial vessels. Original magnification 4 x.

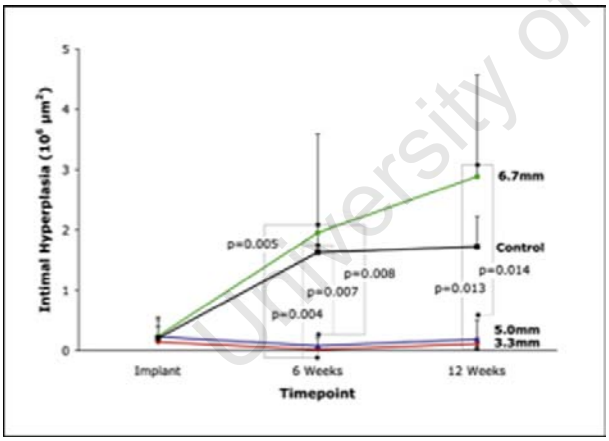

Figure 53 IH of cross sectional area showing the majority of hyperplasia occurring in the first 6 weeks (152).

Immunohistochemical staining of Heparan Sulfate confirmed the presence of an endothelial glycocalyx layer on the luminal surface in both femoral and coronary positions of control veins without mesh support. The pre-implant sample showed no HS staining throughout the vein wall, but stained positively on the vascular endothelial cells *(Fig-52)*.

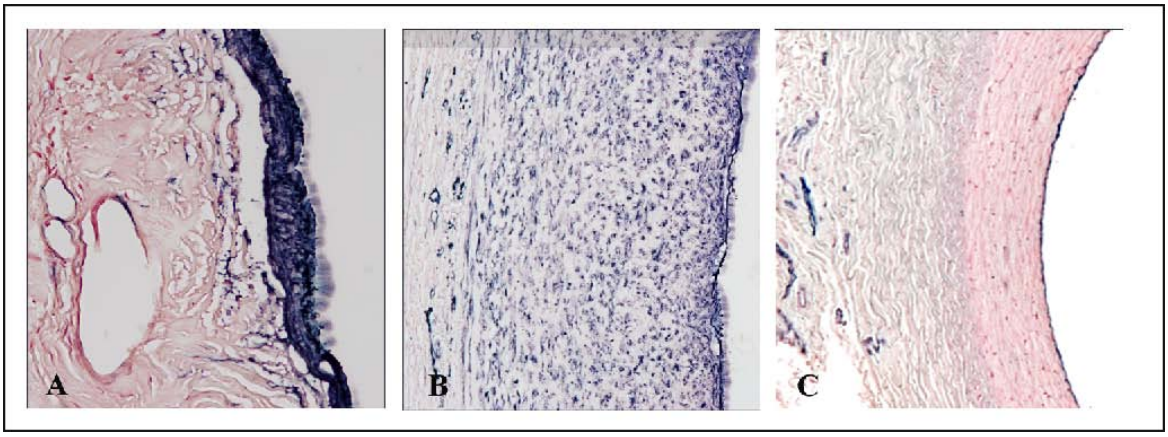

Figure 54 Immunohistochemical staining demonstrating elevation of Heparan Sulfate in stented SV in the femoral (A) and non-stented SV in coronary positions (B), as well as the presence of the endothelial glycocalyx on the luminal surfaces. The pre-implanted SV (C) shows no HS staining in the wall, only in the vascular endothelium. Original magnification 20 x.

5.3 Bioprosthetic Artery graft

Iliac interpositional, porcine, graft was grafted into the iliac artery of a non-human primate (Chacma baboon)

5.3.1 Materials and Methods

The study involved grafting a porcine aortic tissue graft into the iliac circulation for 42 days. Wax embedded tissue was sectioned (3µm) on a Microm HM360 microtome onto coated glass slides and stained. Staining was performed using Elastic Masson's trichrome stain, anti-heparan sulfate for glycocalyx detection, VWF immunofluorescence for endothelium and CD-68/CD-3 double stain for inflammatory cells including macrophages and lymphocytes.

5.3.1.1 Elastic Masson's Trichrome

Sections (3µm) were dewaxed and stained using the Masson's trichrome stain according to *(Appendix A-5)*. Images were taken on a Nikon (90i) microscope.

5.3.1.2 VWF

Standard immunofluorescent techniques as described in *(A-7.1.)* were used to demonstrate the presence of endothelial cells staining using VWF antibody, in combination with a fluorescent secondary antibody. Sections were photographed on the fluorescent microscope (Nikon 90i).

5.3.1.3 Heparan Sulfate

Staining for the presence of heparan sulfate (HS) was performed using standard immunohistochemical technique *(Appendix A-7.2)*. The Abcam (ab2501), A monoclonal antibody rat anti-human HS was applied after Proteinase K digestion for 10 minutes was performed to enhance antibody staining. Primary antibody incubation (in 1% BSA) was performed at 4°C, overnight. A goat anti-Mouse (HRP) bioyinylated secondary antibody was used, followed by Streptavidin peroxidase based visualization

using Histomark True Blue chromogen. Air-dried sections were dipped into xylene, and mounted in entellan. Images were captured on a (Nikon 90i) microscope.

5.3.1.4 Inflammatory Cells

Double immunofluorescent staining was used to stain both macrophages and T-lymphocytes. The method is described in detail in *(Appendix A-7.5)*. The section was incubated with a cocktail of two antibodies, namely monoclonal Mouse anti human CD 68 and polyclonal Rabbit anti human CD 3. Similarly a cocktail of secondary antibodies was used (Donkey anti-mouse Cy3 and Donkey anti-rabbit Alexa 488) for detection. Images were captured using a Nikon 90i fluorescent microscope.

5.3.2 Results

5.3.1 Hyperplasia

There was transanastomotic ingrowth originating from the medial tissue, through the anastomosis to the luminal surfaces both proximally and distally, extending over both the graft as well as the native artery *(Fig-55)*. The pannus layer is made up primarily of SMC and ECM components but in addition contained a large population of inflammatory cells including macrophages and lymphocytes.

5.3.2 Glycocalyx

There is an extensive glycocalyx layer covering the surface of the hyperplasia as demonstrated by immunohistochemical staining of HSPG *(Fig-56)*. The layer of trans-anastomotic ingrowth as well as the native artery also demonstrates strong staining for HSPG differentiating it from the surrounding adventitial tissue. Vascular endothelial cells can be seen staining positive within adventitia.

5.3.3 Inflammation

Double immunofluorescent staining demonstrated an extensive population of macrophages and lymphocytes surrounding the entire graft, including the pannus area. Multi-nucleated foreign body giant cells were also detected by the double stain *(Fig-57)*. The inflammatory cells were seen to cluster at the cut edge of the graft, close to the graft as well as within the pannus.

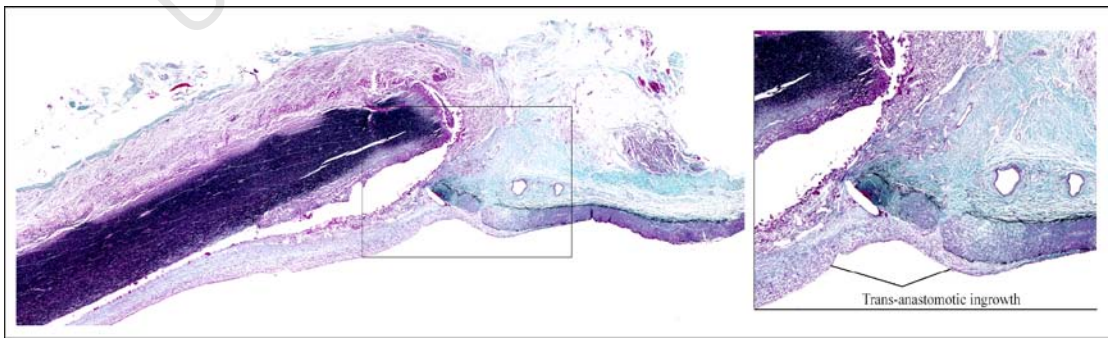

Figure 55 Elastic Masson's trichrome staining of the anatomosis of a bioprosthetic porcine graft, showing the extent of the IH on both the bioprosthetic graft as well as the native artery. Original magnification x 2

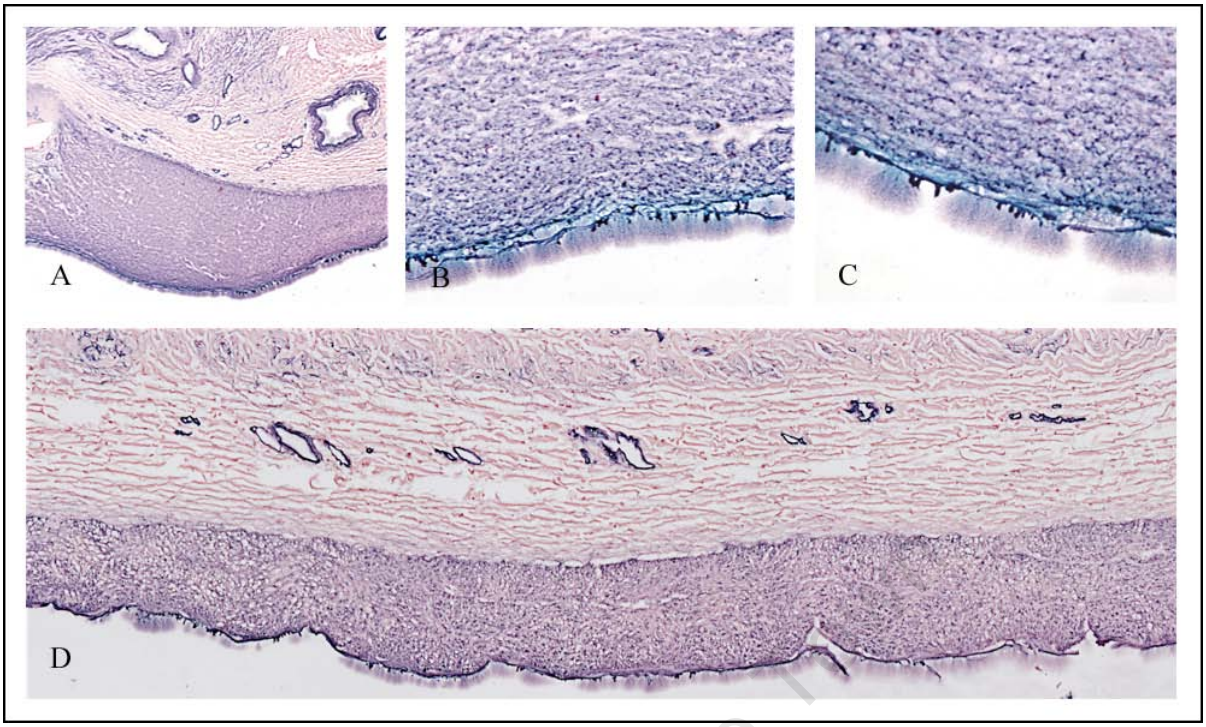

Figure 56 Heparan Sulfate staining showing the positively stained intimal area (IH) and the native artery beneath is negative except for the vessels within the wall, with a glycocalyx on its surface. Magnification 20 x; 40 x; 60 x and 4 x.

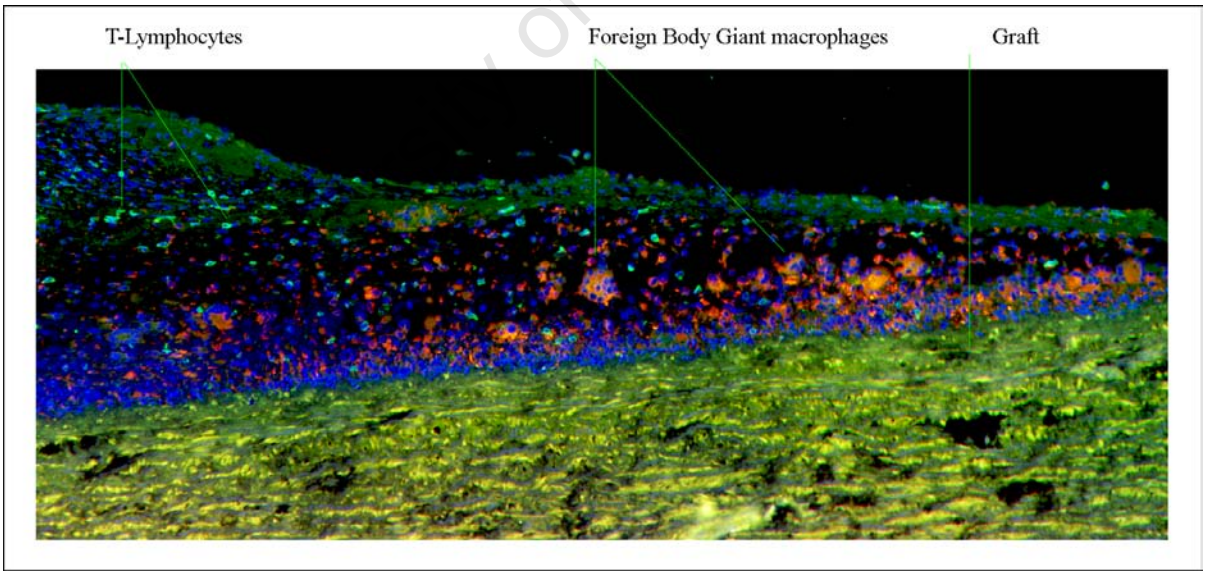

Figure 57 Double immuno-fluorescence of CD 68 positive macrophages in (Cy 3) and CD 3 positive lymphocytes in (Alexa-488) in the pannus edge covering the a-cellular porcine graft. Nuclei are stained with DAPI in blue. Magnification 10 x.

5.4 Discussion

Taking into consideration the points listed below, a comparison was drawn between the three studies described.

- The absence of obesity as a contributory factor to the development of hyperplasia in a different animal model and the absence of a pre-existing pro-inflammatory state compared to that found in the obese and diabetic rats.
- The re-endothelialization that occurs following angioplasty as opposed to the transplant of a living endothelium in a vein graft.
- The significance of an external mesh support on IH considering that the vein is in an arterial position under greater pressure.
- The presence of an endothelial glycocalyx as described in the balloon angioplasty study.
- The existence of a mismatch of elastic properties between the vein graft and the native vessel.

Given the fact that this study was conducted on non-human primates without the presence of obesity or MS, we cannot directly compare the result from balloon angioplasty /stenting in rats with these results. We can however, compare the overall results from the ZFR-L rats (both reinforced and non-reinforced) to these findings. For the purpose of this comparison the table below simplifies the various groups (see Table below).

Table 7 Table describing the groups and animal models used.

1	2	3	4	5
Porcine Bioprosthetic Vascular graft (Baboon)	Non-Reinforced SV (Baboon Femoral pos)	Reinforced SV (Baboon Coronary Pos)	Reinforced Balloon Injury (ZFR-L Rat Carotid)	Non- Stented Balloon Injury (ZFR-L Rat Carotid)

5.4.1 Bioprosthetic Artery Graft.

The porcine bioprosthetic graft in the iliac arterial position in a non-human primate shows extensive transanastomotic IH, characterized by strong HSPG staining throughout the pannus region. There is also an extensive endothelial glycocalyx present along its entire length. The pannus (area of IH) has complete endothelial coverage as confirmed by VWF staining. This is in keeping with the findings seen after carotid balloon injury in the lean Zucker rat. These two models differ with regard to their inflammatory response, as there is a widespread population of inflammatory cells surrounding the bioprosthtic graft, as well as in the pannus area, but which is not seen following balloon injury in the rat after 21 days. The stented balloon injury group does demonstrate a macrophage response but this

was mild in comparison with the extensive response associated with the bioprosthetic graft. This is in spite of decellularization of the graft prior to implantation, that was expected would render it less immunogenic.

Although the bioprosthetic graft may present a suitable non-thrombogenic lumenal surface the transanastomotic ingrowth and inflammatory response remain a concern.

5.4.2 Reinforced SV grafts in CABG

The findings in Chapter 3 and 4, which relate to the degree of IH in the stented carotid artery in the rat model, show decreased IH compared to non-stented balloon injury. This confirms the results in this Chapter when comparing stented SV to non-stented SV grafts. The long-term patency of SV grafts is significantly improved by the use of external mesh reinforcement (153). The external mesh reduces IH by decreasing flow shear stress changes caused by size mismatch of a vein joined to an artery as well as eliminating lumenal irregularities, thereby reducing turbulent blood flow. The histological findings of this study confirm the presence of an endothelium in pre-implanted SV, implanted non-stented SV as well as stented SV in both femoral and coronary positions, as was the case in the balloon injury groups. This suggests that the physical presence of an endothelium, although advantageous, indeed, may not be the necessary criteria for prevention of IH, the question of its viability at the time of reperfusion could be a consideration. Zilla et al. found that the presence of an external mesh around the SV was responsible for the decrease in IH in comparison to the non-stented SV (153). This finding was in spite of both SV being completely endothelialized. There is a noteworthy low presence of inflammatory cells in the SV grafts, both stented and non-stented, similar to what was confirmed in the balloon injured rat. This may be explained by the absence of a pre-existing underlying vascular disease that one would encounter in a clinical scenario, or due to the time point defined by our studies. The presence of inflammatory mediators as characterized by CRP staining, confirms the role of an inflammatory response, even if direct evidence of this is lacking at the time point chosen.

In conclusion, the IH demonstrated by SV grafts and bioprosthetic artery grafts continues to stimulate the development of IH in much the same way as following balloon angioplasty.

Chapter 6

SUMMARY

The emergence of novel techniques to overcome the limitations of PCI are welcome developments in cardiac surgery amidst the overwhelming burden of chronic disease and the high percentage of revascularization requirements following balloon angioplasty and vascular stenting. Coronary artery disease is expected to account for 14.2% of all deaths by 2030, and healthcare budgets are buckling under the load of expensive technology and follow up treatment (155).

Previously, CABG introduced in the 1960s, represented the conventional treatment for coronary artery disease. Subsequently the introduction of PCI in 1977 by Andreas Gruntzig, changed the course of management of heart disease. This brilliant development represented a major accomplishment of twentieth century medicine and became a widely used alternative to open heart surgery. This period of euphoria was short lived, as new problems began to emerge. Between 35%-40% of patients required single or even multiple repeat procedures due to the development of restenosis by IH and introduced the serious risk of acute coronary occlusion or thrombosis of the coronary artery, often resulting in MI or death, and which required emergency CABG. Lastly, there was the realization that the intervention did not alter the natural history of the disease (156).

The introduction of BMS in 1986 reduced stenosis to 20%-25%, but along with this breakthrough, came the complication of late stent-thrombosis. This was partially relieved in 2001 by the development of DES. However, the anti-proliferative coating used on stents was found to inhibit re-endothelialization (156).

Currently some of the most common surgical options for the treatment of coronary occlusion include balloon angioplasty, CABG (vein or prosthetic grafts) and stenting. These techniques all offer temporary relief of the occlusion caused by vascular disease, BUT they all ultimately result in the continued development of neointimal hyperplasia.

The question remains - What to target? Atherosclerosis, MS, Obesity or IH?

Obesity increases the level of IH following PCI. This has been previously established (14, 157, 158). What is the compounding effect of obesity, and is a person of normal weight with atherosclerosis at less risk than an obese person with atherosclerosis? Does DM2 contribute to this increased risk? These questions are central to the ironic situation, in which the very treatment for stenosis, itself results in restenosis, and largely without answers.

The compounding effect of obesity includes several factors that influence the increased risk for adverse outcomes in cardiovascular related complications of obese individuals.

Obesity induces a pro-inflammatory state that exacerbates cardiovascular complications as well as leading to IR and even to EC dysfunction. Wall shear stress increases with increase in body fat (49) Hyperglycaemia and hypertension in obese individuals with DM2 contribute significantly to the

resulting metabolic changes. Pathological changes of beta cell dysfunction are directly related to complications of obesity and DM2. Decreased mRNA adiponectin, together with increased TG, insulin, glucose, plasma LDL, FFA and importantly, the enzyme, heparanase occur in DM2.

Our findings confirm the definite correlation between obesity and IH. Increased body fat in ZFR-F rats resulted in an increase in post angioplasty neointimal hyperplasia in comparison to the ZFR-L control group. The obese ZDF group unexpectedly displayed substantially less IH than the ZFR-L group. Although this group could not be defined as being frank, glucose intolerant, diabetics, as they were not severely hyperglycemic, pathological changes to the islets of the pancreatic islets were nevertheless observed confirming insulin resistance. Previous investigators (99) encountered this same finding in ZDF rats, as well as in Sprague-Dawley diabetic rats. This was explained by the fact that the phenomenon could possibly be due to severe hyperglycemia, resulting in the observed weight loss. This was not, however the case in our ZDF group in this study whose weights were similar to the ZFR-F group and at most these animals were only mildly hyperglycemic. Other investigators have obtained similar findings of decreased IH in severely hyperglycemic diabetic groups (106, 159, 160).

Schiller et al. suggested that reduced intimal thickening could be as a result of increased EC regrowth or normalization of EC phenotype. In that study diabetic animals showed a greater endothelial regrowth albeit with impaired EC function. The idea that re-endothelialization inhibits IH development is not new, but adds support to the possible use of therapeutic agents that improve re-endothelialization. Their data suggested that hyperglycemia and decreased insulin levels could play a role in reducing IH through stimulation of EC regrowth. It may be possible that re-endothelialization, even in the presence of impaired physiological function, would help to inhibit neointimal thickening (160). In contrast, Von Willebrand staining for endothelium in our study showed complete (90 - 100%) endothelialization in most samples of ZFR-F, ZFR-L and ZDF groups. Thus, our finding that was that neointimal hyperplasia was not inhibited, in spite of full endothelial regrowth.

Diabetes and obesity is associated with a low-grade inflammatory state. The hypothesis that this inflammatory state may be a contributory factor in the development of vascular disease, and possibly increase IH following injury, was based on this premise. Our investigation into the effects of injury on several inflammatory cytokines and the possible correlation to IH interestingly, showed elevated staining for adiponectin in the ZDF followed by the ZFR-F and then the ZFR-L groups. In spite of the fact that adiponectin is believed to be protective against inflammation and decreased in obese and diabetic individuals, the findings in this study were not in agreement. There were also high levels of staining for CRP in our ZDF group, that confirm the existence of an underlying pro-inflammatory state, since CRP is a predictive marker for cardiovascular disease (35). CRP staining in the ZFR-F and ZFR-L were relatively high, but less than in the ZDF group.

Our finding of elevated CRP levels in the ZDF group post angioplasty confirms the existence of a heightened inflammatory state (in the absence of inflammatory cells). The presence of diabetes and

obesity are greater CV risk factors and are accompanied by increased CRP plasma levels (108). According to Virmani, raised CRP levels are a prominent finding in atherosclerotic lesions (161).

There was however a zero to low level of staining for IgG in the ZDF group compared to the ZFR-F group, which was strongly positive in some rats, primarily in the intimal region. Of interest, was the result of IgA staining associated with the endothelium of balloon-injured arteries in the ZDF group and negative in the ZDF group. Secondly, when either sera from a balloon injured or non-injured rat were compared when applied to different sections from the above groups that originally stained positive for IgA in the intima and adventitia but not in the media, the media subsequently also stained positive for IgA. This suggests that an immune response could be responsible for the activation of SMC proliferation. Further evidence for this comes from a study by Soleimani et al, in which alloantibody was found to be responsible for enhanced SMC proliferation following carotid artery transplantation in mice. This was completely absent from B lymphocyte deficient mice (162).

The time point defined in our study, although selected to discern primarily the extent of vessel stenosis, was not ideal for the analysis of inflammatory cells, as macrophages and neutrophils typically infiltrate the injured area three to seven days post injury and decreasing thereafter (163). The lack of inflammatory cells in the intimal hyperplasia region of the balloon injured arteries suggests that inflammation possibly was not driving force behind this process, although it may have contributed towards it in the early stages of IH development following injury. Our stented group, however showed the presence of macrophages at 21 days located specifically in the region of the stent struts in response to the foreign material. This confirms previous findings (98, 164). Several studies have associated inflammation with post PCI restenosis, and which have implicated macrophages in the development of IH (134, 164, 165). The response to injury caused by balloon angioplasty differs from that of vascular stenting in that there is only an early neutrophil response and according to Rogers, is devoid of macrophages (166). Following stenting there is a sustained macrophage presence in the intima. Future studies evaluating the effect of inflammation on restenosis could provide much needed therapeutic information for the possible use in DES.

The use of methacrylate resin to facilitate sectioning and preservation of the stent-strut interface introduces problems for immunohistochemistry. Although it certainly is possible to perform immunohistochemistry on certain resin embedded tissue, it is not necessarily a given. Although much research has been carried out by our laboratory into this subject and the resin used in this project was suitable for immunohistochemistry techniques on human and baboon tissue, we encountered some difficulties on rat tissue with certain antibodies, specifically ED-1 (macrophage marker). In spite of antigen retrieval techniques and modified incubation times, this combination of rat tissue embedded in methacrylate resin did not allow accurate staining for this antibody.

Our findings of the I:M ratio (1.4) in the obese groups were in keeping with those previously reported (Desouza-1.4; Shelton-1.37 and Park-1.6), however our I:M ratio in the stented lean group (1.0) was significantly higher than Desouza (0.67), Shelton (0.79) and Park (0.67). This was not due to an

increase in the tunica intima, but rather by the decrease in the medial thickness. This finding of a thinner media in lean rats seems to be confirmed by Park and Shelton. It is interesting to note that the medial thickness of the ZFR-L group is lower than the ZFR-F and ZDF groups in all three scenarios, namely following balloon injury, stented balloon injury as well as in the levels, which extended beyond the stent.

In the stented study, intimal thickening was controlled by the presence of the stent, and the increase in IH at proximal or distal ends beyond the stent substantiated this finding. A stent may provide a treatment for occlusion due to stenosis or atherosclerosis and result in re-endothelialization within the stent region, but the resulting neointimal thickening beyond the stent must result in WSS changes that impact vascular tone and mechanotransduction. These findings support Schiller's hypothesis that EC regrowth may in fact attenuate IH development, however the areas beyond the stent would suggest otherwise. The EC remains a key and vital player in modulating the proliferation and migration of SMC following vascular intervention. There are relatively few studies available on stented carotid arteries in Zucker rats, but our findings relating to the absence of variation in intimal thickness throughout the three groups confirms the finding by Jonas et al.(99), however, the reason for this is still unclear, and further investigation would be beneficial in this regard.

We did not assess the shear stress changes in this study. However, the influence that diameter changes have on the flow of blood through an artery cannot be ignored. The role of shear stress changes within the vessel has been addressed by several investigators (48, 50, 114, 167, 168), and has been shown to have an effect on the development of IH. The effects of wall shear stress (WSS) on EC function have been well described (48, 49), and have been shown to stimulate the production of endothelial glycocalyx. Dimensions of glycocalyx are reduced at atherosclerotic prone lesions (51), and this could explain why glycocalyx dimensions are reduced at bifurcations that experience a reduced WSS. Therefore the EGL is considered to be the first step in the process of mechanotransduction(49). Both high and low WSS is believed to be responsible for glycocalyx disruption, and it may therefore be necessary for an optimum WSS to maintain EC function (67).

In addition, experiments on WSS have mostly been conducted in vitro, based on average calculated WSS, whereas in vivo shear stress varies along the arterial tree. The mean WSS in man is 0.5 Pa compared to 7.0 Pa in rats and 8.8 Pa in mice. This may be due to the decreased arterial diameter in smaller animals with a blood velocity comparable to larger animals (169) This has implications on previous experiments related to WSS with assumptions for mean WSS being inaccurate.

The endothelium was for many years seen to be the barrier between the vascular wall and the blood flow. More recent investigations into the presence and role of the endothelial glycocalyx have altered this perception. Improved techniques to quantify or visualize this layer have shown it to be larger than first imagined. It has also been shown to be vitally involved in the vascular permeability and maintenance of vascular tone. Changes to this meshwork of glycoproteins and PG appear to be the initial reaction to WSS and endothelial denudation and hyperglycaemia (21). The need for a confluent

endothelium seems critical for control of IH post angioplasty, but it is the glycocalyx that senses and translates environmental changes to the cells below it.

One of the important components of the IH tissue are PG. The Movat pentachrome stain conventionally detects GAGs or mucins in formalin fixed, paraffin embedded tissue. Alcian Blue is specific for acid or low pH, sulfated mucins. We therefore performed a Movat stain on our explants balloon injured as well as our stented explants. Our data showed relatively low concentrations of PG in the IH region, however there was more positive staining in the stented, resin embedded samples than after balloon injury alone. Recent studies into the role of PG and the glycocalyx prompted us to further investigate the presence of PG, using the more specific immunohistochemistry technique. Chondroitin sulfates are the most prevalent PG stained by the Movat staining and since strong staining was not present, HS was selected, as it makes up between 50-80% of the glycocalyx. Strong staining for HS was found in the intimal and medial regions as well as demonstration of the glycocalyx on the lumen in some samples.

Several PG have been isolated as playing important roles in mediating the proliferation and migration of VSMC, such as perlecan, HA, versican, decorin and heparan and chondroitin sulfate (32, 53, 55, 60, 167). GAG changes have been noted to take place before changes in SMC phenotype, and this is believed to be central to the formation of IH (170). A study of HS and syndecan-1 levels at surgery showed huge multifold increases with ischemic perfusion alone resulting in EGL components being shed into the circulation, and this could be a trigger for post-operative inflammation (114). Gouveneur demonstrated that HA is incorporated into the glycocalyx in response to WSS (50). Baker showed that in DM2 there is an increase in CS at the expense of HS, and perhaps this could explain why our ZDF group demonstrated a negligible glycocalyx since it is primarily composed of HS (171).

The increase in the enzyme heparanse is the one parameter in which there is a very strong correlation to increased IH (171). HSPG modulate VSMC proliferation, and are essential to counteracting the neointimal response to injury. Increased heparanse expression results in increased neointimal thickness. This heparanase is expressed in the EC themselves and is regulated by high glucose and oxidized LDL levels, and is increased in obese, hyperlipidaemic Zucker rats compared to Zucker lean rats (171). Unfortunately it was beyond the scope of this study to include the study of over-expression of heparanse on SMC proliferation and migration, but further studies in this regard would be valuable in the future.

It has been proposed that HS maintains SMC in a contractile phenotype and that the presence of GAGs and HS reduce the proliferation and migration of SMC in vitro (53). Neointimal hyperplasia has been shown to be decreased following administration of HS. With this in mind, perhaps it is relevant that platelets and inflammatory cells release heparanase, which degrades HS chains (171). Therefore one could say that once inflammatory cells and platelets have resolved, there is an up-regulation of HS and thus the resultant dense layer of EGL demonstrated at 21 days post injury together with a gradual regression in IH, as seen in our experiments. It may be possible that this glycocalyx layer offers a

protective mechanism to handle the changes in shear stress created by a thickened neointima. Perhaps the reduced EGL reported in humans due to hyperglycaemia, may result in higher restenosis rates following PCI. Takagi et al reported that IH after stent deployment in human patients with glucose intolerance is greater than those with normal glucose levels.

The primary weak link between a healthy vasculature and disease appears to be the endothelial cell. If we consider the cascade of events that results from either atherosclerosis or EC injury i.e. glycocalyx disruption; EC dysfunction; shear stress changes; release of inflammatory cytokines; decreased NO availability; SMC proliferation; ECM development and thrombus formation, they are ALL directly linked to, and reliant on, the EC and, if we take it one step further, to the endothelial glycocalyx which is responsible for sensing and transducing shear stress to the EC (49).

Further investigation into the vital role played by the EC, reveals that one of their many important functions seems to revolve around the synthesis and secretion of PG. These seemingly unimportant substances play a fundamental role in modulating vascular tone; vascular permeability; lipid accumulation; inflammation; mechanotransduction and most importantly glycocalyx integrity. FSS has been shown to stimulate the incorporation of HA in the endothelial glycocalyx that may contribute to enhanced EC function (50).

The IH due to vascular intervention from PCI, CABG or vein grafting may all have similar origins. Beginning with a diseased artery with an underlying pro-inflammatory state, leading to vascular stenosis and shear stress changes. Glycocalyx disruption follows with loss of vascular tone and endothelial damage. The consequent release of cytokines, growth factors and PG and activation of the coagulation cascade triggers the formation of IH. The ultimate mechanical intervention itself promotes vascular damage, stimulation SMC migration and proliferation as part of the healing process and development of restenosis.

In spite of an abundance of research and publications in this regard, we are still without a definitive solution to this pathology. Further investigation in pursuit of advanced therapeutic intervention is required in this essential area of research.

Appendix-A

A.1-10% Buffered Formalin (PBS)

PBS (pH7.6) Volume 5L

Table A-1

Constituent	Supplier
42 g sodium chloride [143 mM]	Sigma-S7653 [Steinheim; Germany]
6.4 g disodium hydrogen orthophosphate [9mM]	Merck-Art6346 [Gauteng; SA]
0.7 g sodium dihydrogen orthophosphate anhydrous [1mM]	Merck-Art 6346 [Darmstadt; Germany]

For 10% buffered formalin, make up 1 part formalin:9 parts PBS.

A.2-4% Para formaldehyde (100ml)

Table A-2

Constituent	Supplier
4 g Paraformladehyde 95%	Sigma-Aldrich 15,812-7 [Steinheim; Germany]
90 ml PBS (Table A-1)	

Heat gently to 58-60C under a fume hood, but do not overheat. Add 5-10drops NaOH to clear solution. pH to 7.0-7.5, make up to volume 100 ml with PBS (Table A-1)

A.3-Tris Buffered Saline (TBS) Volume 5L

Table A-3

Constituent	Supplier
30.3 g tris HCl (trizma) [38.5mM]	Sigma-T5941 [Steinheim; Germany]
6.95 g tris Base [11.5mM]	Sigma-saarchem 611 60 00 [Krugersdorp; SA]
43.83 g sodium chloride [150mM]	Sigma-S7653 [Steinheim; Germany]

Make up to 5 L with distilled water, pH7.6-7.8

A.4-Haematoxylin and Eosin Stain

A.4-1 Mayers Haemotoxylin

Table A-4.1

Constituent	Supplier
2 g haematoxylin	Merck-SAAR2822000CB[Gauteng; SA]
50 g potassium alum	Saarchem-111 80 00[Gauteng; SA]
0.2 g sodium iodate	UnivAR 582 34 80[Krugersdorp; SA]
1 L double distilled water	
1 g citric acid	Saarchem-160 5020EM[Gauteng; SA]
50 g chloral hydrate	Saarchem-159 15 00[Gauteng; SA]

Combine the first four constituents in the Table A-4 and gently heatin a warm bath at 37°C. Add the rest of the constituents and boil for 5 minutes. Cool and filter and store in a glass bottle at room temperature.

A.4-2 Eosin/Phloxine

Table A-4.2

Constituent	Supplier
1 g eosin	Merck-341972Q [Poole; UK]
1 g phloxine	Merck-1.115926.0025[Darmstadt; Germany]
Few drops acetic acid	Radchem-A032 [SA]
1 L double distilled water	

Place sections into the haematoxylin solution (Table A-4.1) for 5 minutes and then 5 minutes in running tap water to stain the nuclei blue. Place slides in running tap water for 5 minutes, to differentiate the haematoxylin. Place the sections into the eosin/phloxine (Table A-4.2) for 30 seconds and dip in distilled water followed by dehydration through graded alcohols, 3 changes of xylene and mounting in Entellan *[Merck-Gauteng; SA]*

A-5- Masson's Elastic Trichrome

Verhoeff's Solution

Table A-5.1

Constituent	Supplier
10% alcoholic haematoxylin	Merck-SAAR2822000CB [Gauteng; SA]
10% ferric chloride	Merck-234 05 00 EM [Gauteng; SA]
Lugol's iodine solution (neat)	Merck-322 29 83 KF Steinheim; Germany]
100% alcohol	Illovo [Merebank; SA]

All the constituents were added in equal quantities.

Acid Fuchsin Solution

Table A-5.2

Constituent	Supplier
0.5 g acid fuchsin	Merck-250 10 00 [Krugersdorp;SA]
0.5 ml glacial acetic acid	Radchem-A032 [SA]
100 ml double distiller water	

Phosphomolybdic Acid Solution

Table A-5.3

Constituent	Supplier
1 g phosphomolybdic acid	Sigma-P7390 [Steinheim; Germany]
100 ml double distilled water	

Ligh Green Solution

Table A-5.4

Constituent	Supplier
2% light green	Sigma-L1886 [Steinheim; Germany]
1% acetic acid	Radchem-A032 [SA]

Dewax sections through xylene, graded alcohol to water. Cover with Verhoeff's solution (Table A-5.1) for 15 minutes and rinse in water, followed by differentiation in 2% Ferric chloride to remove

excess black, leaving only the elastin stained black. Immerse sections in Acid Fuchsin solution (Table A-5.2) for 5 minutes and rinse in water, followed by incubation in Phosphomolybdic acid solution (Table A-5-3) for 5 minutes and rinse in water. Apply Light green solution (Table A-5.4) for 1 minute and rinsed in water before rehydrating and mounting in entellan.

Results:

The muscle tissue-stained pink/red

Collagen-blue/green

Elastin and nuclei-black.

A-6-Movat (Modified)

Alcian Blue Solution

Table A-6.1

Constituent	Supplier
1 g alcian blue	Merck-K24319334 [Gauteng; SA]
100 ml double distilled water	

Alcohol/Alkaline Solution

Table A-6.2

Constituent	Supplier
10 ml (25%) ammonia solution	BDH BB100115Q [Gauteng; SA]
40 ml 95% alcohol	Illovo [Merebank; SA]

Von Gieson Counterstain

Table A-6.3

Constituent	Supplier
100 ml picric acid	Fluka 80456[Steinheim; Germany]
10 ml 1% acid fuchsin	Merck-250 10 00 [Krugersdorp;SA]

Bring to the boil and cool before bottling.

Take sections to water. Treat with Alcian blue table (Table A-6.1) for 30 minutes in a coplin jar. Wash slides in running tap water for 10 minutes. Treat with solution in (Table A-6.2) for 3 hours. Wash slides for 20 minutes in running tap water. Stain with Verhoeffs solution in (Table A-5.1) for 30minutes. Rinse briefly in water. Differentiate in 2% ferric chloride until the elastin stains black with nuclei slightly lighter. Wash slides in water for 15 minutes. Counterstain with solution in (Table A-6.3) for 30 seconds. Blot dry and dip in xylene before mounting in entellan.

Results:

Muscle –yellow; Collagen-pink; Elastin-black; Fibrin-red; GAGS-blue

A-7-Immuno-staining

A-7.1-Standard Immunofluorescent Staining

Antibody	Supplier	Cat No:	Antigen Retrieval	Primary Dilution	Secondary Antibody & Dilution
Rabbit Anti-Rat IgG/FITC	Serotec [Oxford; UK	STAR 17B	N/A	1:50	N/A – FITC conjugated primary
Goat Anti-Rab IgA	Komabiotech [Seoul; Korea]	K0211684	N/A	1:50	Donkey X Goat/Alexa 488 (1: 500) [Invitrogen; Ca; USA]
Mouse Anti-ED 1	Serotec [Oxford; UK]	MCA 341R	Proteinase K 10 mins	1:100	Donkey X Mouse Cy3 (1:500) [Jacksons Immunochem; Pennsylvania;USA]
Rabbit Anti-CRP	Abcam [Cambridge; UK]	ab47795	Protease XIV 5 mins	1:50	Donkey X Rabbit Cy3 (1:700) [Jacksons Immunochem; Pennsylvania;USA]
Rabbit Anti-VWF	Abcam [Cambridge; UK]	ab6994	Proteinase K 20 mins	1:400 overnight @4°C	Donkey X Rabbit Cy3 (1:700) [Jacksons Immunochem; Pennsylvania;USA]
CD 3 Rabbit Anti-CD 3	Abcam [Cambridge; UK]	Ab828 500	Pressure cook; Citrtate Buffer pH 6	1:50	Donkey X Rabbit Cy3 (1:700) [Jacksons Immunochem; Pennsylvania;USA]
Mouse Anti Human CD 68	Diagnostech	M0814	Proteinase K 10 minutes	1:100	Goat anti-mouse Alexa 488 [Invitrogen, Ca,USA]

i) Sections (3 µm) cut on a Microm rotary microtome *[HM 360Waldorf; Germany]*, float sections onto warm water before picking them up on a coated glass slide *[Marienfeld-Histobond-Germany]*.

ii) Place slides on a 60°C hot plate for 1 hour. De-wax in xylene (3 changes), followed by alcohol (3 changes) and into running tap water.

iii) Perform antigen retrieval as required for each specific antibody (Table A-7.1.1) using enzyme treatment, Proteinase-K (Diagnostech-S-302080; Denmark) or Protease XIV *[Sigma P5147-1G; Germany]* at 37°C.

iv) Rinse in running tap water, then place in TBS for 10 minutes.

v) Incubate sections with primary antibody, appropriately diluted in 1% BSA in PBS for 1 hour at 37°C (Table A-7.1.1).

vi) Rinse in TBS for 5 minutes with a magnetic stirrer.

vii) Incubate with fluorescent secondary antibody directed at the host in which the primary antibody is made, in the appropriate dilution in 1%BSA in PBS for 2 hours (Table A-7.1.1).

viii) Rinse in TBS for 5 minutes, mount in Vectorshield-DAPI mountant *[Vector H1200 Ca;USA]*, seal the edges with nail varnish and view slide under fluorescent microscope.

A-7.2-Immunohistochemical Staining (Heparan Sulfate)

i) Cut 3 µm sections on a Microm rotary microtome *[HM 360 Waldorf; Germany]* [float sections onto warm water before picking them up on a coated glass slide *[Marienfeld-Histobond; Germany]*.

ii) Place slides on a 60°C hot plate for 1 hour. De-wax in xylene (3 changes), followed by alcohol (3 changes) and into running tap water.

iii) Perform antigen retrieval using enzyme treatment, Proteinase-K *[Diagnostech-S-302080 Denmark]* for 10 minutes at 37°C.

iv) Incubate slides in (3% Hydrogen Peroxide/methanol) for 10 minutes, to block endogenous staining of HRP.

v) Incubate with Mouse Anti-Rat Heparan Sulfate *[ab 2501-Cambridge;USA]*, diluted 1:400 in 1% BSA/PBS for 24 hrs at 4° C in a sealed container.

vi) Rinse in TBS for 15 minutes.

vii) Incubate with secondary antibody Goat Anti-Mouse Biotinylated IgG *[Histomark 71-00-29 KPL-Gaithersburg;USA]* for 30 mins, followed by a 5 min rinse in TBS, and incubation with Streptavidin Peroxidase (Histomark-71-00-38) for 30 mins. Rinse in TBS for 5 mins.

viii) Apply True Blue Peroxidase Substrate *[Histomark-71-00-68 KPL-Gaithersburg;USA]*, un-diluted for 5 mins until colour development is complete. Rinse briefly in water.

ix) Counterstain in 0.25% Neutral Red *[Merck 442 60 00CB; Gauteng; SA]* for 20 seconds only, rinse in water.

x) Air dry sections, dip into xylene, and mount in Entellan *[Merck-Gauteng; SA]*

A-7.3-Double Immunofluorescent Staining (Confocal Microscopy)

i) Place freshly explanted tissue directly into HEPES buffer (A-8.4), without prior fixation.

ii) Incubate in sufficient Proteinase K *[Diagnostech-S-302080; Denmark]* to cover the tissue for 10 minutes with agitation, at 37°C. Rinse well in running tap water.

iii) Incubate with primary antibody cocktail (Rabbit Anti Human VWF; *[Diagnostech M0616; Denmark]* 1:100; Mouse Anti Rat Heparan Sulfate; *[Abcam-ab2501; Cambridge;UK];*1:400 diluted in 1% BSA/TBS, for 2 hours with agitation.

iv) Rinse well in TBS.

v) Incubate with secondary fluorescent antibody cocktail (Donkey Anti-Rabbit Cy3 1:700 *[Jacksons Immunochem; Pennsylvania;USA]* / Goat Anti-Mouse Alexa 488 1:500 *[Invitrogen; Ca; USA]*) in PBS for 2 hours with agitation.

vi) Rinse well in TBS for 15 minutes. Transfer sample onto a slide with a spacer, in HEPES buffer, and cover with a cover slip. View sample using a confocal (Zeiss) microscope using appropriate filters.

A-7.4-Immunohistochemical staining (Insulin)

i) Sections (3 µm) are cut on a Microm rotary microtome *(HM 360Waldorf; Germany),* float sections onto warm water before picking them up on coated glass slide *(Marienfeld-Histobond-Germany).*

ii) Place slides on a 60°C hot plate for 1 hour. De-wax in xylene (3 changes), followed by alcohol (3 changes) and into running tap water.

iii) Perform antigen retrieval using 10 minutes enzyme treatment, Proteinase-K (Diagnostech-S-302080; Denmark) at 37°C. Rinse in running tap water.

iv) Incubate with the primary swine anti guinea-pig Insulin *(A0564 Diagnostech, Denmark)* diluted 1:400 in 1% BSA in PBS, overnight at 4°C.

v) Wash well in TBS.

vi) Incubate in biotinylated Goat anti-rabbit IgG *(Histomark: 71-00-30-KPL, Gaithersburg,MD),* for 30 minutes at room temperature. Wash well in TBS.

vii) Incubate in Streptavidin-peroxidase *(Histomark: 71-00-38-KPL, Gaithersburg,MD)* for 30 minutes and wash well in TBS.

viii) Add chromogen True Blue-HRP *(Histomark: 71-00-68-KPL, Gaithersburg,MD)* until colour change, about 5 minutes.

ix) Do not take through alcohol solutions, counterstain in .25% neutral red for 5 seconds. Rinse quickly in water and air dry before dipping into xylene and mounting in entallan.

A-7.5 Double Immuno-Fluorescence

i) Sections were dewaxed through xylene and brought to water.

ii) Antigen retrieval was performed using the pressure cook technique, for 2 minutes, followed by washing in running tap water.

iii) A combination of antibodies was applied in their appropriate dilutions (in 1% BSA). Mouse anti-human macrophage, CD 68 *(M0814,Diagnostech, Denmark*) and Rabbit anti human CD 3 *(ab818-500 Cambridge;USA)* for 1 hour at room temperature.

iv) Sections were washed in TBS before incubation with a secondary combination, donkey anti rabbit/Cy 3 (Jackson's Immunochemicals, Pennsylvania, USA) and (Goat anti mouse Alexa 488 (Invitrogen, Ca, USA) diluted 1:500 in 1% BSA for 2 hours.

v) Sections were washed in TBS, followed by mounting in Vector shield, dapi mountant. *(Vector H1200 Ca;USA),* and visualized using a triple band filter, Nikon 90I, microscope.

A-8-Resin Processing, Embedding and Staining Schedule

Tissue was harvested and fixed according to protocol, for 24 hrs in 4% Para formaldehyde as described in A-2.

A-8.1-Methylmethacrylate/Butyl Methacrylate Resin

Step No	Solution	Conc	Time(hr:min)	Temp(C)
1	ethanol *[Illovo;SA]*	80%	30 min	4°C
2	ethanol *[Illovo;SA]*	80%	30 min	4°C
3	ethanol *[Illovo;SA]*	90%	30 min	4°C
4	ethanol *[Illovo;SA]*	90%	30 min	4°C
5	2-propanol *[Gauteng; SA]*	100%	60 min	4°C
6	2-propanol *[Gauteng; SA]*	100%	60 min	4°C
7	toluene *[Gauteng; SA]*	100%	60 min	4°C
8	toluene*[Gauteng; SA]*	100%	60 min	4°C
9	toluene-resin sol 1	50%	60 min	4°C
10	resin –sol 1	Pure	Overnight	4°C
11	resin – sol 1	Pure	All day	4°C
12	resin – sol 2	Pure	Overnight	4°C

13	resin – sol 2	Pure	All day	4°C
14	resin – sol 3	Pure	Overnight	4°C
15	resin – sol 3	Pure	All day	4°C
16	Polymerization mixture			-18°C to -20° C

Glass vials are completely filled with polymerization mixture to exclude air, capped and transferred to a deep freezer.

Polymerization is carried out at -18 to – 20°C and completed within 3 days.

A-8.1.1-Solution 1

60 ml methyl methacrylate*: Sigma-Aldrich M5,590-9 [Steinheim; Germany]*

35 ml butyl methacrylate: *Sigma-Aldrich 235865 [Steinheim; Germany]*

5 ml methylbenzoate:*Sigma-Aldrich M2,990-8 [Steinheim; Germany]*

1.2 ml polyethylene glycol 400: *Sigma-Aldrich 20,239-8 [Steinheim; Germany]*

A-8.1.2-Solution 2

100 ml of Solution 1

0.4 g benzoyl peroxide: *Sigma-Aldrich 228877 [Steinheim; Germany]*

A-8.1.3-Solution 3

100 ml of solution1

0.8 g benzoyl peroxide : *Sigma-Aldrich 228877 [Steinheim; Germany]*

A-8.1.4-Polymerization Solution

400 ul of N, N-dimethyl-P-toludine*: Sigm-Aldricha D18,900-6 [Steinheim; Germany]* is added to 100ml of cold (4°C) solution 3 and stirred for a few minutes.

After addition of the accelerator care is taken that the mixture is kept cold at all times.

Note: All resin solutions are stirred for at least 1 hour before use. It is essential that the methacrylate be kept completely dry. It should be stored in bottles containing a drying agent molecular sieve at 4°C.

Reference: Embedding of bone samples in methacrylate: On improved method suitable for bone histomorphometry, histochemistry. and immunohistochemistry. Reinholc G. Erben, University of Munich (146).

A-8.2-Sectioning

A-8.2.1-Tungsten Carbide Blade

6-10 µm thick sections are prepared at room temperature with a Leica SM2500 sliding microtome equipped with a D-profile knife with a tungsten carbide cutting edge. During sectioning the knife and the block are kept moist with 30% methanol. Sections are first floated onto 30%methanol

at 42℃ in a water bath then onto 0.l% aqueous Elmer's glue(Cat No:60308-Canada) at 42℃, picked up on coated slides (Marienfeld; Histobond; Germany), flattened with chloroform vapours, covered by a plastic film, flattened with a rubber roller. Press with a spring clamp and dry for 2 days at 42℃.

A-8.2.2-Saw Ground Technique

Resin blocks were removed from the plastic containers and prepared for sectioning. This involved trimming the block to the start of the tissue using the Buehler high-speed precision saw, polishing the block surface using two grades of water-paper, 600 and 1200 grit. Once dried, the blocks were glued onto coated glass slides using Elmers Ultimate Glue (USA), by placing a drop of glue onto the block and pressing it onto the slide. This was clamped and placed under weight overnight to ensure adherence. The following day the block was sectioned off the slide once again using the high-speed precision saw. The slide containing the thick section, was now polished down to obtain a thinner section. This was fine polished using the fine grit paper for the final section, ready for staining. These sections were stained without resin removal, by placing the slides into haematoxylin at 37°C fro 2 hours, washing in tap water for 30 minutes and staining with Eosin for 30 seconds. No mounting was required.

A-8.3-Deplasticization & Staining (Bladed Sections Only)

1	2-methoxyehtylacetate (*Aldrich-10,988-6)*	20 min	20℃
2	2-methoxyehtylacetate (*Aldrich-10,988-6)*	20 min	20℃
3	2-methoxyehtylacetate (*Aldrich-10,988-6)*	20 min	20℃
4	acetone [*Merck-Gauteng; SA*]	5 min	20℃
5	acetone [*Merck-Gauteng; SA*]	5 min	20℃
6	dist H_2O	5 min	20℃
7	dist H_2O	5 min	20℃

Modified staining techniques are used for staining de-resined sections.

A-8.3.1-Resin H&E

Following removal of the resin place sides into a coplin jar containing haemotoxylin (Table A-4.1) at 60℃ for 1 hour. Rinse in running tap water for 40 minutes. Place slides on a hot plate at 60℃ covered with 1% Eosin/Phloxine (Table A-4.2). Rinse and do not mount.

A-8.3.2-Resin Immunofluorescence

Following removal of resin apply relevant antigen retrieval depending on primary antibody used. For reisn sections Primary and secondary incubations are doubled, but otherwise the protocol is the same as (A-7.1). Depending on primary antibodies available, some antibodies are not possible on resin embedded tissue.

A9. Transmission electron microscopy

Alcian Blue Staining for Transmission Electron Microscopy.

	Constituent	Supplier
A-9.1	Alcian Blue 8 GX Stock Sol [0.05%]	
	1 g alcian blue	Merck-K24319334[Gauteng; SA]
	100 ml acetone/milliQ water (9:1)	
A-9.2	Calcium Chloride Stock Sol 100ml	
	0.588 g calcium chloride [40mM]	BDH-27586[Poole; UK]
	100 ml milliQ water	
A-9.3	EDTA Stock Sol (pH 7.2-7.4) 100ml	
	0.292 g EDTA [10mM]	Sigma-223 60 20 EM[Steinheim; Germany]
	5 ml warm milliQ water	
	1 pellet sodium hydroxide	Sigma-S8045 [Steinheim; Germany]
A-9.4	HBSS 500ml	
	3.320 g sodium chloride [114mM]	Sigma-S7653 [Steinheim; Germany]
	0.375 g potassium chloride [10mM]	Merck-AB004936-500 Gauteng; SA
	0.081 g potassium dihydrogen ortho-phosphate[1.18mM]	Merck-AB004873-500[Gauteng; SA]
	0.144 g magnesium sulphate (7 H_2O) [1.17mM]	BDH-10151
	1.050 g sodium hydrocarbonate [25 mM]	Sigma-

	0.595 g HEPES [5mM]	Sigma-H3375 [Steinheim; Germany]
	0.5 g glucose [5.55mM]	Sigma
A-9.5	Magnesium Chloride Stock Sol	
	10.2 g magnesium chloride [30mM]	Merck[Darmstsdt; Germany]
	50 ml ultra-pure water	
A-9.6	McDowell Fixative	
	20 g para formaldehyde [4%w/v]	Sigma-15,8127[Steinheim;Germany]
	5.8 g sodium dihydrogen ortho-phosphate H_2O[84mM]	Merck-SAAR5822870 EM[Gauteng; SA]
	20 ml gluteraldehyde [1%w/v]	Aldrich-
A-9.7	Toluidine Blue	
	1 g borax	Sigma-719997[Steinheim; Germany]
	1 g toluidine blue dye	Merck-608 25 00 [Gauteng; SA]

A-9.1-Alcian Blue 8 GX Stock Solution

Add Alcian Blue to acetone/ultra-pure water mix. Stir for 1 hr at room temp in a closed vial. Pass through No. 589 filter paper. The residue is recovered from the paper and dried. Store in a dark place at room temperature.

On the day of use, dissolve 150mg dried alcian blue powder in 25ml acidified ultra-pure water (180ml actenoe: 20ml Ultra-pure water) and pass through the following filters (5.0µm; 1.2 µm; 0.22µm;)

A-9.2-Calcium Chloride Stock Sol 100ml

Dissolve calcium chloride in ultra-pure water**.**

A-9.3 EDTA-Stock Sol (pH 7.2-7.4) 100ml

Dissolve EDTA in 50ml water together with sodium hydroxide. Adjust pH to 7.2-7.4 and make up to 100ml with water.

A-9.4-HBSS 500ml

On the day of use, dissolve the salt components in 450ml ultra-pure water and add 6.25ml stcok $CaCl_2$ sol and 1.225ml EDTA stcok Sol. Adjust to 500ml and degas with air (95% air; 5% CO_2) for 1 hour at 37 ℃. Check pH and add 200mg bovine serum albumin.

A-9.5-Magnesium Chloride Stock Sol

Dissolve $MgCl_2$ in water.

A-9.6-McDowell Fixative

Prepare in a fume hood to extract hazardous fumes. Dissolve parafomaldehyde in 250ml water at 60°C. Add1-2 pellets of Sodium Hydroxide until solution is clear. Make up volume to 400ml with ultr-pure water. Add gluteraldehyde and $NaH_2PO_4.H_2O$. Adjust pH to 7.2-7.4 and store at 4°C.

A-9.7-Toluidine Blue

Mix all items together, stir and filter.

A-9.8-Perfusion Fixation

Rats are anaesthetized with Ketamine/Xlazine. A laparotomy is performed exposing the heart, and perfusion through the left ventricle using HBSS for 5 minutes at 8ml/minute.

Perfuse using fixative alone, followed by 30 minutes of McDowell fixative containing alcian blue and $MgCl_{2]}$. The solution must be stirred constantly to prevent aggregation. The left and right carotid arteries were then dissected free and explanted, attached to the aorta, and placed in the McDowell fixative mixture overnight and stained as described below.

A-9.9-Post Fixation of tissue

The following day, tissue was fixed in 2% osmium for 1 to 2 hours in the fume hood and rinsed with distilled water for 5 minutes. This was followed by staining with Uranyl Acetate for 2 hrs, with agitation and protection from light. And washed in ultra-pure water.

A-9.9.1-Uranyl Acetate

Constituent	Supplier
2% uranyl acetate dihydrate	Merck-K2137273 (Darmstadt; Germany)
50% ethanol	Illovo [SA]

Store the solution in a dark bottle at 4°C.

A-9.9.2Lead citrate

Constituent	Supplier
2.66 g lead nitrate	Sigma-L6258 [Steinheim; Germany]
3.52 g trisodium citrate	Merck-582 25 00 EM [Gauteng; SA]
60 ml distilled water	
16 ml of 10N sodium hydroxide(4 g in 100 ml distilled water)	Sigma-S8045 [Steinheim; Germany]
Make up to 100 ml with distilled water	

The solution was mixed and filtered before it was stored at 4°C.

A-9.9.3-Sample preparation

The tissue was dehydrated in each of the ethanol solutions for 15 minutes. Firstly in 50% ethanol, 70% ethanol, 80% ethanol, 90% ethanol and then two times for 20 minutes in 100% ethanol. The tissue was then dehydrated twice in 100% acetone solutions for 20 minutes each.

A-9.10-Spurr Resin Embeddibg

Constituent	Supplier
Spurr Resin Kit	TAAB-S032D [UK]

The tissue was prepared for embedding in Spurr resin, as per kit intructions with different Spurr resin ratio solutions in acetone. The tissue was placed in each solution for an hour at room temperature. The ratio's (Spurr resin : Acetone) of the solutions were 1:2, 1:1 and 2:1. The last solution was 100% Spurr resin with two times for 1 hour at room temperature. The tissue was embedded in Spurr resin in a mould and allowed to polymerize overnight at 70°C.

A-9.11-Sectioning and staining blocks for TEM

Blocks were trimmed with a razor blade to expose the tissue from the block face and get rid of excess resin, thereby minimizing the surface cutting area. Semi-thin sections were cut using an Ultracut (Leica Ultracut) microtome and a glass knife. Sections were mounted on glass slides, heat fixed and stained with toluidine blue for 3-5 mins in order to examine microscopically, to assess the correct area is being cut. Excess dye is rinsed off with distilled water, and the section viewed under light microscope. Ultra-thin sections were cut, sections picked up and placed onto copper grids.

The tissue was stained with Uranyl Acetate for 10 minutes and afterwards with lead citrate for 2 minutes. After staining the grid was immersed in a drop of 10% aqua glacial acetic acid for 1 minute and rinsed in distilled water. The grid was ready for viewing on the TEM.

A-9.12 Viewing TEM samples

Samples were viewed on a Phillips EM420 Transmission Electron Microscope. Grids were placed in the viewing chamber, a vacuum was drawn and the image was located under low magnification (3500 X), before going to a higher magnification and photographs were captured using an AnalySIS computer assisted program.

References

1.Pick. The patients guide to heart valve surgery. 2009.

2.Maton. Human Biology and Health. Science PH, editor.: Englewoods Cliffs, Prentice Hall; 1993.

3.Evanko SP, Tammi MI, Tammi RH, Wight TN. Hyaluronan-dependent pericellular matrix. Adv Drug Deliv Rev. 2007 Nov 10;59(13):1351-65.

4.McGill HC, Jr., McMahan CA, Zieske AW, Sloop GD, Walcott JV, Troxclair DA, et al. Associations of coronary heart disease risk factors with the intermediate lesion of atherosclerosis in youth. The Pathobiological Determinants of Atherosclerosis in Youth (PDAY) Research Group. Arterioscler Thromb Vasc Biol. 2000 Aug;20(8):1998-2004.

5.Hansson GK. Inflammation, atherosclerosis, and coronary artery disease. N Engl J Med. 2005 Apr 21;352(16):1685-95.

6.welfare Aioha. Key indicators of progress for chronic

disease and associated determinants [Technical Review]. 2009.

7.WHO. WHOSIS World Health Statistical information systems. 2008.

8.Hu R, Ma CS, Nie SP, Lu Q, Kang JP, Du X, et al. Effect of metabolic syndrome on prognosis and clinical characteristics of revascularization in patients with coronary artery disease. Chin Med J (Engl). 2006 Nov 20;119(22):1871-6.

9.American. Cardiovascular Disease Death Rates Decline. Science Daily. 2007.

10.Medical-illustration. Nucleus Medical Art.

11.Isomaa B, Almgren P, Tuomi T, Forsen B, Lahti K, Nissen M, et al. Cardiovascular morbidity and mortality associated with the metabolic syndrome. Diabetes Care. 2001 Apr;24(4):683-9.

12.Bellomo A, Mancinella M, Troisi G, Ettorre E, Marigliano V. Diabetes and metabolic syndrome (MS). Arch Gerontol Geriatr. 2007;44 Suppl:61-7.

13.Diabetics. The IDF consensus worldwide defoinition of metabolic syndrome. 2005.

14.Aronne. Cardiovascular disease in obesity: A review of related risk factors and risk-reduction strategies. Journal of Lipidology. 2007;1:575-82.

15.Berg AH, Scherer PE. Adipose tissue, inflammation, and cardiovascular disease. Circ Res. 2005 May 13;96(9):939-49.

16.Skrha J, Prazny M, Hilgertova J, Kvasnicka J, Kalousova M, Zima T. Oxidative stress and endothelium influenced by metformin in type 2 diabetes mellitus. Eur J Clin Pharmacol. 2007 Dec;63(12):1107-14.

17.Nigro J, Potter-Perigo S, Ivey ME, de Dios ST, Evanko SP, Wight TN, et al. The effect of PPAR ligands to modulate glucose metabolism alters the incorporation of metabolic precursors into proteoglycans synthesized by human vascular smooth muscle cells. Arch Physiol Biochem. 2008 Jul;114(3):171-7.

18.Sims FH. A comparison of structural features of the walls of coronary arteries from 10 different species. Pathology. 1989 Apr;21(2):115-24.

19.Franks PW. Obesity, inflammatory markers and cardiovascular disease: distinguishing causality from confounding. J Hum Hypertens. 2006 Nov;20(11):837-40.

20.Cascien. The potential for novel anti-inflammatory therapies for CAD. Nature. 2002:122-30.

21.Nieuwdorp M, van Haeften TW, Gouverneur MC, Mooij HL, van Lieshout MH, Levi M, et al. Loss of endothelial glycocalyx during acute hyperglycemia coincides with endothelial dysfunction and coagulation activation in vivo. Diabetes. 2006 Feb;55(2):480-6.

22.Reitsma S, Slaaf DW, Vink H, van Zandvoort MA, oude Egbrink MG. The endothelial glycocalyx: composition, functions, and visualization. Pflugers Arch. 2007 Jun;454(3):345-59.

23.Shobha. Impaired glucose tolerance and impaired fasting glucose American Family Physician. 2004.

24.Tokuyama Y, Sturis J, DePaoli AM, Takeda J, Stoffel M, Tang J, et al. Evolution of beta-cell dysfunction in the male Zucker diabetic fatty rat. Diabetes. 1995 Dec;44(12):1447-57.

25.Weyer C, Pratley RE, Snitker S, Spraul M, Ravussin E, Tataranni PA. Ethnic differences in insulinemia and sympathetic tone as links between obesity and blood pressure. Hypertension. 2000 Oct;36(4):531-7.

26.Fisman. Cardiovascular Diabetology: Clinical, metabolic & inflammatory facets. Text Book. 2008;45.

27.Scientific. Lipoproteins Good Cholesterol, Bad Choleaterol. Scientific Psychic.

28.Healthy oils, Healthy fats [database on the Internet]. [cited. Available from: *http://www.webmd.com/cholesterol-management/default.htm*.

29.Stary HC, Blankenhorn DH, Chandler AB, Glagov S, Insull W, Jr., Richardson M, et al. A definition of the intima of human arteries and of its atherosclerosis-prone regions. A report from the Committee on Vascular Lesions of the Council on Arteriosclerosis, American Heart Association. Circulation. 1992 Jan;85(1):391-405.

30.Stary HC, Chandler AB, Dinsmore RE, Fuster V, Glagov S, Insull W, Jr., et al. A definition of advanced types of atherosclerotic lesions and a histological classification of atherosclerosis. A report from the Committee on Vascular Lesions of the Council on Arteriosclerosis, American Heart Association. Circulation. 1995 Sep 1;92(5):1355-74.

31.Kipshidze N, Dangas G, Tsapenko M, Moses J, Leon MB, Kutryk M, et al. Role of the endothelium in modulating neointimal formation: vasculoprotective approaches to attenuate restenosis after percutaneous coronary interventions. J Am Coll Cardiol. 2004 Aug 18;44(4):733-9.

32.Noble MI, Drake-Holland AJ, Vink H. Hypothesis: arterial glycocalyx dysfunction is the first step in the atherothrombotic process. QJM. 2008 Jul;101(7):513-8.

33.Ridker PM. Rosuvastatin in the primary prevention of cardiovascular disease among patients with low levels of low-density lipoprotein cholesterol and elevated high-sensitivity C-reactive protein: rationale and design of the JUPITER trial. Circulation. 2003 Nov 11;108(19):2292-7.

34.Krasinski K, Spyridopoulos I, Kearney M, Losordo DW. In vivo blockade of tumor necrosis factor-alpha accelerates functional endothelial recovery after balloon angioplasty. Circulation. 2001 Oct 9;104(15):1754-6.

35.Ridker PM, Danielson E, Fonseca FA, Genest J, Gotto AM, Jr., Kastelein JJ, et al. Rosuvastatin to prevent vascular events in men and women with elevated C-reactive protein. N Engl J Med. 2008 Nov 20;359(21):2195-207.

36.Steffens S, Mach F. Adiponectin and adaptive immunity: linking the bridge from obesity to atherogenesis. Circ Res. 2008 Feb 1;102(2):140-2.

37.Okamoto Y, Folco EJ, Minami M, Wara AK, Feinberg MW, Sukhova GK, et al. Adiponectin inhibits the production of CXC receptor 3 chemokine ligands in macrophages and reduces T-lymphocyte recruitment in atherogenesis. Circ Res. 2008 Feb 1;102(2):218-25.

38.Kishida K, Nagaretani H, Kondo H, Kobayashi H, Tanaka S, Maeda N, et al. Disturbed secretion of mutant adiponectin associated with the metabolic syndrome. Biochem Biophys Res Commun. 2003 Jun 20;306(1):286-92.

39.McNamara DB, Murthy SN, Fonseca AN, Desouza CV, Kadowitz PJ, Fonseca VA. Animal models of catheter-induced intimal hyperplasia in type 1 and type 2 diabetes and the effects of pharmacologic intervention. Can J Physiol Pharmacol. 2009 Jan;87(1):37-50.

40.Nikkari. Smooth Muscle Cell Expression of Extracellular matrix genes after arterial injury. American Journal of Pathology. 1994;144(6):1348-56.

41.Aoyagi M, Yamamoto M, Azuma H, Niimi Y, Tajima S, Hirakawa K, et al. Smooth muscle cell proliferation, elastin formation, and tropoelastin transcripts during the development of intimal thickening in rabbit carotid arteries after endothelial denudation. Histochem Cell Biol. 1997 Jan;107(1):11-7.

42.Virmani R, Kolodgie FD, Farb A, Lafont A. Drug eluting stents: are human and animal studies comparable? Heart. 2003 Feb;89(2):133-8.

43.Farb A, Weber DK, Kolodgie FD, Burke AP, Virmani R. Morphological predictors of restenosis after coronary stenting in humans. Circulation. 2002 Jun 25;105(25):2974-80.

44.Scott NA. Restenosis following implantation of bare metal coronary stents: pathophysiology and pathways involved in the vascular response to injury. Adv Drug Deliv Rev. 2006 Jun 3;58(3):358-76.

45.Geary RL, Nikkari ST, Wagner WD, Williams JK, Adams MR, Dean RH. Wound healing: a paradigm for lumen narrowing after arterial reconstruction. J Vasc Surg. 1998 Jan;27(1):96-106; discussion -8.

46.Gouverneur M, Berg B, Nieuwdorp M, Stroes E, Vink H. Vasculoprotective properties of the endothelial glycocalyx: effects of fluid shear stress. J Intern Med. 2006 Apr;259(4):393-400.

47.Wight TN, Kinsella MG, Qwarnstrom EE. The role of proteoglycans in cell adhesion, migration and proliferation. Curr Opin Cell Biol. 1992 Oct;4(5):793-801.

48.Davies. Hemodynamic shear stress and the endothelium in cardiovascular pathophysiology. Nature Clinical Practice. 2008.

49.Reneman. Wall Shear Stress Revisited. Artery Research. 2009.

50.Gouverneur M, Spaan JA, Pannekoek H, Fontijn RD, Vink H. Fluid shear stress stimulates incorporation of hyaluronan into endothelial cell glycocalyx. Am J Physiol Heart Circ Physiol. 2006 Jan;290(1):H458-2.

51.van den Berg BM, Spaan JA, Rolf TM, Vink H. Atherogenic region and diet diminish glycocalyx dimension and increase intima-to-media ratios at murine carotid artery bifurcation. Am J Physiol Heart Circ Physiol. 2006 Feb;290(2):H915-20.

52.Wight TN, Ross R. Proteoglycans in primate arteries. I. Ultrastructural localization and distribution in the intima. J Cell Biol. 1975 Dec;67(3):660-74.

53.Nugent MA, Nugent HM, Iozzo RV, Sanchack K, Edelman ER. Perlecan is required to inhibit thrombosis after deep vascular injury and contributes to endothelial cell-mediated inhibition of intimal hyperplasia. Proc Natl Acad Sci U S A. 2000 Jun 6;97(12):6722-7.

54.Yao Y, Rabodzey A, Dewey CF, Jr. Glycocalyx modulates the motility and proliferative response of vascular endothelium to fluid shear stress. Am J Physiol Heart Circ Physiol. 2007 Aug;293(2):H1023-30.

55.Merrilees MJ, Beaumont B, Scott LJ. Comparison of deposits of versican, biglycan and decorin in saphenous vein and internal thoracic, radial and coronary arteries: correlation to patency. Coron Artery Dis. 2001 Feb;12(1):7-16.

56.Wight TN. Cell biology of arterial proteoglycans. Arteriosclerosis. 1989 Jan-Feb;9(1):1-20.

57.Wight. Arterial remodelling in vascular disease: a key role for hyaluronan and versican. Frontiers in Bioscience. 2008:4933-7.

58.Heickendorff L, Ledet T, Rasmussen LM. Glycosaminoglycans in the human aorta in diabetes mellitus: a study of tunica media from areas with and without atherosclerotic plaque. Diabetologia. 1994 Mar;37(3):286-92.

59.Farb A, Kolodgie FD, Hwang JY, Burke AP, Tefera K, Weber DK, et al. Extracellular matrix changes in stented human coronary arteries. Circulation. 2004 Aug 24;110(8):940-7.

60.Wight TN, Potter-Perigo S, Aulinskas T. Proteoglycans and vascular cell proliferation. Am Rev Respir Dis. 1989 Oct;140(4):1132-5.

61.Weinbaum. The Structure and Fucntion of the Endothelial Glycocalyx. Annu Rev Biomed Eng. 2007;9:121-67.

62.Perrin. A Role for the endothelial glycocalyx in regulating microvascular permeability in diabetes mellitus. Cell Biochem Biophys. 2007:108115.

63.Fischer JW, Kinsella MG, Clowes MM, Lara S, Clowes AW, Wight TN. Local expression of bovine decorin by cell-mediated gene transfer reduces neointimal formation after balloon injury in rats. Circ Res. 2000 Mar 31;86(6):676-83.

64.Kolodgie FD, Burke AP, Wight TN, Virmani R. The accumulation of specific types of proteoglycans in eroded plaques: a role in coronary thrombosis in the absence of rupture. Curr Opin Lipidol. 2004 Oct;15(5):575-82.

65.Chatzizisis YS, Coskun AU, Jonas M, Edelman ER, Feldman CL, Stone PH. Role of endothelial shear stress in the natural history of coronary atherosclerosis and vascular remodeling: molecular, cellular, and vascular behavior. J Am Coll Cardiol. 2007 Jun 26;49(25):2379-93.

66.van den Berg BM, Nieuwdorp M, Stroes ES, Vink H. Glycocalyx and endothelial (dys) function: from mice to men. Pharmacol Rep. 2006;58 Suppl:75-80.

67.Pries AR, Secomb TW, Gaehtgens P. The endothelial surface layer. Pflugers Arch. 2000 Sep;440(5):653-66.

68.Schober A, Weber C. Mechanisms of monocyte recruitment in vascular repair after injury. Antioxid Redox Signal. 2005 Sep-Oct;7(9-10):1249-57.

69.Gruntzig. Transluminal dilatation of coronary artery stenoses. The Lancet. 1978;311(8058):263.

70.Schwartz RS, Edelman ER, Carter A, Chronos NA, Rogers C, Robinson KA, et al. Preclinical evaluation of drug-eluting stents for peripheral applications: recommendations from an expert consensus group. Circulation. 2004 Oct 19;110(16):2498-505.

71.Touchard AG, Schwartz RS. Preclinical restenosis models: challenges and successes. Toxicol Pathol. 2006;34(1):11-8.

72.Weintraub WS. The pathophysiology and burden of restenosis. Am J Cardiol. 2007 Sep 3;100(5A):3K-9K.

73.Schaefer CA, Kuhlmann CR, Weiterer S, Fehsecke A, Abdallah Y, Schaefer C, et al. Statins inhibit hypoxia-induced endothelial proliferation by preventing calcium-induced ROS formation. Atherosclerosis. 2006 Apr;185(2):290-6.

74.Marx N. PPARgamma and vascular inflammation: adding another piece to the puzzle. Circ Res. 2002 Sep 6;91(5):373-4.

75.Bragt MC, Popeijus HE. Peroxisome proliferator-activated receptors and the metabolic syndrome. Physiol Behav. 2008 May 23;94(2):187-97.

76.Zhao W, Iskandar S, Kooshki M, Sharpe JG, Payne V, Robbins ME. Knocking out peroxisome proliferator-activated receptor (PPAR) alpha inhibits radiation-induced apoptosis in the mouse kidney through activation of NF-kappaB and increased expression of IAPs. Radiat Res. 2007 May;167(5):581-91.

77.Desouza CV, Murthy SN, Diez J, Dunne B, Matta AS, Fonseca VA, et al. Differential effects of peroxisome proliferator activator receptor-alpha and gamma ligands on intimal hyperplasia after balloon catheter-induced vascular injury in Zucker rats. J Cardiovasc Pharmacol Ther. 2003 Dec;8(4):297-305.

78.Svegliati-Baroni G, Candelaresi C, Saccomanno S, Ferretti G, Bachetti T, Marzioni M, et al. A model of insulin resistance and nonalcoholic steatohepatitis in rats: role of peroxisome proliferator-activated receptor-alpha and n-3 polyunsaturated fatty acid treatment on liver injury. Am J Pathol. 2006 Sep;169(3):846-60.

79.Mongiardo A, Curcio A, Spaccarotella C, Parise S, Indolfi C. Molecular mechanisms of restenosis after percutaneous peripheral angioplasty and approach to endovascular therapy. Curr Drug Targets Cardiovasc Haematol Disord. 2004 Sep;4(3):275-87.

80.Kolodgie FD, John M, Khurana C, Farb A, Wilson PS, Acampado E, et al. Sustained reduction of in-stent neointimal growth with the use of a novel systemic nanoparticle paclitaxel. Circulation. 2002 Sep 3;106(10):1195-8.

81.Nageh T, Meier B. Treatment of in-stent restenosis. Int J Cardiol. 2005 Oct 10;104(3):245-50.

82.Windecker S, Juni P. Safety of drug-eluting stents. Nat Clin Pract Cardiovasc Med. 2008 Jun;5(6):316-28.

83.Ozbek. Clinical and Angiographic Results after Implantation of a Passive-Coated Coronary Stent in Patients with Acute Myocardial Infa. J iInvasive Cardiology. 2008;20(1).

84.Tesfamariam B. Local vascular toxicokinetics of stent-based drug delivery. Toxicol Lett. 2007 Jan 30;168(2):93-102.

85.Spurlock ME, Gabler NK. The development of porcine models of obesity and the metabolic syndrome. J Nutr. 2008 Feb;138(2):397-402.

86.Schwartz RS, Edelman ER, Carter A, Chronos N, Rogers C, Robinson KA, et al. Drug-eluting stents in preclinical studies: recommended evaluation from a consensus group. Circulation. 2002 Oct 1;106(14):1867-73.

87.Schwartz RS, Chronos NA, Virmani R. Preclinical restenosis models and drug-eluting stents: still important, still much to learn. J Am Coll Cardiol. 2004 Oct 6;44(7):1373-85.

88.Pasa MB, Pereira AH, Castro Junior C. Morphometric analysis of intimal thickening secondary to stent placement in pig carotid arteries. Acta Cir Bras. 2008 Mar-Apr;23(2):165-72.

89.Finn AV, Gold HK, Tang A, Weber DK, Wight TN, Clermont A, et al. A novel rat model of carotid artery stenting for the understanding of restenosis in metabolic diseases. J Vasc Res. 2002 Sep-Oct;39(5):414-25.

90.Bergman RN, Kim SP, Hsu IR, Catalano KJ, Chiu JD, Kabir M, et al. Abdominal obesity: role in the pathophysiology of metabolic disease and cardiovascular risk. Am J Med. 2007 Feb;120(2 Suppl 1):S3-8.

91.Desouza CV, Gerety M, Hamel FG. Neointimal hyperplasia and vascular endothelial growth factor expression are increased in normoglycemic, insulin resistant, obese fatty rats. Atherosclerosis. 2006 Feb;184(2):283-9.

92.Indolfi C, Torella D, Coppola C, Stabile E, Esposito G, Curcio A, et al. Rat carotid artery dilation by PTCA balloon catheter induces neointima formation in presence of IEL rupture. Am J Physiol Heart Circ Physiol. 2002 Aug;283(2):H760-7.

93.Rinaldi B, Romagnoli P, Bacci S, Carnuccio R, Maiuri MC, Donniacuo M, et al. Inflammatory events in a vascular remodeling model induced by surgical injury to the rat carotid artery. Br J Pharmacol. 2006 Jan;147(2):175-82.

94.Park SH, Marso SP, Zhou Z, Foroudi F, Topol EJ, Lincoff AM. Neointimal hyperplasia after arterial injury is increased in a rat model of non-insulin-dependent diabetes mellitus. Circulation. 2001 Aug 14;104(7):815-9.

95.Lee S, Lim HJ, Park HY, Lee KS, Park JH, Jang Y. Berberine inhibits rat vascular smooth muscle cell proliferation and migration in vitro and improves neointima formation after balloon injury in vivo. Berberine improves neointima formation in a rat model. Atherosclerosis. 2006 May;186(1):29-37.

96.D'Alessandro D, Neri E, Moscato S, Dolfi A, Bartolozzi C, Calderazzi A, et al. Immediate structural changes of porcine renal arteries after angioplasty: a histological and morphometric study. Micron. 2006;37(3):255-61.

97.Horvath C, Welt FG, Nedelman M, Rao P, Rogers C. Targeting CCR2 or CD18 inhibits experimental in-stent restenosis in primates: inhibitory potential depends on type of injury and leukocytes targeted. Circ Res. 2002 Mar 8;90(4):488-94.

98.Virmani R, Farb A. Pathology of in-stent restenosis. Curr Opin Lipidol. 1999 Dec;10(6):499-506.

99.Jonas M, Edelman ER, Groothuis A, Baker AB, Seifert P, Rogers C. Vascular neointimal formation and signaling pathway activation in response to stent injury in insulin-resistant and diabetic animals. Circ Res. 2005 Sep 30;97(7):725-33.

100.Schmidt RE, Dorsey DA, Beaudet LN, Peterson RG. Analysis of the Zucker Diabetic Fatty (ZDF) type 2 diabetic rat model suggests a neurotrophic role for insulin/IGF-I in diabetic autonomic neuropathy. Am J Pathol. 2003 Jul;163(1):21-8.

101.Shafrir. Animal models of diabetes: Frontiers in research. 2001:103-11.

102.Sreejayan N. Vascular Biology Protocols (Methods in Molecular Medicine). Ren J, editor.: Humana Press; 2008.

103.Gabeler EE, van Hillegersberg R, Statius van Eps RG, Sluiter W, Gussenhoven EJ, Mulder P, et al. A comparison of balloon injury models of endovascular lesions in rat arteries. BMC Cardiovasc Disord. 2002 Sep 27;2:16.

104.Sreejayan N. Vascular Biology Protocols. 2008.

105.Purcell C, Tennant M, McGeachie J. Neo-intimal hyperplasia in vascular grafts and its implications for autologous arterial grafting. Ann R Coll Surg Engl. 1997 May;79(3):164-8.

106.Indolfi C, Torella D, Cavuto L, Davalli AM, Coppola C, Esposito G, et al. Effects of balloon injury on neointimal hyperplasia in streptozotocin-induced diabetes and in hyperinsulinemic nondiabetic pancreatic islet-transplanted rats. Circulation. 2001 Jun 19;103(24):2980-6.

107.Caust LJ, Prichard MM. Reversal of Horner's syndrome. J Neurol Neurosurg Psychiatry. 1963 Jun;26:241-3.

108.Altman R. Risk factors in coronary atherosclerosis athero-inflammation: the meeting point. Thromb J. 2003 Jul 17;1(1):4.

109.Schwartz RS, Holmes DR, Jr., Topol EJ. The restenosis paradigm revisited: an alternative proposal for cellular mechanisms. J Am Coll Cardiol. 1992 Nov 1;20(5):1284-93.

110.Kornowski R, Hong MK, Virmani R, Jones R, Vodovotz Y, Leon MB. Granulomatous 'foreign body reactions' contribute to exaggerated in-stent restenosis. Coron Artery Dis. 1999;10(1):9-14.

111.Gurfinkel EP, de la Fuente RL, Mendiz O, Mautner B. Influenza vaccine pilot study in acute coronary syndromes and planned percutaneous coronary interventions: the FLU Vaccination Acute Coronary Syndromes (FLUVACS) Study. Circulation. 2002 May 7;105(18):2143-7.

112.Atoji. Chondroitin Sulfate Proteoglycan in the Extracellular Matrix of the Canine Superior Olivary Nuclei. . Acta Anatomica. 1990;139(2):151-3.

113.Nieuwdorp M. The endothelial glycocalyx: a potential barrier between health

and vascular disease. Cuurent Opinion in Lipidology. 2005;16:507-711.

114.Rehm M. Shedding of the endothelial glycocalyx in patients undergoing major vascular surgery with global and regional ischemia. Circulation. 2007;116:1896-906.

115.Takumida M, Wersall J, Bagger-Sjoback D, Harada Y. Observation of the glycocalyx of the organ of Corti: an investigation by electron microscopy in the normal and gentamicin-treated guinea pig. J Laryngol Otol. 1989 Feb;103(2):133-6.

116.Vora JP, Zimsen SM, Houghton DC, Anderson S. Evolution of metabolic and renal changes in the ZDF/Drt-fa rat model of type II diabetes. J Am Soc Nephrol. 1996 Jan;7(1):113-7.

117.Marsh SA, Powell PC, Agarwal A, Dell'Italia LJ, Chatham JC. Cardiovascular dysfunction in Zucker obese and Zucker diabetic fatty rats: role of hydronephrosis. Am J Physiol Heart Circ Physiol. 2007 Jul;293(1):H292-8.

118.Nakagawa T. Uncoupling of VEGF with NO as a mechanism for diabetic nephropathy. Diabetes Res Clin Pract. 2008 Nov 13;82 Suppl 1:S67-9.

119.Chow F, Ozols E, Nikolic-Paterson DJ, Atkins RC, Tesch GH. Macrophages in mouse type 2 diabetic nephropathy: correlation with diabetic state and progressive renal injury. Kidney Int. 2004 Jan;65(1):116-28.

120.Bakker W, Eringa EC, Sipkema P, van Hinsbergh VW. Endothelial dysfunction and diabetes: roles of hyperglycemia, impaired insulin signaling and obesity. Cell Tissue Res. 2009 Jan;335(1):165-89.

121.Wallitt EJ, Jevon M, Hornick PI. Therapeutics of vein graft intimal hyperplasia: 100 years on. Ann Thorac Surg. 2007 Jul;84(1):317-23.

122.Lemson MS, Tordoir JH, Daemen MJ, Kitslaar PJ. Intimal hyperplasia in vascular grafts. Eur J Vasc Endovasc Surg. 2000 Apr;19(4):336-50.

123.van den Berg B. Glycocalyx perturbation: cause or consequence of damage to the vasculature? AM J Physiol Heart Circ Physiol. 2006;290:H2174-H5.

124.Vink H, Duling BR. Identification of distinct luminal domains for macromolecules, erythrocytes, and leukocytes within mammalian capillaries. Circ Res. 1996 Sep;79(3):581-9.

125.Erdely A, Freshour G, Maddox DA, Olson JL, Samsell L, Baylis C. Renal disease in rats with type 2 diabetes is associated with decreased renal nitric oxide production. Diabetologia. 2004 Oct;47(10):1672-6.

126.Hayashi K, Kanda T, Homma K, Tokuyama H, Okubo K, Takamatsu I, et al. Altered renal microvascular response in Zucker obese rats. Metabolism. 2002 Dec;51(12):1553-61.

127.Baylis C, Atzpodien EA, Freshour G, Engels K. Peroxisome proliferator-activated receptor [gamma] agonist provides superior renal protection versus angiotensin-converting enzyme inhibition in a rat model of type 2 diabetes with obesity. J Pharmacol Exp Ther. 2003 Dec;307(3):854-60.

128.Frode TS, Medeiros YS. Animal models to test drugs with potential antidiabetic activity. J Ethnopharmacol. 2008 Jan 17;115(2):173-83.

129.Holst JJ, Vilsboll T, Deacon CF. The incretin system and its role in type 2 diabetes mellitus. Mol Cell Endocrinol. 2009 Jan 15;297(1-2):127-36.

130.Weir GC, Bonner-Weir S. Five stages of evolving beta-cell dysfunction during progression to diabetes. Diabetes. 2004 Dec;53 Suppl 3:S16-21.

131.Zeyda M, Stulnig TM. Adipose tissue macrophages. Immunol Lett. 2007 Oct 15;112(2):61-7.

132.Yudkin JS, Stehouwer CD, Emeis JJ, Coppack SW. C-reactive protein in healthy subjects: associations with obesity, insulin resistance, and endothelial dysfunction: a potential role for cytokines originating from adipose tissue? Arterioscler Thromb Vasc Biol. 1999 Apr;19(4):972-8.

133.Pei H, Gu J, Thimmalapura PR, Mison A, Nadler JL. Activation of the 12-lipoxygenase and signal transducer and activator of transcription pathway during neointima formation in a model of the metabolic syndrome. Am J Physiol Endocrinol Metab. 2006 Jan;290(1):E92-E102.

134.Gaspardone A, Versaci F, Tomai F, Citone C, Proietti I, Gioffre G, et al. C-Reactive protein, clinical outcome, and restenosis rates after implantation of different drug-eluting stents. Am J Cardiol. 2006 May 1;97(9):1311-6.

135.Virmani R, Kolodgie FD, Farb A. Drug-eluting stents: are they really safe? Am Heart Hosp J. 2004 Spring;2(2):85-8.

136.Rogers C, Edelman ER. Endovascular stent design dictates experimental restenosis and thrombosis. Circulation. 1995 Jun 15;91(12):2995-3001.

137.Hoffmann R, Takimoglu-Boerekci M, Langenberg R, Knackstedt C, Franke A, Radke PW, et al. Randomized comparison of direct stenting with predilatation followed by stenting on vessel trauma and restenosis. Am Heart J. 2004 Apr;147(4):E13.

138.Howard BV, Rodriguez BL, Bennett PH, Harris MI, Hamman R, Kuller LH, et al. Prevention Conference VI: Diabetes and Cardiovascular disease: Writing Group I: epidemiology. Circulation. 2002 May 7;105(18):e132-7.

139.Piatti P, Di Mario C, Monti LD, Fragasso G, Sgura F, Caumo A, et al. Association of insulin resistance, hyperleptinemia, and impaired nitric oxide release with in-stent restenosis in patients undergoing coronary stenting. Circulation. 2003 Oct 28;108(17):2074-81.

140.Rippstein P, Black MK, Boivin M, Veinot JP, Ma X, Chen YX, et al. Comparison of processing and sectioning methodologies for arteries containing metallic stents. J Histochem Cytochem. 2006 Jun;54(6):673-81.

141.Kim JY, Ko YG, Shim CY, Park S, Hwang KC, Choi D, et al. Comparison of effects of drug-eluting stents versus bare metal stents on plasma C-reactive protein levels. Am J Cardiol. 2005 Nov 15;96(10):1384-8.

142.Daemen J, Serruys PW. Drug-eluting stent update 2007: part II: Unsettled issues. Circulation. 2007 Aug 21;116(8):961-8.

143.Pritchard DI. Sourcing a chemical succession for cyclosporin from parasites and human pathogens. Drug Discov Today. 2005 May 15;10(10):688-91.

144.Peltier S, Oger JM, Lagarce F, Couet W, Benoit JP. Enhanced oral paclitaxel bioavailability after administration of paclitaxel-loaded lipid nanocapsules. Pharm Res. 2006 Jun;23(6):1243-50.

145.Daemen J, Serruys PW. Drug-eluting stent update 2007: part I. A survey of current and future generation drug-eluting stents: meaningful advances or more of the same? Circulation. 2007 Jul 17;116(3):316-28.

146.Erben RG. Embedding of bone samples in methylmethacrylate: an improved method suitable for bone histomorphometry, histochemistry, and immunohistochemistry. J Histochem Cytochem. 1997 Feb;45(2):307-13.

147.Glagov S, Bassiouny HS, Sakaguchi Y, Goudet CA, Vito RP. Mechanical determinants of plaque modeling, remodeling and disruption. Atherosclerosis. 1997 Jun;131 Suppl:S13-4.

148.Forough R, Lea H, Starcher B, Allaire E, Clowes M, Hasenstab D, et al. Metalloproteinase blockade by local overexpression of TIMP-1 increases elastin accumulation in rat carotid artery intima. Arterioscler Thromb Vasc Biol. 1998 May;18(5):803-7.

149.Williamson. The role of endothelial cell attachment to elastic fibre molecules in the enhancement of monolayer formation and retention, and the inhibition of smooth muscle cell recruitment . Biomaterials. 2007;28:5307-18.

150.Santhosh. Endothelial cell growth factor (ECGF) enmeshed with firbin matrix enhances proliferation of EC in vitro. Biomaterials. 2001;22:2769-76.

151.Serruys PW, Ormiston JA, Onuma Y, Regar E, Gonzalo N, Garcia-Garcia HM, et al. A bioabsorbable everolimus-eluting coronary stent system (ABSORB): 2-year outcomes and results from multiple imaging methods. Lancet. 2009 Mar 14;373(9667):897-910.

152.Zilla P, Human P, Wolf M, Lichtenberg W, Rafiee N, Bezuidenhout D, et al. Constrictive external nitinol meshes inhibit vein graft intimal hyperplasia in nonhuman primates. J Thorac Cardiovasc Surg. 2008 Sep;136(3):717-25.

153.Zilla P, Wolf M, Rafiee N, Moodley L, Bezuidenhout D, Black M, et al. Utilization of shape memory in external vein-graft meshes allows extreme diameter constriction for suppressing intimal hyperplasia: a non-human primate study. J Vasc Surg. 2009 Jun;49(6):1532-42.

154.Sung P. Vascular graft update:Safety and Performance. 1984.

155.Molina JA, Heng BH. Global trends in cardiology and cardiothoracic surgery--an opportunity or a threat? Ann Acad Med Singapore. 2009 Jun;38(6):541-5.

156.Braunwald E. Effects of coronary-artery bypass grafting on survival. Implications of the randomized coronary-artery surgery study. N Engl J Med. 1983 Nov 10;309(19):1181-4.

157.Rana JS, Li TY, Manson JE, Hu FB. Adiposity compared with physical inactivity and risk of type 2 diabetes in women. Diabetes Care. 2007 Jan;30(1):53-8.

158.Gruberg L, Mehran R, Dangas G, Hong MK, Mintz GS, Kornowski R, et al. Effect of plaque debulking and stenting on short- and long-term outcomes after revascularization of chronic total occlusions. J Am Coll Cardiol. 2000 Jan;35(1):151-6.

159.Park SJ, Shim WH, Ho DS, Raizner AE, Park SW, Hong MK, et al. A paclitaxel-eluting stent for the preventin of coronary restenosis. N Engl J Med. 2003 Apr 17;348(16):1537-45.

160.Schiller NK, Timothy AM, Chen IL, Rice JC, Akers DL, Kadowitz PJ, et al. Endothelial cell regrowth and morphology after balloon catheter injury of alloxan-induced diabetic rabbits. Am J Physiol. 1999 Aug;277(2 Pt 2):H740-8.

161.Virmani R, Liistro F, Stankovic G, Di Mario C, Montorfano M, Farb A, et al. Mechanism of late in-stent restenosis after implantation of a paclitaxel derivate-eluting polymer stent system in humans. Circulation. 2002 Nov 19;106(21):2649-51.

162.Soleimani B, Katopodis A, Wieczorek G, George AJ, Hornick PI, Heusser C. Smooth muscle cell proliferation but not neointimal formation is dependent on alloantibody in a murine model of intimal hyperplasia. Clin Exp Immunol. 2006 Dec;146(3):509-17.

163.Welt FG, Rogers C. Inflammation and restenosis in the stent era. Arterioscler Thromb Vasc Biol. 2002 Nov 1;22(11):1769-76.

164.Farb A, Sangiorgi G, Carter AJ, Walley VM, Edwards WD, Schwartz RS, et al. Pathology of acute and chronic coronary stenting in humans. Circulation. 1999 Jan 5-12;99(1):44-52.

165.Fukuda D, Shimada K, Tanaka A, Kawarabayashi T, Yoshiyama M, Yoshikawa J. Circulating monocytes and in-stent neointima after coronary stent implantation. J Am Coll Cardiol. 2004 Jan 7;43(1):18-23.

166.Rogers C, Welt FG, Karnovsky MJ, Edelman ER. Monocyte recruitment and neointimal hyperplasia in rabbits. Coupled inhibitory effects of heparin. Arterioscler Thromb Vasc Biol. 1996 Oct;16(10):1312-8.

167.Kenagy RD, Fischer JW, Lara S, Sandy JD, Clowes AW, Wight TN. Accumulation and loss of extracellular matrix during shear stress-mediated intimal growth and regression in baboon vascular grafts. J Histochem Cytochem. 2005 Jan;53(1):131-40.

168.Osterberg K, Mattsson E. Intimal hyperplasia in mouse vein grafts is regulated by flow. J Vasc Res. 2005 Jan-Feb;42(1):13-20.

169.Greve JM, Les AS, Tang BT, Draney Blomme MT, Wilson NM, Dalman RL, et al. Allometric scaling of wall shear stress from mice to humans: quantification using cine phase-contrast MRI and computational fluid dynamics. Am J Physiol Heart Circ Physiol. 2006 Oct;291(4):H1700-8.

170.Bingley. Relationship of glycosaminoglycans and matrix changes to vascular smooth muscle cell phenotype modulation in rabbit arteries aftetr acute injury. J Vasc Surgery. 2001;33:155-64.

171.Baker AB, Groothuis A, Jonas M, Ettenson DS, Shazly T, Zcharia E, et al. Heparanase alters arterial structure, mechanics, and repair following endovascular stenting in mice. Circ Res. 2009 Feb 13;104(3):380-7.

Appendix-B

Comparison of Processing and Sectioning Methodologies for Arteries Containing Metallic Stents

Peter Rippstein, Melanie Black, Marie Boivin, John P Veinot, Xiaoli Ma, Yong-Xiang Chen, Paul Human, Peter Zilla, Edward R O'Brien.

Journal of Histochemistry & Cytochemistry (2006) 54: 673-681

Utilization of shape memory in external vein-graft meshes allows extreme diameter constriction for suppressing intimal hyperplasia: A non-human primate study

Peter Zilla, Michael Wolf, Nasser Rafiee, Lovendran Moodley, Deon Bezuidenhout, Melanie Black, Paul Human, Thomas Franz.

Journal of Vascular Surgery (2009)